Review

Evolution in the Design of Water Oxidation Catalysts with Transition-Metals: A Perspective on Biological, Molecular, Supramolecular, and Hybrid Approaches

Ajeet Kumar Singh and Lisa Roy*

Read Online

ACCESS | Metrics & More | Article Recommendations

ABSTRACT: Increased demand for a carbon-neutral sustainable energy scheme augmented by climatic threats motivates the design and exploration of novel approaches that reserve intermittent solar energy in the form of chemical bonds in molecules and materials. In this context, inspired by biological processes, artificial photosynthesis has garnered significant attention as a promising solution to convert solar power into chemical fuels from abundantly found H_2O. Among the two redox half-reactions in artificial photosynthesis, the four-electron oxidation of water according to $2H_2O \rightarrow O_2 + 4H^+ + 4e^-$ comprises the major bottleneck and is a severe impediment toward sustainable energy production. As such, devising new catalytic platforms, with traditional concepts of molecular, materials and biological catalysis and capable of integrating the functional architectures of the natural oxygen-evolving complex in photosystem II would certainly be a value-addition toward this objective. In this review, we discuss the progress in construction of ideal water oxidation catalysts (WOCs), starting with the ingenuity of the biological design with earth-abundant transition metal ions, which then diverges into molecular, supramolecular and hybrid approaches, blurring any existing chemical or conceptual boundaries. We focus on the geometric, electronic, and mechanistic understanding of state-of-the-art homogeneous transition-metal containing molecular WOCs and summarize the limiting factors such as choice of ligands and predominance of environmentally unrewarding and expensive noble-metals, necessity of high-valency on metal, thermodynamic instability of intermediates, and reversibility of reactions that create challenges in construction of robust and efficient water oxidation catalyst. We highlight how judicious heterogenization of atom-efficient molecular WOCs in supramolecular and hybrid approaches put forth promising avenues to alleviate the existing problems in molecular catalysis, albeit retaining their fascinating intrinsic reactivities. Taken together, our overview is expected to provide guiding principles on opportunities, challenges, and crucial factors for designing novel water oxidation catalysts based on a synergy between conventional and contemporary methodologies that will incite the expansion of the domain of artificial photosynthesis.
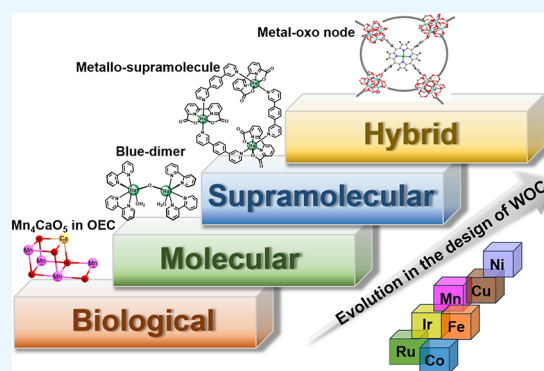
1. INTRODUCTION

The rapid increase in global energy demands coupled to climatic concerns have intensified development of alternative sustainable, environment-friendly, and affordable energy perspectives. In this context, artificial photosynthesis has garnered significant attention as a viable approach to meet these crucial societal needs, whereby the abundant solar energy is stored in chemical bonds to be used later as solar fuels.[1−6] Indeed, photocatalytic and electrocatalytic pathways are promising strategies to utilize visible light as the primary source of energy to drive the reaction of water splitting and provide practical solutions to a clean and green hydrogen fuel economy.[7−14] Notably, water splitting consists of the following two half-cell reactions to generate the solar fuel hydrogen and release molecular oxygen:

$$2H_2O(l) \rightarrow O_2(g) + 4H^+(aq) + 4e^- \tag{1}$$

$$4H^+(aq) + 4e^- \rightarrow 2H_2(g) \tag{2}$$
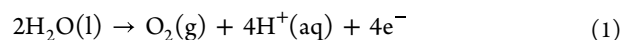
where eq 1 and 2 are water oxidation and reduction reactions, respectively. Out of these two steps, water oxidation requires high overpotential, $E° = 1.23$ V vs normal hydrogen electrode (NHE), due to involvement of multiple electron−proton releases, escalating the energetic input, and widely considered

Scheme 1. Generalized Theme for Typical Solar Light Driven Photocatalytic Water Splitting, Showing the Active Site of the Mn₄CaO₅ Cubane in Photosystem II
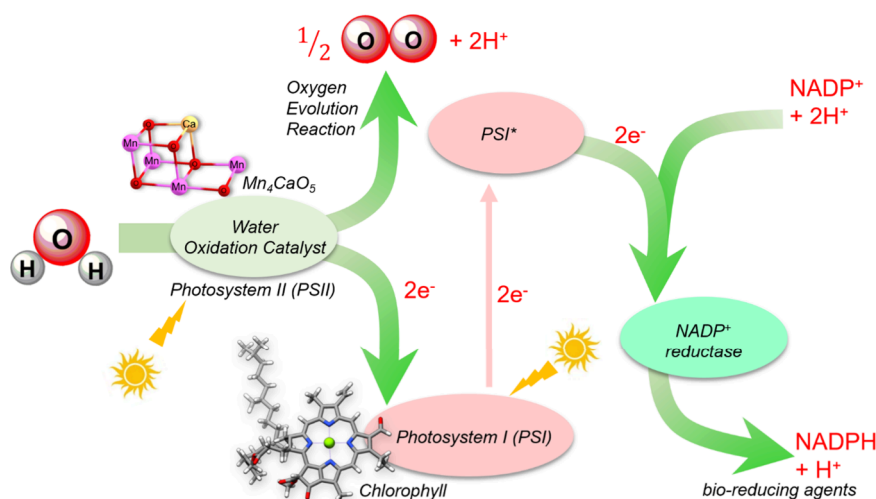
Reprinted with permission from ref 4. Copyright 2014 the Royal Society of Chemistry.

as the bottleneck of homogeneous electrochemical production of H_2 from H_2O.[15−17] Specifically, the O−O bond formation, during the oxygen evolution reaction (OER), is a challenging task due to high endergonicity of the redox events, coupled to significant electronic and structural reorganization.[18−21] In fact, water oxidation often requires overpotentials of 400 mV or higher, that results in almost 25% energy loss to drive the splitting process.[22] Therefore, it is of paramount importance to identify an ideal and efficient water-oxidizing catalyst which should be robust and overcome the thermodynamic and kinetic requirement for water oxidation under mild conditions.[4,23]

As discussed in details in section 2.1, Nature adopts a unique and intricate sunlight driven biochemical machinery for water oxidation to O_2 in the oxygen evolving complex (OEC) of photosystem II (PSII) (Scheme 1).[24−28] The critical O−O bond forming event is coupled to release of two protons, O_2 generation and rapid release, followed by a water-binding event. Interestingly, all these processes are manifested by assistance from appropriate oxidation states on manganese, proximity and binding of water molecules to the Mn core and Ca^{2+}, and hydrogen bonding networks of the neighboring amino acid residues (Figure 2, vide infra). Simultaneously, the reducing equivalents such as electrons and protons derived from water are utilized to drive the reduction of CO_2 to carbohydrate during the carbon fixation event. This fundamental yet intriguing biological process is the central strategy to harvest solar energy into chemical form and leads to sustenance of life on earth.[5]

As demonstrated in the literature, in the past few decades, significant research efforts have been invested to understand the structural and functional principles of the water oxidation event in PSII.[29−31] Understanding the oxygen evolution reaction in the OEC has been primarily focused. The OEC consists of an oxo-bridged tetranuclear manganese−calcium cluster (Mn₄CaO₅) at its active site. Complementary spectroscopic and computational techniques have unearthed in-depth insights on this riveting mechanism, that leads to a four-electron redox chemistry of two water molecules in the OEC, encompassing five sequential intermediate states in the Kok cycle, resulting in the crucial O−O bond formation (see

Figure 2, vide infra).[31−37] X-ray diffraction techniques with free-electron lasers (XFEL) and other advanced spectroscopic approaches have contributed immensely to elaborate the geometric and electronic templates that are involved in the plausible substrate water coupling and release of dioxygen,[38−41] providing a solid foundation for future functional studies.[42,43] Thus, the biological photosynthetic complex serves as a natural platform which could be probed to provide useful guidelines in the quest for light-driven artificial water splitting catalyst (Scheme 1).[20,44−46]

Over the years, several biomimetic analogs have been identified which mimic the structural and electronic properties of the inorganic core of Nature's water oxidation catalyst.[47−52] This resulted in synthetic endeavors of a plethora of oxo-bridged oligonuclear complexes, mostly buildup of manganese, displaying beautiful chemical architectures, albeit with less success as compared to the efficiency of the biological water oxidation catalyst.[53] Furthermore, several experimental and synthetic studies have attempted to draw inspiration from the photochemical processes of PSII, to achieve conversion of solar energy into chemical energy and fuels in an elegant manner, rather than mimicking the structural components of the complicated and sophisticated photosynthetic device. Thus, a number of well-defined molecular catalysts[19] have been deployed to facilitate water splitting in electrolyzers and photoelectrochemical devices.[54] In addition to initial explorations with rare, expensive and toxic noble metals like ruthenium and iridium,[55] present scientific thrust relies on low-cost and abundant non-noble first-row transition metals like manganese, iron, cobalt, nickel, and copper, with tailored coordination environment, electronic structure and solvent medium.[56] In addition, the humongous success of supramolecular chemistry in selective chemical transformations and organized assemblage of photochromophores have opened up new avenues in supramolecular catalysis,[57] particularly the subfield of photoredox catalysis. This has paved the way for emergence of bioinspired supramolecular water oxidation catalysts, utilizing the fundamental concepts of noncovalent interactions, and consisting of mono-, bi-, and polynuclear metallic sites.[58,59] Utilizing supramolecular principles, mononuclear catalysts are confined in vesicles or fibers to enable

spatial proximity of two catalytic centers during O−O bond formation, and improves catalytic efficiency.[58,59] However, despite considerable increase in the number of active water oxidation catalysts (WOCs), thermal instability and kinetic challenges are key issues that prevent their practical implementation, critical for a sustainable future.[18]

In the recent past, several review articles and perspectives have highlighted the structural features and methodological development in artificial water splitting.[4,18,20,21,60] However, to the best of our knowledge, there has been no concise report that outlines collectively the advancements in water oxidation by conventional molecular catalysts, multinuclear inorganic cores, supramolecular and hybrid catalysts[61] and focuses on their catalytic functions from a structural−functional−mechanistic perspective, acquired through both experimental and computational techniques. Therefore, in this review, we briefly discuss the present knowledge on the complexity and the mechanistic intricacies involved in the tightly controlled reaction center in nature's photosynthetic device (Scheme 1, Figure 2). This should provide guidance to understand the evolution of several biomimetic and nonbiomimetic structural and functional analogues of the oxygen evolving complex and offer proper directions for modifying the chemical environment of the synthetic catalyst to attain the desired efficiency in artificial water oxidation. Furthermore, we present a critical overview on the recent progress on WOCs, with representative examples in the field of homogeneous molecular catalysts, structural biomimetic cores, supramolecular and hybrid catalysts identified in the past decade (Figure 1).[4,18,20,21,61]
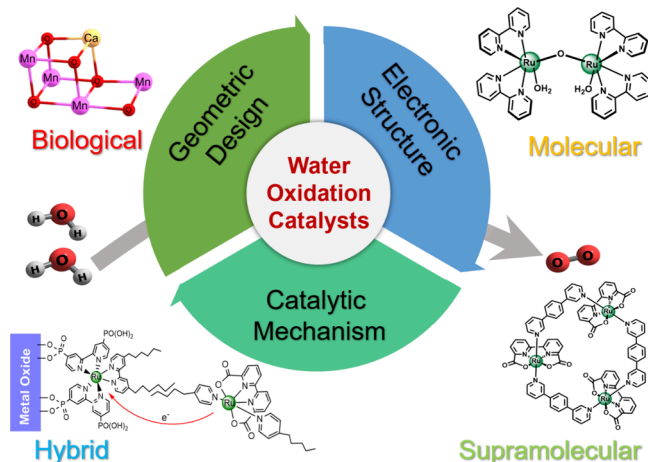

Figure 1. Schematic representation of the various water oxidation catalysts and their salient features discussed in this review.

We identify the challenges faced in artificial water oxidation, and present our outlook on the prospect of various chemical approaches for future design of transition-metal-based catalysts with high catalytic activity. This article is by no means a comprehensive account of the vast literature on biological and artificial water oxidation, neither it covers an overview on photoredox catalysis for solar fuel generation. Furthermore, this article does not address the vast field of heterogeneous water oxidation by metal-oxides, electrodes etc. The readers are encouraged to consult recently published review articles for a detailed narrative.[4,18,20,21,60−65]

2. BIOLOGICAL WATER OXIDATION

2.1. Principle of Natural Photosynthesis. The oxygenic photosynthetic reaction occurs at PSII which is a multipigment protein complex, comprising of four chlorophyll-a and two pheophytin-a molecules. Visible light shining on the antenna complexes generates an excitation energy that induce a charge separation in the chlorophyll-a and pheophytin-a assembly. This subsequently leads to a charge-separated radical pair comprising of the radical cation P680$^{\bullet+}$ and the radical anion Pheo$^{\bullet-}$.[20] Incidentally, the oxidation potential of P680$^{\bullet+}$ is the highest known oxidizing potential in biology, estimated to be ca. + 1.2 to 1.3 V,[65] and therefore, it is primarily responsible for successive four-electron oxidations of the manganese−calcium cluster, Mn_4CaO_5, or the water oxidizing molecular machine present in photosystem II (PSII) subunit. The radical pair (P680$^{\bullet+}$ and Pheo$^{\bullet-}$) undergoes electron/hole transfer steps to avoid oxidizing neighboring chlorophylls by the radical cation.[65] The intermediacy of the redox-active tyrosine residue (Y_z) next to P680$^{\bullet+}$ results in donation of an electron from the former to the latter, within 20−250 ns, to regenerate the initial state of P680.[65] The tyrosine radical cation reversibly loses one proton to a neighboring histidine residue, forming a neutral $Y_z^{\bullet}$ radical.[20,65,66]

The four electron transport events lead to transient storage of four oxidizing equivalents or holes in the OEC, with alternate release of protons to maintain charge neutrality. The series of five redox intermediate states (S_i) ($i = 0−4$) in the Kok cycle (also known as the oxygen cycle or the S-state cycle) designate the number of stored oxidizing equivalents in the Mn_4CaO_5 cluster (Figure 2).[67] The original Kok model was
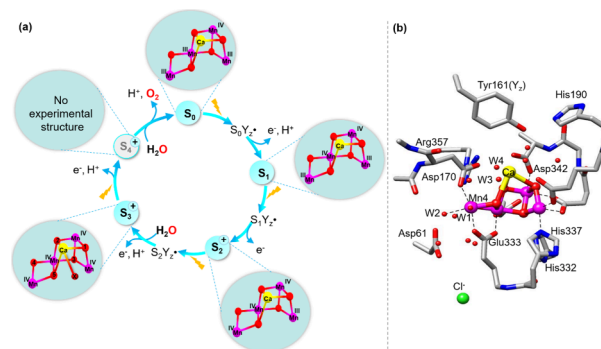
Figure 2. (a) Stages of the five S_i states in the catalytic Kok cycle. Reprinted with permission from ref 67. Copyright 2023 Springer Nature. (b) Ball and stick representation of the active site of the oxygen evolving complex in photosystem II (not to scale). Color code: Mn (magenta), O (red), Ca (yellow), C (gray), N (blue), O (green). H atoms are not shown for clarity. Reprinted with permission from ref 76. Copyright 2021 the Royal Society of Chemistry.

developed by Kok and co-workers as early as 1970,[68] based on Joliot's flash-induced oxygen evolution pattern (FIOP) experiments.[69] Over the past five decades the kinetic FIOP model has evolved enormously to contribute to molecular-level understating of the OEC. As shown in Figure 2a, accumulation of four oxidizing equivalents in the S_4 state convert it back to the S_0 state, with simultaneous release of O_2 from oxidation and deprotonation of two coordinated H_2O molecules.[67] Thus, it consists of alternate electron/proton removal steps as proposed by Klauss[70] as well as two water-binding events in the $S_2 \rightarrow S_3$ and $S_4 \rightarrow S_0$ states.[71−74] The four states, S_0 to S_3^+,

in the sequential water-splitting mechanism can be trapped and identified spectroscopically, while the fifth state (S_4^+) has fleeting existence and has not been probed experimentally so far.[67,75] The chemical energy extracted from water oxidation and the reducing equivalents are temporarily stored in the plastoquinone for eventual utilization during CO_2 fixation to carbohydrate.[76]

2.2. Geometric and Electronic Structure of the OEC.

An understanding of the structural complexity of the oxygen evolving complex in photosystem II imparts requisite leads to design efficient molecular catalysts. Although crystallization of the photosynthetic reaction center was reported back in 1985 by Deisenhofer et. al,[77] it was almost after two decades that the X-ray diffraction (XRD) structure of the membrane-embedded PSII enzyme from oxygenic photosynthetic bacteria was probed by Krauss and others at a resolution of 3.8 Å.[78] The first crystallographic structure of PSII revealed unique placement of the protein residues and the metal cofactor.[78] Further refinement of the structure at 3.5 Å with X-ray absorption fine structure (EXAFS), electron paramagnetic resonance (EPR) and electron nuclear double resonance (ENDOR) studies by Ferreira et. al reflected that the OEC consists of a heterometallic oxo-bridged Mn_3CaO_4 cubane structure.[29] Improved crystallographic models at higher resolutions resolved the atomic placements of all the four Mn ions and the Ca^{2+} ion. It is depicted that the inorganic core of the OEC consists of three Mn and one Ca^{2+} ion arranged in an asymmetric cubane-like structure like a distorted-chair, with bridging -oxo groups, and a fourth distant and dangling Mn (Mn4) attached to the core by corner oxo groups (Figure 2b).[76] In addition, there are four terminal water molecules (W1 to W4), close to the metal centers, out of which two are attached to Mn4 and two to Ca. It is believed that these water molecules act as substrates during oxidation. Latest studies have also demystified the identity of the associated amino acid residues (as shown in Figure 2b), the coordination ligand environment around each metal center, secondary coordination sphere, hydrogen bonding networks, chloride binding, charge balance, and proton gradient.[76] The crucial tyrosine residue (Y_z) is hypothesized to be in close proximity to the OEC and engage in hydrogen bonding with the inorganic core. Ca^{2+} is believed to coordinate these hydrogen bond networks around the OEC through electrostatic balance, bind one substrate water molecule, and facilitate nucleophilic attack on a bridging oxo ligand during O−O bond formation. Spectroscopic and computational studies have indicated that functional substitution of Ca^{2+} with Lewis acidic Sr^{2+} impart similar structural and electronic environment, but with diminished efficiency for O_2 evolution capability of the cluster.[79] Furthermore, high resolution XRD at 1.9 Å indicates existence of two Cl^- ions at the entrance of hydrogen bonding network,[80] which might function as either water inlet channels or proton exit channels, and assist in protein alteration. Recent studies on room temperature crystallographic snapshots at 1.89 Å of the OEC provide clarity on the mobility of the water molecules encircling the cubane during S_2 to S_3 transition, emphasizing on the coordination of the amino acid and H-bond networks during proton and water shuttles.[81]

Several spectroscopic evidence have captured the dynamism in the Mn_4CaO_5 cofactor, indicating that it can attain more than one stable conformation, especially in the S_2 state (Figure 3).[75,76] Interestingly, EPR spectroscopy showed two distinct signals for the most probable intermediate of the S_2 state: a
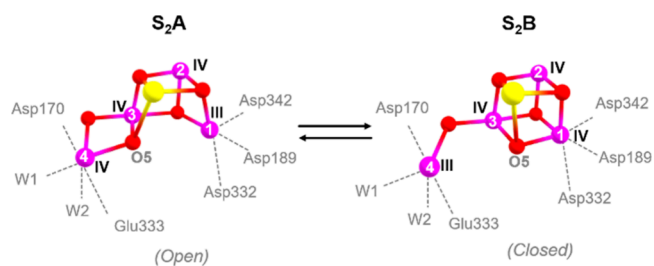

Figure 3. Valence isomeric forms at S_2 state of the OEC showing open (left) and closed (right) cubane structures. Mn−Mn distance $\sim$2.7−2.9 Å in the cubane; Mn1−O5 distance is 3.2 Å in the open and 1.87 Å in the closed structure. Reprinted with permission from ref 82. Copyright 2012 John Wiley and Sons.

multiline signal at $g \approx 2.0$ corresponding to a low-spin ($S \approx 1/2$) ground state.[83−85] Additionally, several studies under varied conditions indicated a higher spin ($S \approx 5/2$) ground electronic configuration due to exhibition of $g \geq 4.1$. Later, a pioneering work by Pantazis et. al put forth the possibility of exchange of the bridging O5 oxygen (see Figure 2), between Mn1 and Mn4, leading toward two structural forms: open cubane (A form) and closed cubane (B form) (Figure 3),[82] by rationalization of Umena et al.'s XRD data of the PSII at 1.9 Å resolution.[80] However, recent X-ray absorption near edge spectroscopy (XANES) analysis of the membrane-bound oxo-bridged Mn_4CaO_5 cluster at room temperature propose that the OEC can be described by one structural form of the S_2 state, while structural data under cryogenic temperatures indicate the possibility of two structural forms at the S_2 state.[86] Notably, the two interconvertible flexible structural forms although are isoenergetic, but represent different oxidation states of the manganese ions, III−IV−IV−IV for the open (A) form and IV−IV−IV−III for the closed (B) form, respectively (Figure 3). Consequently, the cofactor attains different spin multiplicities at the ground state of the S_2 state. The open cubane structure exhibits essentially antiferromagnetic interactions in the mixed valence manganese cluster while the closed cubane display ferromagnetic interactions between the Mn(1,2,3) bundle and the pendulous Mn(4) ion, leading to ground low-spin and high spin states respectively and the observance of the different EPR signals.[75,82]

Despite the similarity in the Mn−Mn distances ($\sim$2.7−2.9 Å in the cubane) in the open and the closed forms, the nature of the Mn−O bonds and distances (Mn1−O5 distance is 3.2 Å in the open and 1.87 Å in the closed structure, Figure 3) are unique that results in multiple scattering effects.[82] Furthermore, the equilibrium between the low spin and high spin isomers in the S_2 state is pH dependent as demonstrated by EPR, time-resolved UV−vis absorption spectroscopy and DFT studies by Rutherford and co-workers.[87] Low-temperature (<150 K) experiments[88] indicate a facile transition of the high spin S_2 model to the S_3 state, lending support to the hypothesis that low-spin conformer A exists initially, followed by transition to the high spin B form. Systematic comparison of the computational models of the S_0-S_3 states with spectroscopically identified intermediates provide additional information on the heterogeneity of the structure of the water oxidizing enzyme. It is generally believed that S_0 (III−IV−III−III) and S_1 (III−IV−IV−III) retain low-spin open cubane structure, with minimal geometric and electronic structure difference that is responsible for their easy interconversion.[89] Moreover, the three-electron/two-proton oxidized S_3 state also features
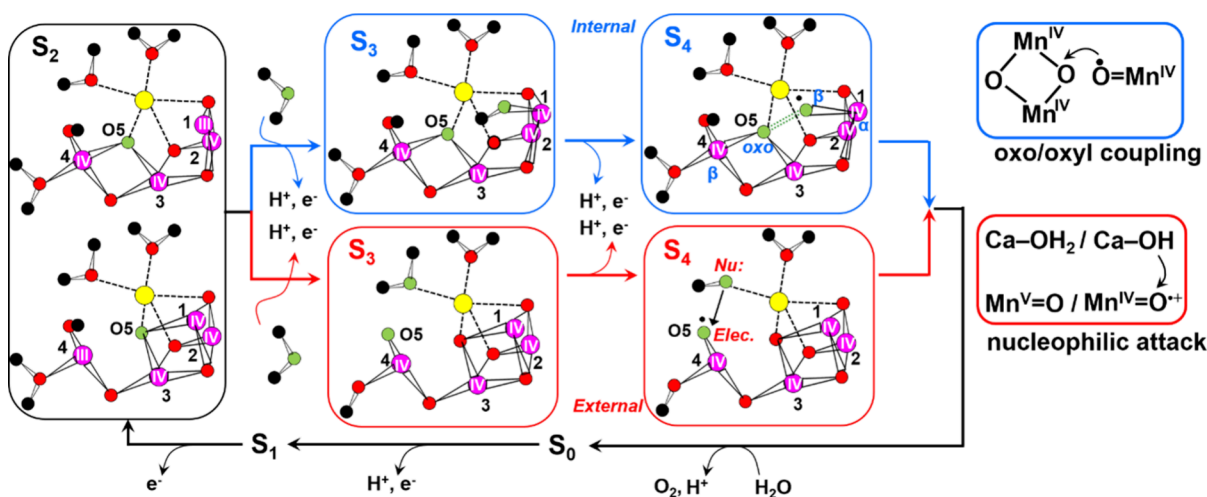
Figure 4. Possible catalytic pathways of O−O bond formation: (I) nucleophilic attack (red boxes) and (II) oxo/oxyl radical coupling (blue boxes). Reprinted with permission from ref 91. Copyright 2013 American Chemical Society.

heterogeneity and adopts the open conformation due to water molecule insertion. This is because conversion of the open cubane structure to the closed cubane allows greater solvent access to Mn4 which can hold two terminal water molecules. Indeed, high-field EPR measurements suggests a modified S_3' intermediate, featuring an oxidized cofactor with closed cubane structure (resembling B type) and a five-coordinated Mn4.[90]

2.3. Mechanism of Water Oxidation in PSII. Spectroscopic, X-ray analysis and quantum chemical studies filter out the possibilities of O−O bond formation which occupies the center stage in biological water oxidation. In particular, the O5 oxygen is considered as the substrate site (Figure 3 and green colored bridging oxygen in Figure 4), which correlates with the observed redox changes and the role of Ca^{2+} ion in the mechanism. Recent evidence converge to two different possible pathways for the O−O bond formation, either inside or outside the cubane structure, initiating from two different structures at the S_2 state. Representations of both the pathways are shown in Figure 4.[91]

Notably, interconversion of two isomeric forms at S_2 is facilitated by swapping a single spin and occurs at a marginal energetic expense (1 kcal/mol),[82] as predicted by DFT calculations on the XRD structural data, thereby allowing smooth valence exchange. FTIR spectroscopy[92] studies reveal the insertion of an additional water substrate on the vacant coordination site on Mn1 at the S_3 state, presumably due to elongation of the Mn1−O5 bond in the open cubane structure that leads to radical coupled O=O dioxygen bond formation. This internal mechanism also known as oxo/oxyl coupling (Figure 4, top) was originally suggested by Siegbahn et al. from density functional theory (DFT) calculations of the OEC,[71,93] and recently supported by XFEL serial crystallography by Suga et al.[94] Interestingly, the three Mn ions (1, 3, 4) that hold the oxo and the oxyl ligands are reduced to + III state on O−O bond formation and subsequent O_2 release. In the external mechanism also known as the water nucleophilic attack (Figure 4, bottom), oxidation of the substrate water to O_2 is carried out on the highly oxidized pendulous Mn4 ion (Figure 4). Here, a water or a hydroxyl ligand (W3) attached to Ca^{2+} acts as a nucleophile to facilitate an acid−base coupling and attacks the electrophilic terminal O5 bound to Mn4, which may be an Mn^V-oxo or a Mn^{IV}-oxyl center, to couple the two

oxygen atoms. Present studies on biological water oxidation mainly focus on the overall high oxidation state of the manganese−calcium cluster, corresponding to the electronic configuration: $Mn^V Mn^{IV}_3$.[42] The reactivity and property of separately synthesized simpler chemical models of first row transition metals provide inspirations toward the occurrence of O−O bond through nucleophilic attack of a nearby water. Although, initially it was hypothesized that $Mn^V=O$ best represents the electrophile,[95−97] recent evidence propose $Mn^{IV}−O^\bullet$ (oxyl) to be a better site for substrate oxidation, hinting toward a possible electronic rearrangement of the metal−oxygen moiety.[97] Theoretical analyses also predicted high activation energies ensuing from the $Mn^V=O$ intermediate, suggesting that the oxyl-radical bound Mn^{IV} is the likely site for O−O coupling.[71,98−100] However, in a recent report, Siegbahn has indicated nonconformity of the water nucleophilic attack mechanism due to overtly large barriers, in the range of 29.8−48.6 kcal/mol, predicted by DFT calculations at B3LYP/LACVP for six different case studies, involving different open/closed structures and overall spin of the cluster.[101] Thus, the mechanistic intricacies of the O−O bond formation during water oxidation are still perplexing. It may be noted, that the natural process may consists of blending of both these mechanisms, instead of following one predominantly. Contrasting mechanistic studies by Zhang and Sun suggests the formation of a Mn^{VII}-dioxo intermediate as the dangling metal site for water oxidation in the S_4 state of the Kok cycle.[18] Extensive DFT studies by Li and others reveal that the existence of a $Mn^{VII}=O$ moiety is very unlikely, due to the large energetic cost involved in transition from S_3 to S_4 (+33.8 kcal/mol at B3LYP/LACVP) as compared to the insignificant endergonicity of the analogous transformation with all Mn^{IV} ions (+5.7 kcal/mol).[102] In a latest theoretical study, Messinger, Sun, and others[103,104] indicate that unlike cyanobacterial photosystems, the S_3 state of higher plants are devoid of the additional Mn-bound oxygenic ligand necessary for a "radical coupling" through the $Mn^{IV}−O^\bullet$ (oxyl) moiety in an open-cubane cluster, as shown in Figure 4 (bottom). The authors further propose that the S_3 state in higher plants undergo considerable structural modifications on binding of water and attain a specific conformation that enables the dangling $Mn^V=O$ exhibit a "nucleophilic oxo-oxo coupling"

with a μ^3-oxo group of the closed-cubane motif in the resulting unbound S_4 state (Scheme 2). Notably, this mechanism is

Scheme 2. Graphic Illustration for O−O Bond Formation and $^3O_2$ Release Due to W2(Terminal oxo)−O5(μ_3-oxo) Coupling in $S_4^{B,unbound}*^a$

$\Delta G^{\ddagger}_{O-O} = 12.5 \sim 14.1$ kcal/mol

$\Delta G_{O-O} = -2.9 \sim 3.5$ kcal/mol
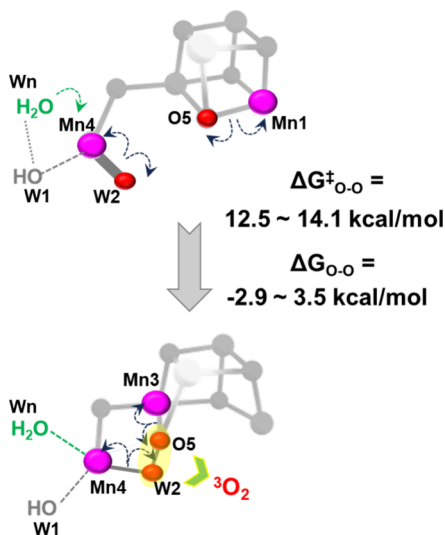
^{a}Energetics for O_2 release shown are at B3LYP*-D3(BJ)/SMD ($\varepsilon = 6.0$)/ SDD (Mn, Ca), cc-pvtz(-f) (C, N, O, H) level of theory.[103]

rather sluggish as compared to radical coupling, justifying that the conformational changes due to water insertion is a prerequisite for O_2 release. The relative energetics at B3LYP*-D3(BJ)/SMD ($\varepsilon = 6.0$)/SDD (Mn, Ca), cc-pvtz(-f) (C, N, O, H) level of theory are found to be consistent with experimental findings relevant for higher plants and features a complementary pathway to the existing radical coupling mechanism.

Alternative ideas about the mechanism of O−O bond formation are also rife in the literature. This is primarily because of the involvement of several proton release and electron transfer chain reactions (as shown in Figure 2) that occur efficiently within the photoactive protein matrix of the OEC, other than the accentuated O−O bond formation event. Renger proposed that oxidation of the tyrosine residue Y_z to Y_z^{ox} by the P680$^{\bullet+}$ radical cation is kinetically limiting through a nonadiabatic electron transfer step that leads to rearrangements of the hydrogen-bonding networks.[105] On the contrary, the Y_z^{ox} induced oxidations of the catalytic framework in the S_3 state are kinetically limited by triggering processes which are sluggish as compared to the nonadiabatic electron transfer. Thus, the reduction of Y_z^{ox} by the WOC provides an optimum facility for the energetically uphill process of O_2 formation and release in the S_3 state itself.[105] Quantum mechanics/molecular mechanics (QM/MM) analysis of the tyrosine oxidation and intramolecular proton transfer reaction in photosystem II by Shoji, Yamaguchi and others emphasized on the possibility of O−O bond formation in the S_3 state triggered by electron transfer from the manganese−calcium cluster to Y_z.[108] On a similar footing, Pushkar et al. predicted a low-barrier O−O bond formation in the S_3 state, prior to the final S_4 redox state in the Kok cycle, by a combination of spectroscopic, crystallographic and DFT studies.[109] An interesting assessment on this subject has been put forth by O'Malley et al. through density functional theory modeling and intrinsic bond orbital

analysis of the reaction path in photosystem II.[106,107] As shown in Figure 5, the authors propose concerted movement of two
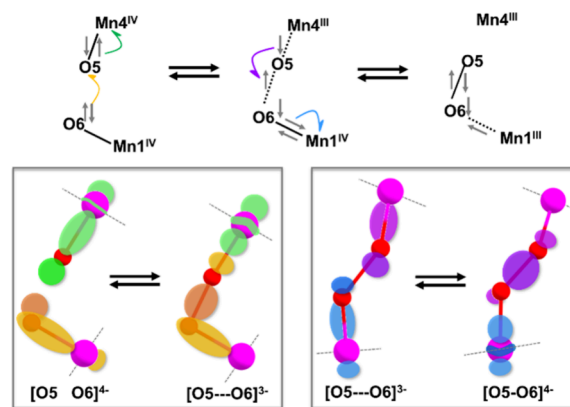
Figure 5. Alternative mechanism of O−O bond formation with representations of important molecular orbitals. Reprinted with permission from refs 106, 107. Copyright 2018 American Chemical Society, Copyright 2020 American Chemical Society.

electrons to Mn1 and Mn4 from the coordinated oxo groups, i.e., O6 and O5, respectively, that results in an unoccupied σ_{2p}^* orbital which streamlines low barrier nascent O−O bond formation. Furthermore, the relatively short O−O bond is predicted to reflect a dynamic equilibrium model. The authors further emphasize that O−O bond forming event in the S_4 state requires the oxidation of Mn^{IV} to Mn^V or Mn^{IV}-oxyl. Such transformation is feasible at an electrode potential of +2.7 to +4.7 V in an acidic aqueous solution.[110] However, the electrode potential offered by the Y_z^{ox}/Y_z is merely +1.1 V,[111] suggesting the requirement of a site-induced metal electrode potential to facilitate Mn^{IV} oxidation by Y_z^{ox}. Since no evidence for such oxidation is observed at S_4 state,[112] O'Malley et al. are of the opinion that equilibriums shown in Figure 5 results in electron transfer from the OEC to Y_z^{ox}, facilitating formation of peroxo[110] and superoxo linkages, that ultimately releases triplet oxygen to instigate a new cycle.[113] However, the peroxo intermediates in the S_3 state are criticized of being minor species and do not hold consistency with spectroscopic data.[114] Undoubtedly, better clarity is required on the final steps of covalent O−O linkage formation, release of O_2 and further water binding events during the transition from S_3 to S_0 in the Kok cycle.[103,104] Nevertheless, knowledge of the biological water oxidation catalyst provides crucial lessons to improve designing of artificial water oxidation catalysts that we discuss below.

2.4. Insights for Biomimetic Water Oxidation.

Increasing efforts to understand the operation of the water oxidizing catalyst in nature have parallelly instigated the field of biomimetic approaches for designing homogeneous and heterogeneous devices for artificial water oxidation. We summarize here some of the crucial insights obtained from photosynthetic water oxidation that should prove beneficial for the development of novel WOC.[31,67,115]

2.4.1. The Necessity of Multinuclear Environment for Four-Electron Water Oxidation Mechanism.

The fact that water oxidation in PSII requires release of four electrons (Figure 2a) to create covalent O−O linkage is challenging in the presence of mono- or di- nuclear motifs, since each of the metal ions provide catalytic support by minute changes in their electronic structure, and thereby facilitating alteration of the

charge and multiplicity of the entire cluster. It further emphasizes on the feasibility of multielectron transfer processes by utilization of metallic clusters, which can also serve as redox reservoirs[116−118] and transfer electrons to the substrates on need. It is expected that an ideal WOC would host multiple electrons without noticeable structural adjustments, similar to the biological water oxidizing enzyme where three out of four Mn ions participate in the redox chemistry.[105] Thereby, it makes tetra- or polynuclear metallic sites as ideal hotspots to perform multioxidation reactions and emerge as promising functional models to oxidize water.[119]

2.4.2. Spin-Flipping Reactions. It is important to note that 3d transition metals demonstrate an array of oxidation states with variable spin multiplicities, due to spin flipping mechanism achievable at low energetic expense, and displaying diversified chemistry.[121,122] Biological water oxidation is also hypothesized to follow the spin-flip mechanism. During direct oxo-oxyl coupling mechanism (Figure 6a), the predicted
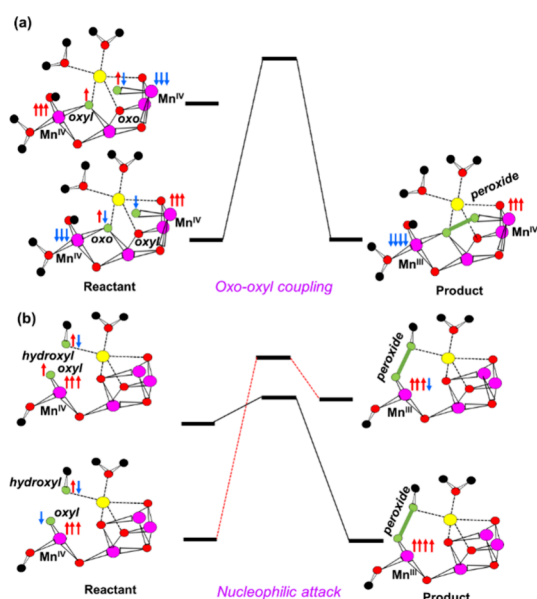
Figure 6. Electronic structure during O−O bond formation in PSII as predicted from computational studies for (a) direct oxo-oxyl coupling and (b) nucleophilic attack mechanism. Reprinted with permission from ref 120. Copyright 2013 American Chemical Society.

barrier is very low (11.3 kcal/mol).[93,123] Siegbahn reasoned that such a low barrier is observed due to antiferromagnetic interaction between the high spin Mn^{IV} (up spin) and oxygen radical (down spin) with another high spin Mn^{IV} (down spin)-oxo that leads to the reduction of the second metal center by one antiparallel spin electron (Figure 6a). Thus, a smooth transition of electrons can take place from one bond to another without any spin-crossing to generate the peroxide product. This also reiterates the necessity of greater than one Mn center for feasible O−O bond formation. However, for the nucleophilic attack, electron transfer from the closed-shell water or hydroxyl ligand requires the high spin Mn^{IV} and the radical oxygen to have all parallel spins. This is only possible on spin-flip crossing on the reactant side (Figure 6b), which leads to a higher barrier. Thereby, design of novel catalysts should utilize this strategy and biomimetic models should judiciously follow the spin-balance rule to achieve similar efficiency.

2.4.3. Ca^{2+} and $Cl^{−}$ Ions Are Essential in Nature's Water Oxidation Reaction. As already discussed in section 2.2, several dicationic and tricationic metal ions have been explored to occupy Ca^{2+} site in the OEC. However, only Sr^{2+} was found to functionally compete with Ca^{2+}. In addition, the possibility of a nucleophilic attack from a Lewis acidic Ca^{2+} bound hydroxide or a water molecule on an electrophilic high-valent manganese-oxo group has also been postulated.[124−126] Interestingly, X-band and Q-band EPR[114] and Mn ENDOR spectroscopic studies indicate that the electronic structure of the OEC remains unaltered on Ca^{2+} exclusion which suggests that it could have functions during coupled electron−proton relays, rather than providing structural integrity. However, recent studies also indicate Ca^{2+} to critically bound the substrate water through a Mn−O−Ca bridge and provide thermal stability to the water oxidizing cluster in PSII. In addition, chloride ions are postulated to have roles in proton transfer channels and to balance the charge developed due to amino acid residues. Hence, it is imperative to consider the crucial roles of Lewis acidic earth abundant metal centers like Ca^{2+} and proton-relay promoting $Cl^{−}$ ions in innovative designs and strategic assemblage of artificial models for the water oxidation process.

2.4.4. Amino Acid Side Chains and Extended H-Bond Networks. Amino acid residues proximal to the manganese−calcium cluster are important to maintain charge balance and electron/proton channels. The redox potential for oxidation of water is significantly decreased during proton transfer steps if the releasing protons are bound through H-bonding.[70] Indeed, it has been observed experimentally that H-bonded water molecules have profound role during catalytic water oxidation.[127] Notably, molecular dynamics simulations with crystal structures of photosystem II reveal a series of hydrogen-bond wires, starting from the Mn cluster, and extending toward the Cl1 and O4 channels.[36] Such wires are believed to carry out proton transfer in the PSII networks.[36,128,129] In fact, it is crucial to take notice of the secondary coordination sphere and the prolonged H-bonding network of the OEC while designing synthetic catalysts. The amino acid residue containing polypeptides can be replaced by judicious choice of organic and inorganic groups providing appropriate biomimetic local coordination. However, many of the peripheral polypeptides in PSII are utilized for binding antenna pigments and assembling the reaction center with the O_2 evolution component.[130−132] Importantly, deletion mutagenesis that selectively removes peripheral polypeptides to make PSII core complexes indicate higher specific rate of O_2 evolution due to smaller antenna size.[130]

3. MOLECULAR CATALYSTS

Identification of an efficient water-oxidation catalyst to facilitate hydrogen generation has escalated in the past few decades, resulting in the development of homogeneous molecular catalysts, primarily made up of ruthenium, iridium, and manganese.[60] Pioneering work by Meyer and co-workers in 1982 led to the development of the coveted blue dimer complex,[133] which instigated the development of molecular devices for artificial photosynthesis. This led to the synthesis of a significant number of mononuclear and polynuclear transition metal containing coordination complexes, capable of water splitting reactions at alkaline pH, by modifying the ligand geometry and the central transition metal, with varied oxidation and spin states, in order to achieve desired redox

features during artificial water oxidation.[4,18] However, most of the synthesized complexes suffer from premature degradation in solution, leading to the deposition of metallic oxides on the electrodes, which have less favorable catalytic activity, compared to their molecular analogues.[4] This uncertainty in long-term stability of molecular catalysts for water oxidation led to a decline in their exploration in the recent years. While a perspective on metallic oxides is out of scope of this review, we focus on notable developments of transition metal containing molecular catalysts in this section with an objective to understand the evolution of atom-efficient molecular water oxidation catalysts, functionally built up of insights from biological oxygen releasing mechanism. Special focus has been given to highlight the fascinating intrinsic catalytic activities of these molecules that augment their possibility for hetero-genization in supramolecular and hybrid artificial (photo/electro) catalytic devices.[18]

The so-called blue dimer, which is actually *cis,cis*-$[Ru^{III}(bpy)_2(H_2O)]_2(\mu\text{-}O)^{4+}$ ion (bpy = 2,2′-bipyridine), highlighted the role of proton coupled electron transfer (PCET) processes during activation of water.[134] The library of WOCs developed after it also emphasized on the crucial role of PCET.[4] Since water oxidation involves 4 H^+/4 e^-, it suggests that the catalyst should consists of metals with low-lying vacant *d*-block to accommodate the electrons released from water to form the O_2 molecule. This naturally implies easy accessibility of high oxidation state on the metal center, promoted by the associated ligand. Notably, successive electron transfer (ET) processes results in highly charged intermediates, which would resist further electron removal, and hence become unsuitable for oxidation. Alternatively, on PCET the desired oxidation state on the metal can be attained at low energetic expense. Furthermore, in such cases, the pK_a of the water bound to the metal is changed, resulting in a feasible transformation to the hydroxo or oxo unit.[60] The redox-noninnocence or electron releasing power of the ligand on application of suitable photochemical, electrochemical or thermal energy is increased subsequently on going from aqua, to hydroxo to oxo coordination, thus facilitating the otherwise challenging multielectron oxidation. Hence, an aqua ligand or a vacant coordination site is imperative to generate the metal-oxo group which ultimately leads to the crucial O−O coupling. Furthermore, to rationally design a successful WOC, the choice of ligand and the additional substituents such as electron donating and withdrawing groups also play a crucial role. Additionally, the ligand should be structurally and electronically robust to resist solvent exchange in aqueous condition. Moreover, the overall complex should meet the desired solubility under the experimental conditions, by incorporation of additional functionalities in the ligand framework and enhancing the possibility of its anchorage on the working electrodes. Lately, noninnocent ligands such as semiquinones[135] and mox[4−] $(N^1,N^{1'}\text{-}(1,2\text{-phenylene})bis(N^2\text{-}$methyloxalamide)[136−138] are found to display ligand based electron transfers facilitating water oxidation through metal−ligand cooperativity in ruthenium and copper complexes, respectively.

3.1. Mechanism of Water Oxidation. As mentioned earlier in this section and prior revelation of the biological oxygen evolution mechanism (Figure 4 and Scheme 2), to carry out water oxidation, it is imperative for the molecular catalyst to accommodate multiple positive charges and generate a high valent metal-oxo/oxyl species. It is generally

achieved starting from a coordinatively unsaturated metal complex which host the substrate aqua ligand. Scheme 3 shows

Scheme 3. Mechanism of O−O Bond Formation through Water Nucleophilic Attack (WNA) (left, red) and Interaction between Two M−O Moieties (I2M) (right, blue)
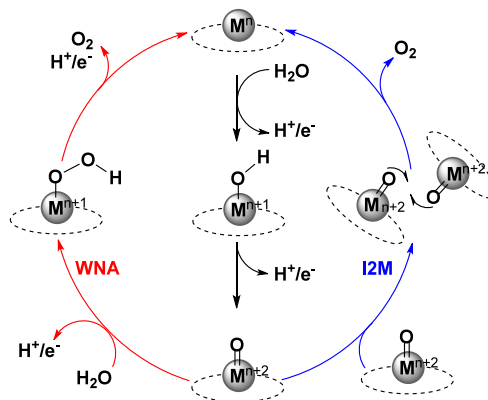
Reprinted with permission from ref 139. Copyright 2017 John Wiley and Sons.

the generation of the metal-oxo species undertaking two consecutive PCET pathways. Thereby two different conduits are followed to pursue O−O bond formation in the subsequent steps based on the nature of this *in situ* developed high-valent metal-oxo intermediate: (a) water nucleophilic attack (WNA) and (b) interaction between two M=O units (I2M). In the WNA mechanism, one solvent water molecule acts as the nucleophile and attacks the sufficiently electrophilic M=O moiety, resulting in the hydroperoxo O−O bond linkage (M-OOH) on top of the metal center. The O−O bond is a manifestation of the interaction between the HOMO of the second H_2O molecule and the LUMO of the metal-oxo group. Consequently, cleavage of the M−O bond and release of O_2 leads to a precatalytic reduced metal complex. In the I2M mechanism, the oxygen on the M=O unit develops radical character. Hence, the O−O coupling takes place between two high spin radical intermediates, either in an intra- or intermolecular fashion, leading to an M−O−O−M moiety. Subsequent oxidation and O_2 evolution from this transient intermediate deliver the starting complex (Scheme 3).

Notably, either of the two conduits pursued in Scheme 3 is largely dependent on the over potential and the concentration of *in situ* generated crucial intermediates. Earlier it has been reported that each of the PCET processes is associated with $\Delta G = 1.23$ kcal/mol. Hence, for the second and third PCET, the energetic requirements are 2.46 and 3.69 eV, respectively.[139] However, the I2M mechanism lacks the third PCET step, thus being favored at low over potential situation As pointed out by Reek and co-workers, a minimal over potential of about 0.3 eV is a fundamental requirement of WNA over radical oxo coupling via I2M.[139] Presumably, the energetic build up is due to the formation of the highly unstable metal-hydroperoxide (M−O−O−H) intermediate, which is absent in the I2M mechanism. Hence, comparing the energetic requirement of M-OOH and M−OH in WNA is incorrect.[139] Rather, a scaling relationship for the binding energies of M−OH and M=O species should be followed, such as

$$\Delta G_{M-OH} = 0.5 \times \Delta G_{M=O} + K_{(O,OH)} \qquad (3)$$

where $K_{(O,OH)}$ is a constant depending on the materials considered. The factor 0.5 indicate that O group binds through a double bond and OH group binds through a single bond toward the metal. Notably, for truly radical-oxo species, the M=O double bond character is lowered.[139] Nevertheless, for rational design of catalysts, the I2M mechanism is preferred, which is primarily facilitated by the concentration of the *in situ* developed metal-oxo species. Further, intramolecular coupling of two M=O units in a binuclear set up is often found to be less efficient than the mononuclear paths, due to the lack of an optimum metal−metal distance.[59]

3.2. Ruthenium Catalysts.
Meyer's blue-dimer (**1**, Figure 7) is the first well-characterized and extensively studied
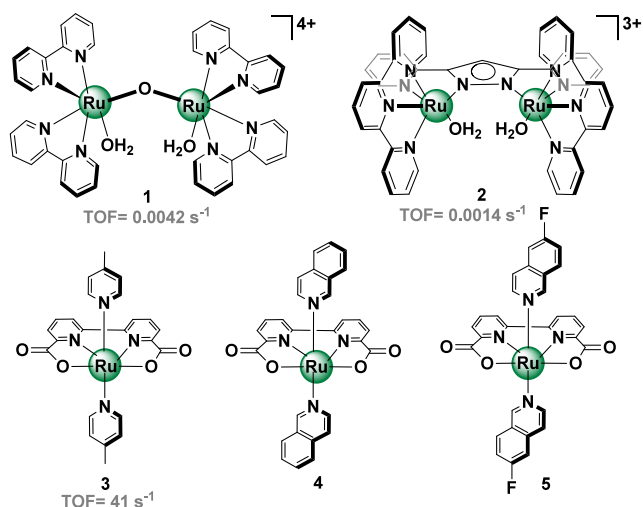
Figure 7. Molecular structures of Ru-based water oxidation catalysts.[133,140−143]

WOC.[133] It gained significant attention due to its unprecedented ability to release O_2 in the presence of a sacrificial oxidant, Ce(IV). It consists of two pseudo-octahedral Ru(III) centers coordinated to a near-linear bridging μ-oxo ligand and coupled to two bipyridine groups in *cis* fashion and one aqua group on the sixth coordination site. Although initial cyclic voltammetry studies from the Meyer group were inconclusive about the protonation states of the involved water substrate and the role of the μ-O ligand in oxidizing it,[133] later reports highlighted on the pH-dependency of this catalyst.[144] Furthermore, in spite of having reasonable catalytic activity with turnover number (TON) of 13 and turnover frequency of 4.2×10^{-3} s^{-1},[133,145,146] the deactivation of **1** due to anion coordination instead of aquation impedes its utilization in technological advancement.[147] Nevertheless, detailed electrochemical, spectroscopic and quantum mechanical studies in the last four decades have unfolded comprehensive understanding on the physical properties and chemical reactivity of **1**,[148,149] that provides a qualitative landscape of catalyst evolution and rational design of robust and efficient catalysts.

Extensive mechanistic investigations of **1** based on redox states, undertaken by Hurst and others,[148−150] indicated that the oxygen evolving complex consists of Ru^{V}Ru^V oxidation state. To rationalize this observation, it is believed that at the onset $[(H_2O)Ru^{III}(bpy)_2(\mu\text{-}O)Ru^{III}(bpy)_2(OH_2)]^{4+}$ releases one H$^+$ and one e$^-$ at 0.79 V (against NHE) to generate

$[(H_2O)Ru^{III}(bpy)_2(\mu\text{-}O)Ru^{IV}(bpy)_2(OH)]^{4+}$.[15] This is followed by further oxidation of 3H$^+$ and 3e$^-$ simultaneously at an energetic expense of 1.22 V to facilitate the formation of the catalytically active species, $[(O)Ru^V(bpy)_2(\mu\text{-}O)\text{-}Ru^V(bpy)_2(O)]^{4+}$.[15] Hence, the catalyst undergoes oxidation of a total of 4H$^+$ and 4e$^-$ requisite for oxidizing water to dioxygen, particularly displaying 2e$^-$/2H$^+$ oxidation at each Ru=O redox centers, due to strategic disposition of two metal centers by a μ-O bridging ligand. Moreover, in order to accommodate oxidation state of Ru beyond + III, it is hypothesized that this active species remains in equilibrium with $[(\bullet O)Ru^{IV}(bpy)_2(\mu\text{-}O)Ru^{IV}(bpy)_2(O\bullet)]^{4+}$, imparting oxyl character to the terminal O^{2-} moieties.[15,151] Furthermore, the crucial O−O coupling step has been probed actively by labeling experiments. Initial labeling experiments of $[(H_2^{18}O)\text{-}Ru^{III}(bpy)_2(\mu\text{-}O)Ru^{III}(bpy)_2(^{18}OH_2)]^{4+}$ conducted with $H_2^{16}O$ in 0.1 M CF$_3$SO$_3$H and appropriate quantity of Ce(IV) resulted in ~13% $^{18}O^{18}O$.[150] This highlighted the possibility of a bimolecular or intramolecular O−O coupling pathway. However, increasing the concentration of CF$_3$SO$_3$H to 0.5 M resulted in comparable amounts of $^{16}O^{18}O$ and $^{16}O^{16}O$ with diminished quantity for $^{18}O^{18}O$ product.[150] Observation of an appreciable amount of $^{16}O^{18}O$ product indicated water nucleophilic attack on one of the Ru=O redox sites.

Computed catalytic mechanism of O−O bond formation in **1** by Yang and Baik predicted low-spin weak antiferromagnetic coupling in $[(O)Ru^VORu^V(O)]^{4+}$ due to the mixing of dπ and δ orbitals along the Ru−O−Ru bridge.[151] This energetically relaxed staggered conformer together with an unbound water molecule has been considered as the reference energy state (**a**, Scheme 4). Explicit interaction of the unbound water molecule to the two Ru^V=O cores results in formation of a high-spin antiferromagnetically coupled species (**a***) that displays oxyl radical character due to intramolecular electron transfer. This 2e$^-$ transfer to the Ru centers initiates O−O coupling process by cleavage of the H−OH bond and formation of RuO−OH coupling to generate the hydroperoxo intermediate **b**, through a multisite electron transfer proton transfer (ET/PT). This is the rate-determining step with an estimated barrier of 25.9 kcal/mol. Thereby, sequential events such as proton transfer/ electron transfer, disproportionation and intramolecular oxidation formally yields the Ru^{III}/Ru^{IV} superoxo complex **c**. In order to release triplet O_2, an intersystem crossing is predicted that recovers the catalytically inactive core of **1**, i.e., $[(H_2O)Ru^{III}ORu^{III}(OH_2)]^{4+}$ ion. Although this proposed mechanism does not account for the quantitative geometric changes or the role of the orbitals on the μ-oxo bridge on redox processes, it provides a conceptual understanding of the catalysis.

Further studies with geometrical derivatives of the blue dimer suggested that the O^{2-} bridge is not imperative for catalytic activity. Second, it was important to prevent disintegration of the backbone of the μ-O linked ruthenium dimer. This realization ensued development of related ruthenium-based binuclear catalysts with rigid bridging ligands, particularly N containing polypyridyl heterocycles such as in Llobet's $[(H_2O)Ru(tpy)(\mu\text{-}bpp)Ru(tpy)(OH_2)]^{3+}$ (complex **2**, where tpy = 2,2′:6′,2″-terpyridine, bpp = 3,5-bis(2-pyridyl)pyrazolate, Figure 7), which displays a 3-fold faster oxygen evolution reactivity than blue dimer with a TOF of 0.014 s^{-1}.[140] It is believed to follow the intramolecular I2M mechanism due to proximal disposition of two Ru−OH$_2$ groups, rigidly held together by the pyrazolate ligand.

Scheme 4. Proposed Mechanism of O−O Bond Formation in 1 Starting from $[(O)Ru^VORu^V(O)]^{4+}$ as Proposed by Yang and Baik[150,151]a
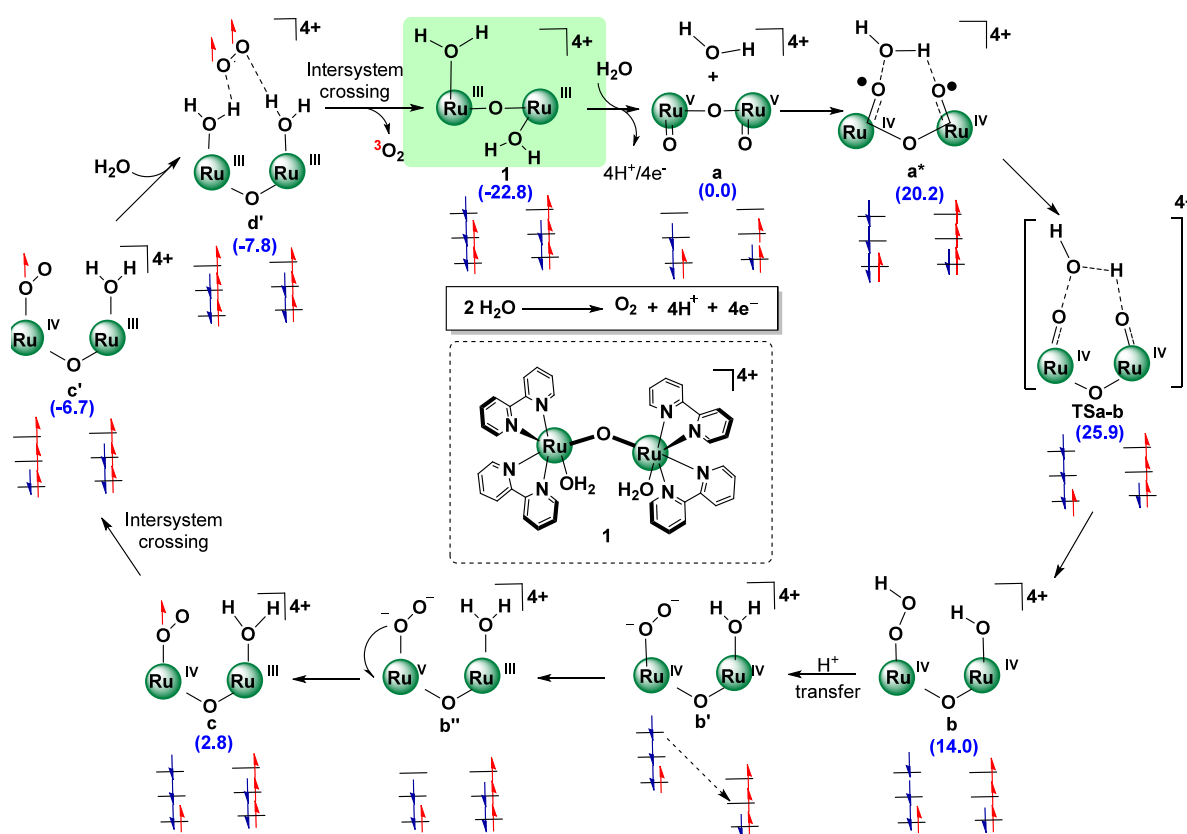
Reprinted with permission from ref 151. Copyright 2006 American Chemical Society. aRelative free energies given in parentheses (blue) are evaluated at B3LYP/cc-pVTZ(-f)/LACV3P(Ru) level of theory.

Siegbahn et al. reinvestigated the mechanism of water oxidation by the artificial water oxidizing Meyer's Blue-dimer (**1**) and Llobet's catalyst (**2**), particularly focusing on the transition state of O−O coupling through interaction of the M−O units or the direct coupling (DC) and attack of a nucleophilic water molecule or the acid−base (AB) mechanism.[152] As shown in Scheme 5, the authors considered all the possible redox and chemical steps in both protonated and nonprotonated species, signifying the removal of only 3H+ in the initial step for the former case, as opposed to conventional removal of 4H+ in the latter case. Careful evaluation revealed that complex **1** favors an AB mechanism over the DC mechanism by 3.9 kcal/mol, through intermediacy of **1a** which consists of a distinct protonated oxygen before the O−O coupling takes place. Interestingly, the initial ET/PT steps starting from complex **1** to intermediate **1a** was predicted to be rate-limiting, with a barrier of 22.0 kcal/mol. However, complex **2** prefers a DC mechanism through a nonprotonated species, **2a** with a comparable rate-limiting O₂ release barrier of 21.9 kcal/mol.

The multimetallic manganese−calcium cubane-like cluster in OEC prescribed the requirement of a multinuclear framework for biomimetic synthetic catalyst to accommodate four redox equivalents during water oxidation. However, preparation of tailor-made binuclear ruthenium catalyst is dwindled with synthetic challenges. Soon it was evident that a single transition metal site was adequate for carrying out necessary electronic transformations. This led to the development of a family of

well-defined single-site Ru(NNN) based promising WOCs by Meyer, Thummel, and others.[154,155] Lately, many efforts have been invested to compensate the pyridyl/bipyridyl/polypyridyl groups by carboxylate-bridging neutral ligands (complexes **3**−**5**, Figure 7), allowing clear perceptions on the mechanisms of water oxidation. This led to the development of more efficient catalysts. In fact, the mononuclear catalyst **3**, Ru(bda)(pic)₂ [bda = 2,2′-bipyridine-6,60-dicarboxylate; pic = 4-methylpyridine] and **4**, Ru(bda)(isoq)₂ [isoq = isoquinoline] are reported to oxidize water through intermolecular I2M interaction of two radical Ru^IV species (Figure 8).[109,121] In case of **3**, a dimer is hypothesized to generate an [HOHOH]⁻ linkage, with an impressive TON of 2000 and a TOF of 41 s⁻¹.[141] The two Ru^IV-oxyl radical species are low-spin doublet entities which can couple either through the energetically degenerate antiferromagnetic or ferromagnetic interactions, leading to a closed-shell peroxide bridging.[156] Interestingly, the involvement of the dimer is experimentally evident from the second-order rate expression for O₂ evolution.[141] Furthermore, the π-stacking interaction between the axial bda ligands and hydrophobic effects of the Ru(IV)-oxyl radical in complex **4** are reported to favor low-barrier O−O coupling processes.[142] Introduction of halogen groups in -bda ligands such as fluorine (complex **5**, Figure 7) further increases the catalytic efficacy of this family of carboxylate ligand containing ruthenium complexes.[143] Indeed, the outstanding activities of the recently reported ruthenium catalysts surely raises hope to develop

Scheme 5. (a) Protonated Direct Coupling (DC) Mechanism for Water Oxidation Using Meyer's Blue-Dimer and (b) Nonprotonated Acid−Base Mechanism for Water Oxidation Using Llobet Catalyst[a]
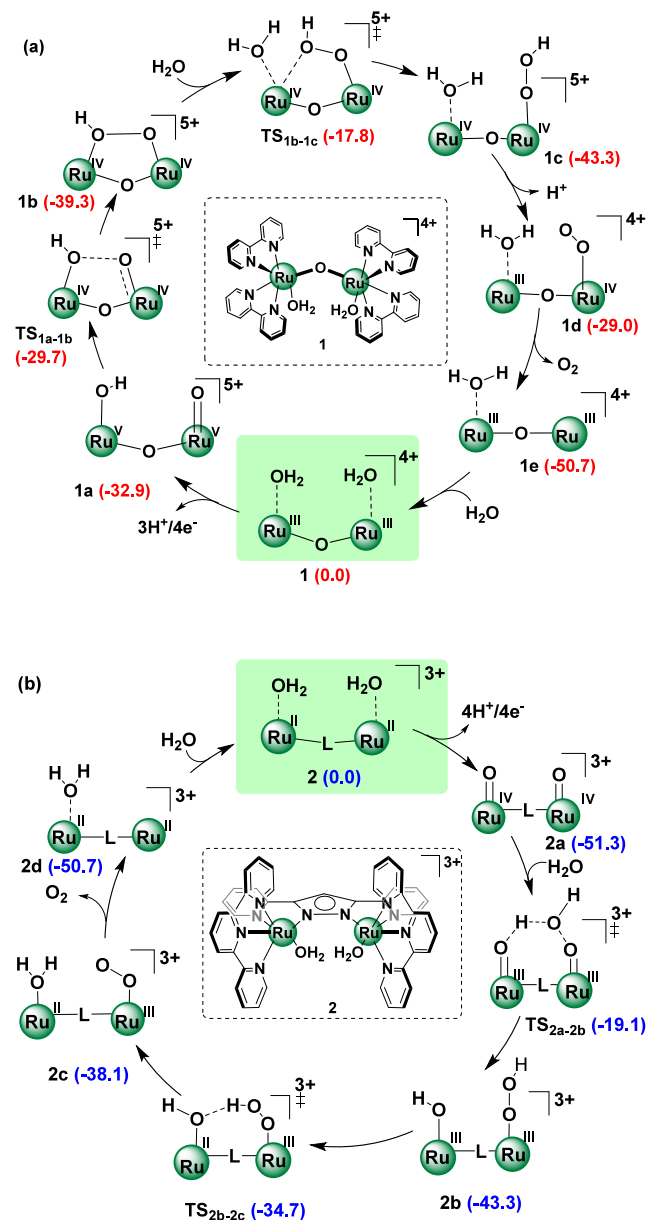
Reprinted with permission from ref 152. Copyright 2011 the Royal Society of Chemistry. [a]Relative free energies given in parentheses (red, blue) are evaluated at B3LYP/CC-PVTZ(-f)/LACV3P level of theory.

Figure 8. Calculated transition state structure of **4:4** dimer O−O bond formation displaying noncovalent face to face $\pi-\pi$ stacked interacting geometric arrangement.[153] Distances shown are in units of Å. Color coding: C (black), H (white), N (blue), O (red), Ru (green).

Figure 9. Molecular structures of Ir-based water oxidation catalysts.[157−160]

novel catalysts with high thermal and electronic stability, for easy incorporation into artificial photosynthetic devices.

3.3. Iridium Catalysts.

The tremendous success of Ru based WOCs inspired the parallel development of iridium containing classic mononuclear and binuclear catalysts. The Bernard group in 2008 first reported the family of cyclometalated iridium complexes, $[Ir(ppy)_2(H_2O)_2]^+$ (ppy = phenylpyridine) (**6**, Figure 9) with two phenyl-pyridine ligations and two coordinated water molecules.[157] This robust complex catalyzes water with a total turnover per unit hour of 2490/168,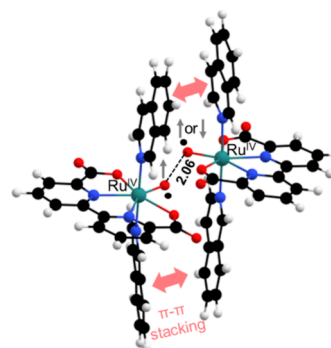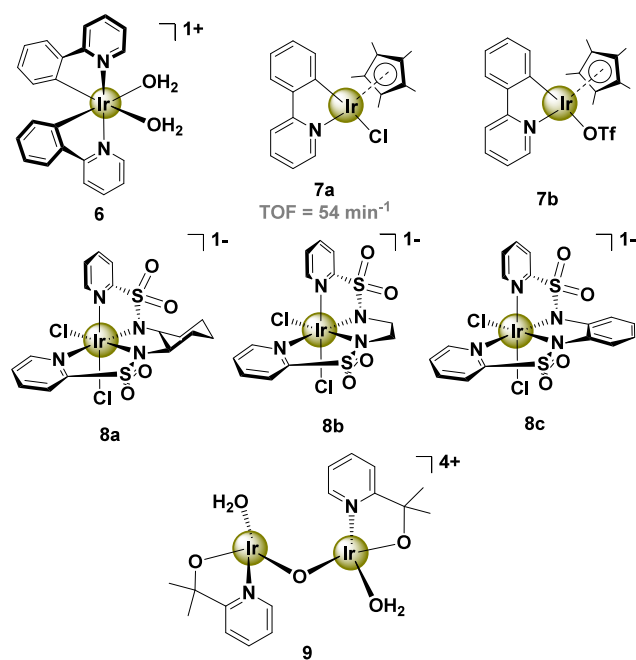 by utilizing Ce^{4+} as the oxidant.[157] The utilization of Ce^{4+} is relevant to the four single electron oxidation process of photosynthesis. Vilella et al. proposed an electrophilic Ir^V-oxo moiety as the active species of complex **6**, under different pH conditions, as shown in Scheme 6. Computational studies at B3LYP/6-311+G(d,p) reveal that the O−O bond formation is instigated by nucleophilic attack of water on the oxo ligand. In this acid−base mechanism, the iridium-oxo group in the $[(ppy)_2Ir^V{=}O(X)]^n$ framework {with X = OH_2 (n = +1), X = OH^- (n = 0), X = O^{2-} (n = −1)} is the Lewis acid accepting two electrons from the attacking water while the associated ligands act as Brønsted base preferably accepting a proton.[161] Hence, the energetic expense for O−O bond formation is mainly dependent on the basicity of the ancillary ligand, apart from the electrophilicity of the target -oxo moiety. An anionic $[(ppy)_2Ir^V{=}(O)_2]^{1-}$ species (Scheme 6, extreme right) consisting of two units of X = O^{2-} has the greatest proton affinity and facilitates O−O bond formation with a barrier of 14.5 kcal/mol, whereas a similar O−O coupling requires a

Scheme 6. Protonation States of Ir^V-Oxo Active Species of Complex 6, $[(ppy)_2Ir^V=O(X)]^n$ {with X = OH$_2$ (n = +1), X = OH$^-$ (n = 0), X = O^{2-} (n = −1)}
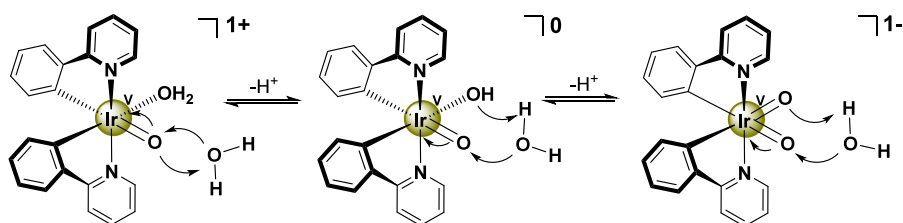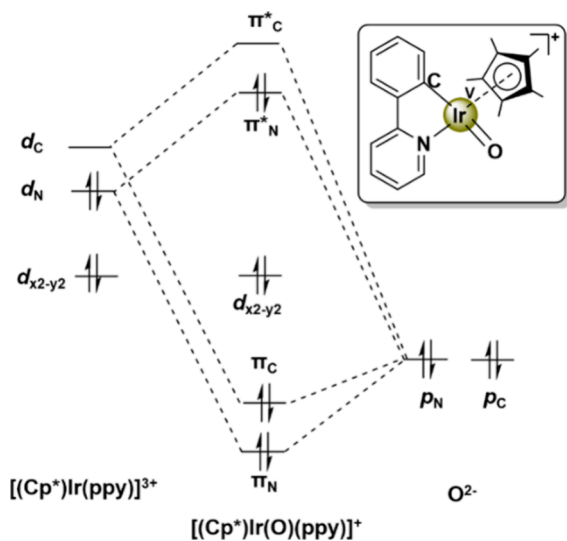

higher barrier when X = OH$^-$ (20.2 kcal/mol, Scheme 6, center) or OH$_2$ (25.9 kcal/mol, Scheme 6, extreme left).

Analysis of the frontier molecular orbitals of structural alternatives of **6** demonstrated mixed valence metal and ligand characterized highest occupied molecular orbitals (HOMOs) due to strong correlation between metal-based d-orbitals and ligand-based π-orbitals.[157] This led to the development of analogous complexes with tunable ligand substitutions, featuring electron withdrawing or electron-donating groups to optimize reactivity and stability. For instance, complex **7a**, $[(Cp^*)Ir^{III}(ppy)Cl]$ (Cp* = pentamethylcyclopentadienyl), which is a member of the family of half-sandwich complexes synthesized by Crabtree and co-workers, demonstrated improved reactivity with an initial TON of 54 and a lifetime of several hours.[162] This indicates the necessity of strongly donating ligands to facilitate smooth accessibility to a high oxidation state on the metal (for, e.g., Ir^V). Electronic structure of the DFT predicted active species of **7b** reveals a pseudo octahedral arrangement of $(t_{2g})^4$ electronic configuration in the metal-based d-orbitals of $[(Cp^*)Ir(ppy)]^+$ which combines with the p-orbitals of O^{2-} ligand (Figure 10). Since the doubly

Figure 10. Molecular orbitals of $[(Cp^*)Ir(O)(ppy)]^+$, i.e., active species of **7b**. Reprinted with permission from ref 158. Copyright 2009 American Chemical Society.

occupied $d_{x^2-y^2}$ orbital does not overlap with any of the O^{2-} p-orbitals and remains essentially nonbonding in nature, metal-based d_N and d_C appropriately oriented toward the -oxo group through the pyridine (N) and the phenyl (C) centers, respectively, develop $d\pi/p\pi$ interactions to distribute six electrons in two bonding (π_N and π_C) and two antibonding molecular orbitals (π_N^* and π_C^*) of $[(Cp^*)Ir(O)(ppy)]^+$

(Figure 10). The doubly occupied π_N^* and unoccupied π_C^* results in a singlet species which is slightly higher in energy than the triplet intermediate (3.7 kcal/mol), where each of the π_N^* and π_C^* are singly occupied. The low-lying antibonding π^* orbitals on the Ir^V=O moiety possess large electrophilicity and have significant contributions from the -oxo group. This electronic configuration thus facilitates O—O coupling via oxo-nucleophilic attack and regenerates the starting Ir^{III} diamagnetic octahedral complex.[162,163]
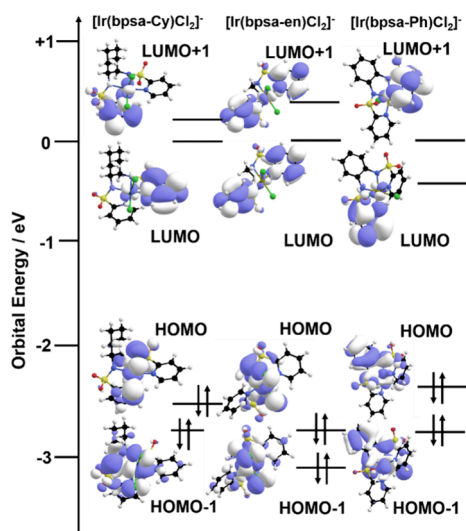
Despite the enhanced catalytic activity of complexes with Cp* ligands, these half-sandwich complexes undergo immature degradation upon oxidation. To improve the stability of the iridium complexes, several alternative strongly σ-donating ligands have been proposed like N-heterocyclic carbene, pyridine amide, pyridinium carbene, etc.[164−166] Recently, a novel family of tetra dentate bpsa {bpsa = bis(pyridine-2-sulfonamide)} ligands have been designed by the Bernhard group which envelops an Ir(III) center to develop an anionic octahedral complex with the two remaining coordination sites occupied by Cl$^-$ ligands (Figure 9).[159] The efficient strong electron donating environment could stabilize high valent metal center and assist catalytic activities under harsh water oxidation conditions. The more rigid ligand frameworks with cyclohexane and phenylene substituents in $[Ir(bpsa-Cy)Cl_2]^-$, (**8a**, Cy = cyclohexane) and $[Ir(bpsa-Ph)Cl_2]^-$ (**8c**, Ph = phenylene) displaying C_1-symmetry exhibit higher catalytic activity with TON values of 1820 and 3540, than the more flexible C_2-symmetric ethylene linker containing $[Ir(bpsa-en)Cl_2]^-$ (**8b**, en = ethylene) complex with a TON value of mere 53.[159] Cyclic voltammetry experiments indicated non-innocence of the sulfonamide group in the electrochemical oxidation process. Frontier orbital diagrams from DFT calculations of **8a**, **b**, and **c** as shown in Figure 11 reveals that the energy of the HOMO for three complexes is in reasonable agreement with the experimentally observed oxidation potential.[159] Careful analysis reveals that the HOMO of **8c** is considerably destabilized as compared to the other two complexes. This indicates involvement of the phenylene spacer in delocalization of the electron cloud in **8c** which presumably favors the oxidation process by stabilizing the high valent metal-oxo intermediate. Furthermore, the HOMO−LUMO energy gap is least for **8c** and highest for **8b**, correlating with their respective catalytic behaviors and further emphasizes on the efficiency of the robust ligand design.[159]

Another strategy in homogeneous water oxidation by iridium containing organometallic complexes involved replacement of the oxidatively degrading Cp* ligand with stable oxidant-resistant chelates that can withstand the harsh water oxidizing conditions and discontinuing the use of sacrificial oxidant like Ce^{4+}. The most intriguing catalytic mixture on the loss of Cp* through oxidative degradation is obtained from the precatalyst, Cp*Ir(pyalk)OH (pyalk = 2-pyridyl-2-propa-

Figure 11. Frontier orbital diagrams of **8a**, **8b**, and **8c** based on DFT calculations at B3LYP/LANL2DZ level of theory. Reprinted with permission from ref 159. Copyright 2016 American Chemical Society.

noate), which results in an extreme blue-colored homogeneous solution.[1] The solution consists of a robust μ-oxo binuclear $[(pyalk)Ir^{IV}-O-Ir^{IV}(pyalk)]$ core (**9**, Figure 9), retaining the pyridyl chelating ligand and exhibiting efficient water oxidation catalysis. Interestingly, the pyalk ligand consists of a $-CMe_2$ unit at the benzylic position which facilitates electron donation to achieve high valent state on Ir as well as resists self-degradation.[160,167−169] Several isomeric forms of **9** were studied using X-ray crystallography, UV−visible spectrum, and computational studies to unravel the probable structure of the homogeneous catalytically active species.[160,168] Since blue coloration is a well-known characteristic of Ir(IV)−O−Ir(IV) species, important absorbance in the visible region (550−750 nm) were studied in details by time-dependent DFT (TD-DFT) calculations at ωB97xd/LANL2TZ(f),6-311G(d,p) level of theory.[160] Ir(IV)-oxo dimers display a combination of nonbonding metal d and antibonding μ-oxo p orbitals in the Ir−O−Ir bridge (Figure 12). Hence the HOMO → LUMO (725.5 nm) and HOMO−1 → LUMO (584.7 nm) electronic transfers in closed-shell-singlet (CSS) and open-shell-singlet (OSS) systems are best described as n → π^* excitations
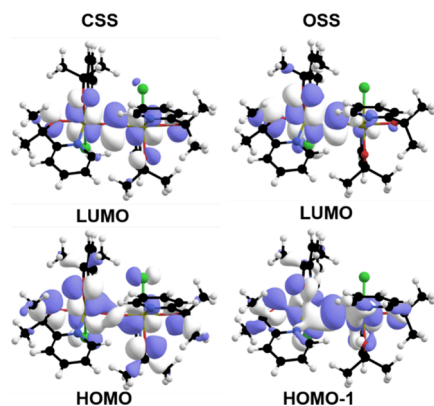
involving a conjugation of Ir d-orbitals and oxygen p-orbitals rather than traditional Laporte forbidden $d \rightarrow d$ transitions. Furthermore, lower-wavelength absorbance at ∼430 nm appears to be typically ligand to metal charge transfer (LMCT) resulting in an absorption band. This clearly suggests that the metal-centered transitions are responsible for the visible spectra and color. However, recent work from Crabtree, Brudvig, and others indicates that these crystallographically identified iridium-oxo dimers are not the active species for oxidation catalysis. To demystify the molecular species for homogeneous catalysis, the authors employed a mixture of binuclear iridium-oxo complexes together with $NaIO_4$ as the oxidant. This resulted in a $Na[Ir(pyalk)Cl_4]$ coordination precursor which exhibits catalytic activity of oxygen evolution comparable to **9**, without the need of a sacrificial oxidant.[168]

One genuine concern regarding iridium-based WOC is their molecular instability. Synthetic molecular iridium complexes undergo oxidative modifications to IrO_x or complete degradation to metal nanoparticles that get deposited on the electrode materials and exhibit high catalytic activity.[20] Hence, it is difficult to distinguish between homogeneity and heterogeneity of the observed catalysis. In fact, the organic linkers might be retained in the heterogeneous material and impart structural and catalytic properties like the molecular analogue. One such example is the MOF-immobilized [Cp*Ir] complex with modified 2-phenylpyridine.[170] However, development of heterogeneous phases from catalytically active molecular scaffolds is a major challenge toward well-defined homogeneity. Recently, Crabtree has discussed several solutions to this heterogeneity problem in a recent review article.[169] Nevertheless, it is important to go beyond the measurement of O_2 evolution in attempts to develop robust molecular iridium catalysts.

3.4. Manganese Catalysts. Inspirations from the elemental description of Mn_4Ca cubane structure in the natural oxygen evolving complex, coupled to high natural abundance, low-cost and extensively rich redox chemistry of manganese, together with the current thrust on identifying catalysts with inexpensive non-noble transition metals streamlined major efforts to synthesize manganese complexes and biomimetic multinuclear clusters relevant to PSII. The fact that the OEC consists of tightly arranged manganese ions resulted in an array of possible biomimetic structural analogues with varied ligand scaffolds, oxidation states and nuclearity as reviewed recently.[21,171] Owing to the structural resemblance with the OEC in PSII, myriads of tetranuclear manganese cubane complexes were explored at the initial stage. These tetranuclear manganese systems feature varied oxidation states such as $Mn(II)_4$, $Mn(III)_3Mn(IV)$, $Mn(IV)_4$, $Mn(III)_2Mn(IV)_2$, and $Mn(IV)_4$ with intriguing architectures.[171] Some of the earlier multinuclear manganese models consisted of tetranuclear manganese adamantane structures with $[Mn^{IV}_4O_6]^{4+}$ aggregates, coordinated to 1,4,7-triazacyclononane ligands, developed by Wieghardt et al.[172] Later a family of manganese adamantane shaped complexes were synthesized from ligand exchange reactions of $[Mn_4O_6(bpea)_4](ClO_4)_4$ with tridentate amine and iminodicarboxylate ligands by Armstrong and others.[173] Dismukes reported a phosphine based mixed valent μ-oxo bridged $Mn(III)_2Mn(IV)_2$ cubane complex,[174] while Vincent et al. synthesized nonplanar butterfly type complexes of the types $[Mn_4(\mu_3-O)_2(\mu-O_2CR)_7(bpy)_2]^{n+}$ (R = Me, Et, Ph) displaying $Mn(II)_2Mn(III)_2$ to $Mn(III)_4$ oxidations.[175] Christou and others reported

Figure 12. Frontier orbital diagrams of **9** based on TD-DFT calculations at ωB97xd/LANL2TZ(f),6-311G** level of theory. CSS = closed shell singlet, OSS = open shell singlet. Reprinted with permission from ref 160. Copyright 2016 American Chemical Society.

a soluble manganese-oxo cluster consisting of 12 Mn centers which performs water oxidation at a very low overpotential (334 mV) and slightly acidic conditions.[116]

Owing to the importance of the calcium ion in the water oxidation carried out by the OEC, specifically in the S_3 state, several manganese—calcium heterometallic cubane compounds resembling the OEC have been developed, featuring a dangling manganese center linked by an oxo bridge.[178] The calcium ion is believed to have a crucial role in the bioassembly of the cluster, solvent association and catalytic activity.[176,179,180] Agapie and co-workers prepared a distinctively cuboidal structural model of the Mn_3Ca—cubane (Figure 13a, extreme
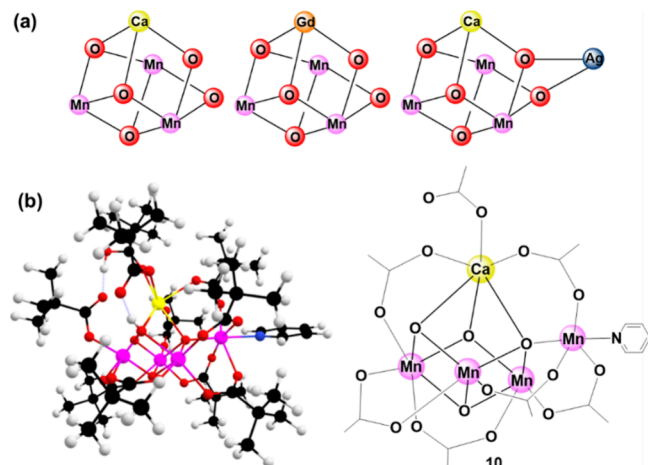

Figure 13. (a) Inorganic core of Mn-based Agapie's heterometallic complexes.[176] (b) Zhang's Mn_3CaO_4—Mn cubane with schematic diagram.[177] Color coding: C (black), H (white), N (blue), O (red), Mn (pink).

left), reminiscent of the subsite in the natural OEC, in an attempt to characterize the potential role of the calcium ion

during attainment of high oxidation states on the manganese centers in the biological heterometallic cluster.[176] Later, the authors replaced the Ca^{2+} ion with heavy metals like Gd^{3+} (Figure 13a, center) and thereafter coordinated a Ag^+ ion (Figure 13a, extreme right) at the fifth site of the parent cluster to prepare topological models of the OEC that display both the cubane core and the dangler transition metal motif in order to provide more detailed response to the overall redox potential of the biological catalyst by these redox inactive ions.[79,176,179,180] Specifically, inclusion of these ions modulate the basicity of the coordinating μ-oxo ligands and exerts a rational strategy for the construction of multinuclear OEC-analogues.

In a recent work, Zhang and co-workers have synthesized a biomimetic Mn_4CaO_4 cubane with a dangling Mn ion (Figure 13b) which has the closest structural and stoichiometric resemblance to the biological OEC.[171,181] As a result of the $Mn(III)_2Mn(IV)_2$ oxidation state of the inorganic core, the cluster illustrates redox properties similar to the S1 state of the OEC, distinctive from other cubane mimics. Furthermore, the complex shows EPR signals at $g \approx 4.9$ and 2.0, similar to the findings for the OEC in the S_2 state.[181] In a theoretical study, Pantazis and co-workers have rationalized the emergence of $g \approx 4.9$ from a $S = 5/2$ ground spin state.[182] However, the authors could not identify any low-spin energetically accessible candidate to elucidate the $g = 2.0$ signal, despite employment of a range of computational techniques including the highly reliable density matrix renormalization group (DMRG) method.[181] Hence, computational studies indicate that the absence of a labile -oxo bridge in the Zhang's model results in the lack of a valence isomer, unlike the characteristic electronic structure of the OEC in the S_2 state. Nevertheless, Zhang's model provides guidelines for spectroscopic and magnetic properties of the biological cluster in various S-states preceding the O—O bond formation.[182]
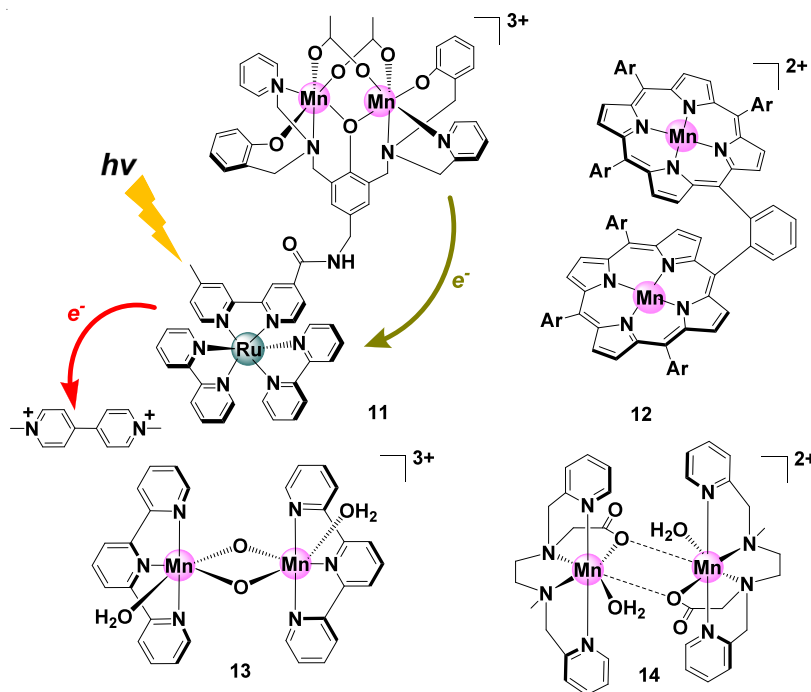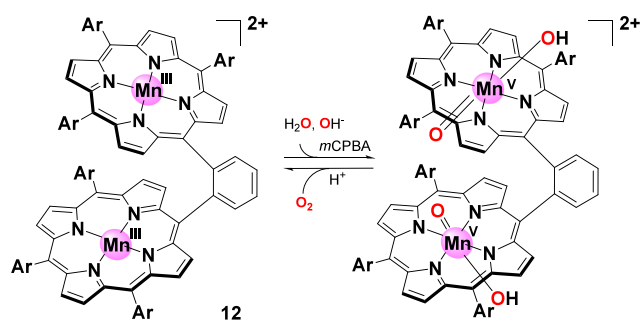

Figure 14. Molecular structures of Mn-based water oxidation catalysts. Ar = $4\text{-}^tBuC_6F_4$, $2,4,6\text{-}(Me)_3C_6H_2$, and C_6F_5.[183,184]

The early structural mimics of the OEC also consisted of myriads of Mn-based dinuclear frameworks with μ-oxo bridges and comprised of nitrogenous bipyridine, terpyridine, phenanthroline or multidentate ligands.[185−187] Although these complexes failed to replicate the elemental structural motif of the tetranuclear Mn−Ca cubane, they provided better understanding on the coordination chemistry of manganese. This ultimately led to the creation and characterization of a series of heterobimetallic redox-active manganese clusters with covalently attached ruthenium sensitizers, such as [Ru-(bpy)$_3$]$^{2+}$ (bpy = bipyridyl) unit by Åkermark and co-workers (11, Figure 14).[183,188] Flash-photolysis led to a sacrificial electron transfer from the ruthenium photosensitizer that created a hole on Ru^{II} and triggered replenishment from the adjacent manganese donor sites. This approach represents a more realistic prototype of a chromophore-WOC assembly carrying out light-induced photoredox events analogous to green plants. EPR measurements further confirmed the generation of Mn^{III} ion in the presence of a photosensitizer array.[188] In addition, it was reported that metal-to-metal displacement and ligand environment are decisive in excited state quenching and intramolecular charge transfer.[188] However, most of these heteronuclear assemblies were subjected to preferential catalyst decomposition over water oxidation.[21]

The early functional models of the OEC, developed by Naruta and co-workers in 1994, consisted of binuclear manganese triphenylporphyrin (TPP) linked via an o-phenylene bridge.[184,189] The complexes consisted of three different aryl substitutions, such as 4-^{t}BuC$_6$F$_4$, 2,4,6-(Me)$_3$C$_6$H$_2$, and C$_6$F$_5$ (12, Figure 14). Out of these three models, Mn-TPP featuring C$_6$F$_5$ exhibited the highest reactivity (TON of 9.2) at the expense of a higher oxidation potential.[184] Mass spectrometric control experiments with H$_2$^{16}O and H$_2$^{18}O revealed that O$_2$ released was in the following ratio, ^{16}O$_2$: ^{16}O^{18}O: ^{18}O$_2$ = 1:2:1 indicating that the evolved dioxygen originated from solvent water. Mechanistic underpinnings demonstrated that the two Mn^{III}−OH units are oxidized to two Mn^V=O units (Scheme 7) which readily transform to peroxo bridging Mn^{IV}−O−O−Mn^{IV} due to convenient spatial disposition of the -oxo groups. Thereby, OH$^-$ attack on the metal centers replace the peroxy moiety and release O$_2$ with the regeneration of the dimeric precursor. This was further confirmed by using $meta$-chloroperoxybenzoic acid (mCPBA) as the oxidant in a later study.[189]

Thereafter, the groups of Crabtree and Brudvig synthesized the dimeric terpyridine complex, [(H$_2$O)(tpy)Mn(μ-O)$_2$Mn-(tpy)(OH$_2$)]$^{3+}$ (13, Figure 14) which catalyzed water oxidation in the presence of chemical oxidants such as potassium oxone (KHSO$_5$) or sodium hypochlorite (NaOCl).[191,192] Careful evaluation of the crystal structure of this complex revealed a mixed valence bis(μ-oxo) Mn(III)−Mn(IV) electronic structure with one aqua ligand dangling on each site. These exchangeable water ligands are crucial during oxidation by NaOCl. A modest catalytic turnover of 4 was observed for O$_2$ evolution from 13. However, UV−vis spectroscopy indicated the formation of permanganate which likely develops due to oxidative decomposition and dissociation of the terpy ligand and precipitation of manganese ions.[191,192] Additionally, consumption of OCl$^-$ in large excess compared to the quantity needed for evolution of O$_2$ further suggested oxidative ligand decomposition. Additionally, isotope labeling studies confirmed that 75% of the evolved O$_2$ originated from solvent water and the rest from OCl$^-$.

Despite the drawbacks concerning the oxidative stability of the ligand moiety, complex 13 is an interesting synthetic functional mimic which enhances the understanding on O$_2$ evolution in photosynthetic water oxidation. Crabtree, Brudvig, and others reported that the rate-limiting step consists of development of a formal Mn^V=O intermediate, which serves as the active component for O−O bond formation.[192] The structural correlation with the OEC due to the μ-oxo linkages bridging the manganese ions led to a similar hypothesis for O−O bond formation in either of the complexes. Later Lundberg and others conducted DFT calculations to investigate the mechanism of water oxidation by 13, focusing primarily on the water activation step and realized that the highly oxidized Mn^V state is not the sole factor for water activation (Figure 15a).[190] The authors proposed that a Mn^{IV}-oxyl radical species is essential to promote O−O bond formation in both model and biological systems. Comparing the energies of different Mn^{IV}−Mn^V reactant complexes displaying varied spin states, the authors predicted a doublet species consisting of a high-spin Mn^{IV} (S = 3/2, unpaired β electrons) oxidation state of the catalytically active manganese ion, antiferromagnetically coupled to the oxyl radical (S = 1/2, unpaired α electron) and the catalytically inactive high-spin Mn^{IV} (S = 3/2, unpaired α electrons) as the most stable magneto-structural conformer (Figure 15b). The calculated barrier for O−O bond formation with water (23 kcal/mol at B3LYP/LACV3P** level of theory) is in well agreement to the experimental estimation.[190−192] Furthermore, calculations on inactive Mn^V=O dimers revealed a singlet oxidation state which turned out to be catalytically inactive and emphasized on the requirement of an electron-deficient radical intermediate for water nucleophilic attack.[190]

To summarize, the proposed mechanism for O$_2$ evolution by 13 facilitated by an oxygen transfer agent (OX) can be hypothesized to constitute of three parallel mechanistic conduits: (a) nucleophilic attack of OX on the terminal putative oxo ligand of Mn^V=O moiety to release O$_2$ (Figure 15a, left gray route), (b) attack of solvent water on the terminal oxo ligand in a similar fashion (Figure 15a, right black route), and (c) comproportionation of the H$_2$O−Mn^{IV}(μ-O)$_2$Mn^{IV}−O$^\bullet$ species with the starting reactant, 13, to deliver two units of catalytically inactive H$_2$O−Mn^{IV}(μ-O)$_2$Mn^{IV}−

Scheme 7. High-Valent Mn^V=O Porphyrin Dimer Generated from a Mn^{III} Precursor of Complex 12^a
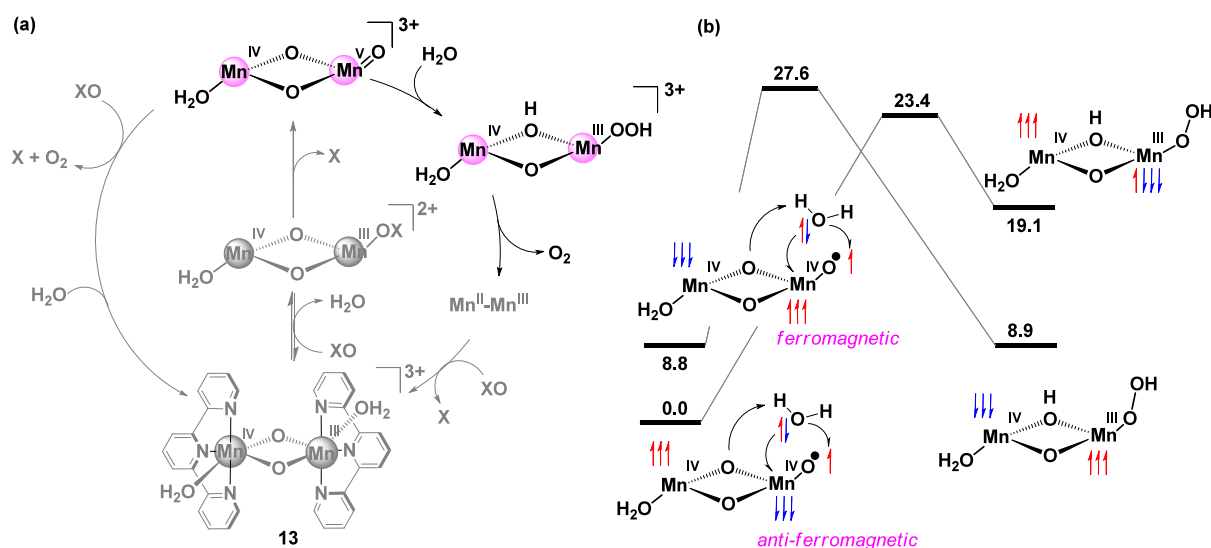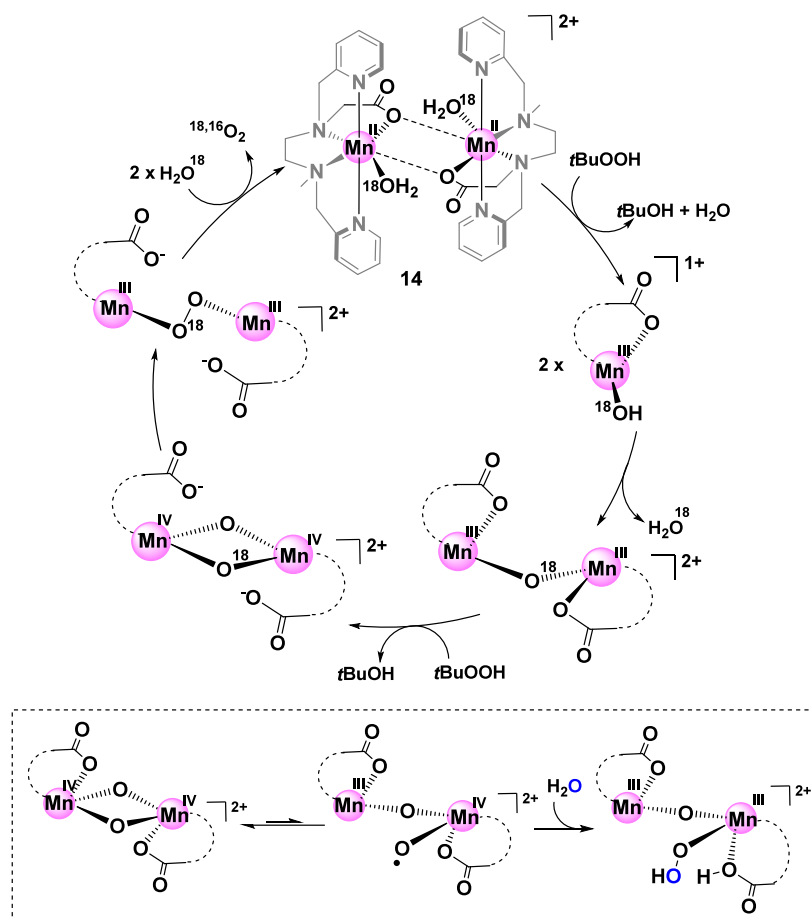

Reprinted with permission from ref 189. Copyright 2003 John Wiley and Sons. ^{a}mCPBA= $meta$-chloroperoxybenzoic acid. Ar = 4-^{t}BuC$_6$F$_4$, 2,4,6-(Me)$_3$C$_6$H$_2$, and C$_6$F$_5$.

Figure 15. (a) Reaction scheme for O_2 evolution by the Mn-terpy dimer complex, **13**, focusing on the O–O bond formation step. (b) Molecular structures of Mn-based water oxidation catalysts. Ar = 4-^{t}BuC$_6$F$_4$, 2,4,6-(Me)$_3$C$_6$H$_2$, and C$_6$F$_5$. Reprinted with permission from ref 190. Copyright 2004 American Chemical Society.

Scheme 8. Catalytic Cycle for Water Oxidation by 14

Reprinted with permission from ref 194. Copyright 2011 the Royal Society of Chemistry.

OH$_2$ binuclear terpyridine complexes (Figure 15a, central gray route) which indicates that water oxidation is a complicated phenomenon and largely depends on specific reaction engineering.[193]

Later, McKenzie and co-workers reported a dinuclear manganese complex **14**, [Mn$^{II}_2$(H$_2$O)$_2$(mcbpen)] (where mcbpen = *N*-methyl-*N'*-carboxy-methyl-*N,N''*-bis(2-pyridylmethyl)ethane-1,2-diamine) (Figure 14) which was

initially developed as a bioinspired mimic of lipoxygenase.[194,195] Interestingly, complex **14** consists of two seven coordinate manganese centers with two carboxylate ligand bridges. EPR and UV−vis spectroscopic studies together with electrochemical methods indicated generation of high-valent compounds on treatment of complex **14** with *tert*-butyl hydroperoxide (TBHP) in acetonitrile or methanol solvent. Presumably, metal−oxygen cleavage leads to monomers of Mn^{III} species which might recombine to form $Mn_2^{III,III}$-μ-oxo or further oxidize in the presence of TBHP to form $Mn_2^{IV,IV}$-bis-μ-oxo (Scheme 8).

Computational studies by McGrady and others considered both the monomer and the dimer constituting pathways.[196] However, the authors proposed that the diamond core $Mn_2^{IV,IV}$-bis-μ-oxo structure is unreactive and reorganizes into a Mn^{III}−$(\mu$-O$)$−$Mn^{IV}O^{\bullet}$ radical intermediate which facilitates O−O bond formation in the presence of water to generate a hydroperoxide intermediate (Scheme 8, inset). This is reminiscent of coupling between Mn(IV)O$^{\bullet}$ with the bridging −Mn(IV)−$(\mu$-O$)$−Mn(IV) through oxo/oxyl radical mechanism in Mn−Ca cubane of PSII.[91,93] Furthermore, computational studies on Mn-mcbpen elaborated the crucial role of the carboxylate moiety in abstracting proton from the residual water. This is in addition to experimental endeavors that suggested the active role of the carboxylate ligand in stabilizing various catalytic species through coordination and noncoordination modes. Such characteristic carboxylate shifts are prevalent in nonheme iron enzymes as well.[197]

3.5. Iron Catalysts. There has been a growing consensus in the organic and bioinorganic fields to harness the chemistry of iron for varied reactions. Low cost and toxicity coupled to high natural abundance of iron, and its ability to attain several high oxidation states to promote fascinating redox chemistry have constituted it to be an ideal element in catalysis. Hence, the family of earth abundant metal containing water oxidation catalysts has further been expanded by inclusion of iron-based molecular catalysts. Albeit, inclusion of iron as a promising water oxidizing agent also relies on specially designed ligand frameworks that can support the high valent requirement. This challenging aspect led to the design of the Fe^{III}-TAML complexes (**15**, Figure 16, TAML= tetra amido macrocyclic
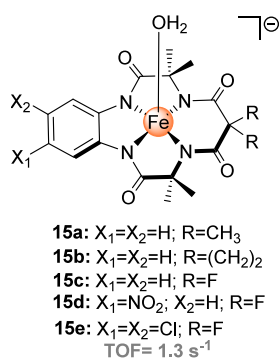

Figure 16. Chemical structures of Fe^{III}-TAML complexes (**15**).[198]

ligand) by Collins and others.[198] Varied ligand scaffolds tuning the substituents led to diversified electronic properties of the Fe^{III}-TAML complexes that were further investigated for water oxidation by ceric ammonium nitrate (CAN) at pH 0.7.[198] Notably, complex **15a** showed no discernible water oxidation activity in acidic medium. However, **15b**−**e** displayed a gradual

increment in the rate of dioxygen liberation, emphasizing on the crucial role of electron-withdrawing substituents in the ligand scaffold, reaching TOF of 1.3 s^{-1} for **15e**. Interestingly, simpler iron precursors like $[Fe(bpy)_3](NO_3)_2$ or $Fe(NO_3)_3$ and others did not show evolution of O_2 in presence or absence of TAML ligand, thus fortifying the unique chemistry of Fe^{III}-TAML complexes.[199]

Quantum chemical calculations proposed two competitive pathways for O−O bond formation by Fe^{III}-TAML complexes. Density functional theory and multireference second-order perturbation theory studies by Cramer and others indicated two proton-coupled electron transfer steps followed by a single electron-transfer from the ligand that generated the putative $TAML^{+\bullet}$−Fe^V−O intermediate, with a formal oxidation state of Fe^{VI} on the metal center.[200] Subsequent O−O bond formation is initiated by a proton relay mechanism consisting of a water nucleophilic attack and three additional water molecules in the local solvation shell, leading to the product hydroperoxide coordinated to iron (Figure 17, **TS$_{WAT}$**).
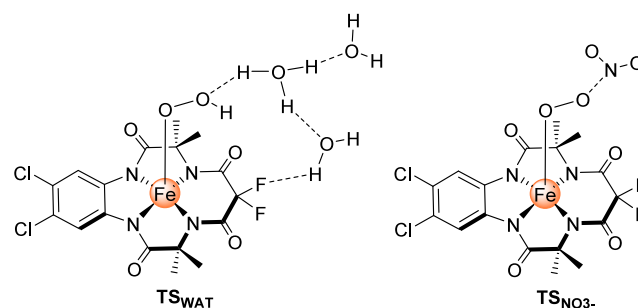

Figure 17. Structures of transition states of **15e** catalyzed O−O bond formation by water (**TS$_{WAT}$**)[200] and nitrate (**TS$_{NO_3-}$**)[201] attacks.

However, the predicted barriers for this step were found to be sensitive to the choice of DFT, ranging from 6.8−35.3 kcal/mol, providing little credence to the direct water attack in the O−O bond formation. Later, Liao et al. revisited this mechanism and proposed an alternative pathway consisting of a nitrate ion attack of CAN on the Fe^V−O intermediate (Figure 17, **TS$_{NO_3-}$**).[201] The authors proposed that B3LYP*-D2 level of theory favored water attack, while M06L functional preferred a nitrate attack. Furthermore, computations on ligand degradation pathways indicated the possibility of both water and nitrate attack on the aromatic ligand scaffold. In fact, the direct water attack on ligand was found to have a lower barrier than that of O−O bond formation according to B3LYP*-D2 energetics.[201] Additionally, the authors proposed that **15a** with methyl groups replacing two fluoride groups leads to a competitive C−H oxidation mechanism, that renders inactivity of the complex for water oxidation.[201] Since the oxygen evolving capability as well as the stability of Fe-TAML complexes are largely dependent on the electronic structure of the derivative complexes, it is therefore essential to maintain a balance between electron donation and withdrawal in the design of modified TAML complexes.[199,202]

Nonheme iron complexes are classic choice for oxygen activation and thereby efficient oxidants for C−H or C═C functionalization. Readily available iron-oxo or hydroperoxo species are potential candidates for O−O bond formation and thereby explored for their catalytic activity toward water oxidation by Fillol and Costas.[203] This resulted in investigations of a broad family of tetra and pentadentate neutral

homogeneous iron containing complexes with varied coordination sites and nitrogenous ligands (shown in Figure 18) such
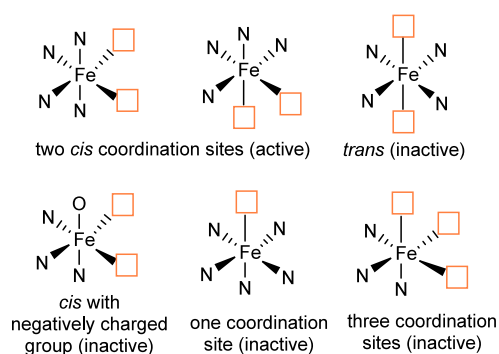
Figure 18. Active and inactive forms of iron based WOCs. Reprinted with permission from ref 199. Copyright 2018 John Wiley and Sons.


TOF = 0.23 s⁻¹ (at pH = 1)
= 0.06 s⁻¹ (at pH = 2)
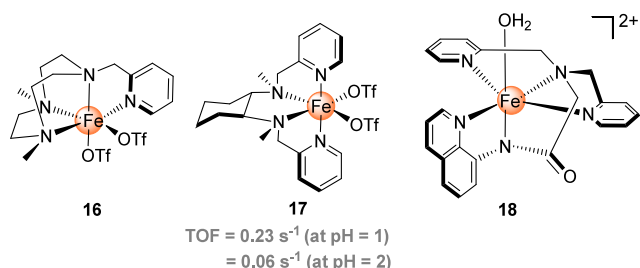
Figure 19. Nonheme iron based molecular water oxidation catalysts.

as $[Fe(OTf)_2(^{Me2}Pytacn)]$ (**16**, Figure 19, where ^{Me2}Pytacn = 1-(2′-pyridylmethyl)-4,7-dimethyl-1,4,7-triazacyclononane)), $[Fe(OTf)_2(mcp)]$ (**17**, Figure 19, where mcp = (N,N'-dimethyl-N,N'-bis(2-pyridylmethyl)-cyclohexane-1,2-diamine)), $[Fe(OTf)_2(bpbp)]$ (bpbp = N,N'-bis(2-pyridylmethyl)-2,2′-bipyrrolidine), $[Fe(OTf)_2(mep)]$ (mep = N,N'-dimethyl-N,N'-bis(2-pyridylmethyl)-ethane-1,2-diamine), $[Fe(OTf)_2(tpa)]$ (tpa = tris(2-pyridylmethyl)amine), $[Fe(OTf)_2(tmc)]$ (tmc = trimethylcyclam), and $[Fe(NCCH_3)(^{Me}Py_2CH\text{-}tacn)](OTf)_2$. Interestingly, position of the coordination site relative to the ligand scaffold modulates the catalytic activity. Catalyst **17** with two free cis coordination sites was found to have higher catalytic activity than the TAML complexes. Utilizing Ce^{IV} or NaIO$_4$ as the oxidant at pH = 1 and 2 resulted in TON as high as >350 and >1000 and TOF of 0.23 s^{-1} and 0.062 s^{-1}, respectively.[203,204] However, $[Fe(OTf)_2(tmc)]$ and Fe(NCCH$_3$)(^{Me}Py$_2$CH-tacn)](OTf)$_2$ having two trans coordination sites and a single coordination site respectively (Figure 18) were found to be inactive toward water oxidation.

To elucidate the reaction mechanism, kinetic studies of model complex **16** were carried out to monitor the evolution of oxygen and the consumption of Ce^{IV} using UV−vis titration.[204] Based on the experimental evidence, the authors proposed that $[Fe(X)_2(L^{N4})]$ type complexes follow a common mechanism (Scheme 9). Mass-spectra measurements indicated formation of a $[Fe^{IV}(O)(OH_2)(L^{N4})]^{2+}$ resting state which is proposed to undergo oxidation by Ce^{IV} to generate a highly reactive Fe^{V}O(OH) species. This postulated that the high-valent intermediate is immediately attacked by a solvent

Scheme 9. Postulated Mechanism for Water Oxidation by Iron Complexes Based on Tetradentate Nitrogen Ligands
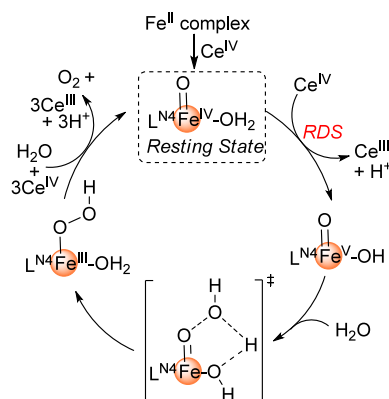
Reprinted with permission from ref 204. Copyright 2013 John Wiley and Sons.

water molecule to undergo the crucial O−O bond formation and liberation of O$_2$ (Scheme 9). Subsequent study by the authors highlighted that structural modification of the ligand backbone is decisive in catalytic activity.[204] While the presence of strongly electron-withdrawing substituents at the para position significantly enhanced the catalytic performance, positioning of fluorine or methyl at the ortho position had adverse effects, suggesting that these substituents restrict coordination of substrate to the iron center.[204]

Recently, Meyer and co-workers have designed a six coordinate mononuclear Fe^{III} complex, $[Fe^{III}(dpaq)(H_2O)]^{2+}$ (**18**, Figure 19); (where dpaq = 2-[bis(pyridine-2-ylmethyl)]-amino-N-quinolin-8-yl-acetamido) for electrocatalytic water oxidation in propylene carbonate.[205] At $E° = 1.58$ V vs NHE, Fe^{III}(OH$_2$)$^{2+}$ is converted to Fe^{V}(O)$^{2+}$ following a PCET mechanism, which reacts with water to give rise to the intermediate peroxide, Fe^{III}(O−OH$_2$)$^{2+}$. Further, the peroxide intermediate undergoes PCET oxidation of d^5 Fe^{III}(OOH)$^{2+}$ to d^3 Fe^{V}(OO)$^{2+}$ for rapid liberation of O$_2$ with simultaneous attack of H$_2$O to regenerate the parent complex **18**.

3.6. Cobalt Catalysts. Inorganic cobalt salts have long been known to oxidize water.[21] However, cobalt salts in the presence of chemical oxidants form cobalt oxides that inhibit the catalytic activity and impose significant hurdles in the path for discovery of cobalt based WOCs. The interest in cobalt-based systems started developing with Nocera's discovery of an *in situ* generated Co^{2+}-phosphate (Co-Pi), characterized by extended X-ray absorption fine structure (EXAFS) studies, that indicated bis-oxo/hydroxo bridged metal subunits organized in higher ordered clusters, working at neutral pH and a low overpotential of 1.25 V vs NHE.[206] This revelation led to several breakthroughs in cobalt based WOCs, analogous to other abundant transition metals like manganese or iron. However, the instability of the Co^{II} metal center inhibited synthesis of robust catalysts, unlike ruthenium or iridium complexes, channeling significant efforts toward design of optimum ligand scaffolds.

In 2011, Berlinguette and co-workers reported a stable cobalt based complex capable of reversible electrochemical water oxidation and coordinated by the unusual 2,6-(bis(bis-2-pyridyl)methoxy-methane)-pyridine (Py5) ligand (**19**, Figure 20).[207] Some of the crucial features that imparts stability to this complex are (1) accommodation of multiple redox levels
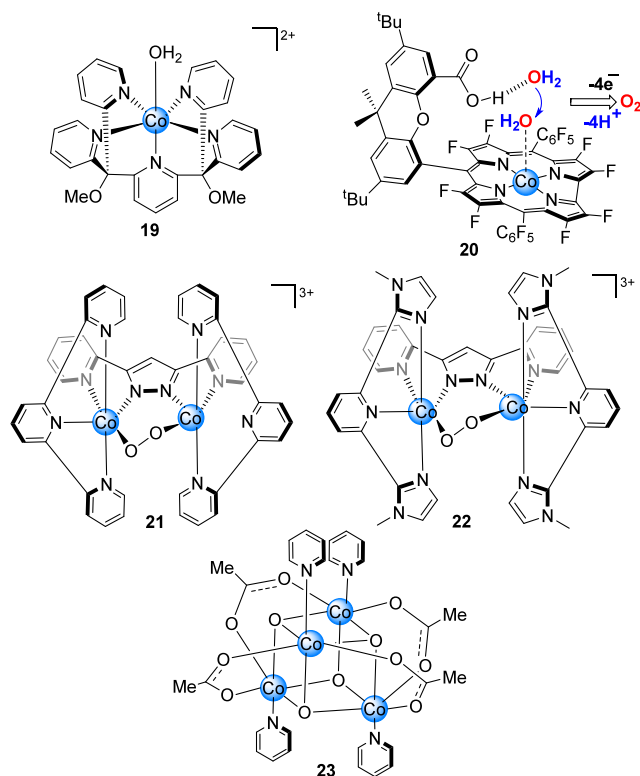
Figure 20. Cobalt based molecular water oxidation catalysts.[207−211]

by the metal ion; (2) oxidatively stable pyridine ligand environment; (3) chelating effect strengthens the Co−N trans ligand and (4) aqua ligand coordinated at the fundamental stage to promote proton coupled electron transfer (PCET). Indeed, this complex exhibited a redox wave at ∼0.75 V vs NHE corresponding to the redox couple $[Co^{III}-OH]^{2+}/$ $[Co^{II}-OH_2]^{2+}$. The pH dependency of this couple is evident from a modification of the signal to an extent of −59 mV for each pH unit, until pH = 11.7, which furthermore solidifies the possibility of a PCET for the initial step (Scheme 10).

Scheme 10. Proposed Mechanism for Water Oxidation Catalyzed by $[(Py5)Co-OH_2]$ (19)
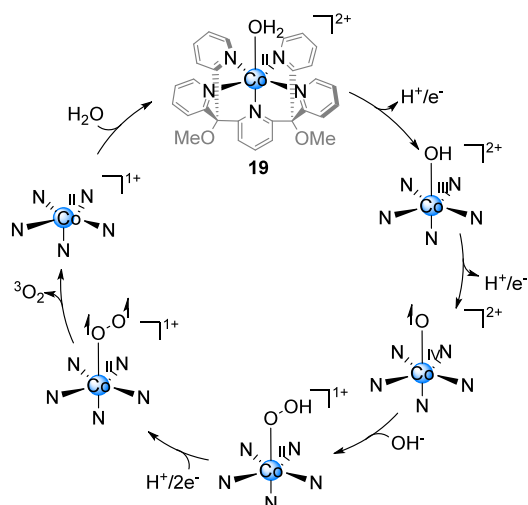
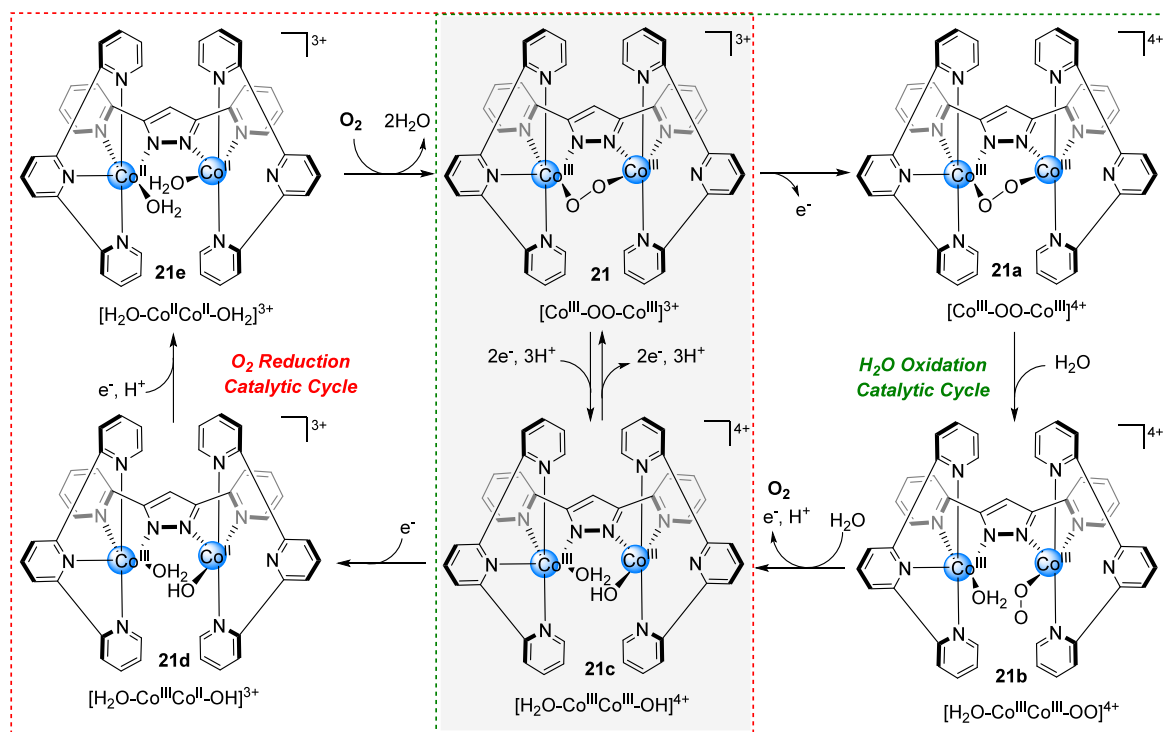Reprinted with permission from ref 212. Copyright 2015 John Wiley and Sons.

Apparently, the water ligand facilitates access to high oxidation states through PCET at low redox potentials.[207] A subsequent pH independent redox wave at 1.40 V vs NHE and pH = 7.6−10.3 demonstrated single electron transfer involving the $[Co^{IV}-OH]^{3+}/[Co^{III}-OH]^{2+}$ couple. This was followed by a large increment in the current density that signified oxidation of water. However, at pH > 10.3, the redox event shifts toward a PCET process of the $[Co^{IV}=O]^{2+}/[Co^{III}-OH]^{2+}$ couple. This results in a nucleophilic attack of water or OH⁻ on the Co^{IV}-oxo intermediate (Scheme 10).

Baik and co-workers have recently studied the mechanism of Co-Py5 (complex **19**) with the help of quantum chemical models.[212] The authors conducted extensive electronic structure analysis to identify the characteristics of the Co^{IV}−oxyl resting state. It was found to feature an energetically stable intermediate-spin quartet state, instead of the low-spin doublet state. Furthermore, significant spin polarization of the terminal oxygen predicted an intramolecular electron transfer from O → M. Analysis of the calculated spin density postulated the resting state to be a biradicaloid species, $[Co^{II}-(^\bullet O^\bullet)]^{2+}$, representing a cobalt-oxene unit, instead of the formally accepted Co^{IV}-oxo. The authors had proposed similar radical species $[Ru^{IV}-O^\bullet]$ for the formally accepted $[Ru^V=O]$ intermediate in blue dimer (**1**, Scheme 5)[148] which was responsible for an oxyl radical attack on the water molecule. Apparently, in first row transition metal containing complexes, high spin configurations are easily accessible due to partially filled 3d orbitals that enhances the oxyl radical character to achieve a biradicaloid oxene moiety featuring a zero-oxidation state on the oxygen center.[207] Perhaps because of this new reactive intermediate, the Co-Py5 complex displayed remarkable catalytic oxidation.

A new route toward macrocyclic redox noninnocent ligand coordinated cobalt complexes has been opened by Nocera and co-workers by investigating the cobalt hangman corrole complexes (**20**, Figure 20), that features a hanging carboxylic acid, fabricating the "hangman cleft".[208] Notably, two water molecules, one of which resides in the primary coordination sphere of the metal and the other held tightly by H-bond network within the secondary coordination sphere, are easily accommodated in the hangman cleft bringing about the possibility of oxygen evolution reaction (OER) (Figure 20). Furthermore, the corrole ligand consists of auxiliary fluorinated phenyl groups (C_6F_5) at the *meso-* positions that are believed to increase the oxidizing power of the framework by ∼0.4 V. Introduction of β-pyrrole fluorination in the porphyrin macrocycle enhances the PCET capability by an additional 0.5−0.6 V.[208]

Representative examples of binuclear Co-based complexes although limited, but are well-characterized structurally and mechanistically with X-ray crystallography and kinetic investigations. One such intriguing example is the dinuclear cobalt-μ-1,2-peroxo complex consisting of bis(2-pyridyl)-3,5-pyrazolate (bpp⁻) and 2,2′;6′:2″-terpyridine (trpy) ligands, $[Co^{III}_2(trpy)_2(\mu\text{-}bpp)(\mu\text{-}1,2\text{-}O_2)]^{3+}$ (**21**, Figure 20), built by Llobet and others to mimic the structural complexity of the Ru-based Blue Dimer, demonstrating thermodynamic stability and kinetic inertness.[209,210] Interestingly, this binuclear cobalt-peroxo complex was initially generated to device 4e⁻ reduction of dioxygen to water.[209] It was facilitated by 1e⁻ reductants such as octamethylferrocene (Me₈Fc) in acidic medium consisting of trifluoroacetic acid (TFA) in acetonitrile solvent at room temperature. Monitoring individual steps in the overall

Scheme 11. Oxygen Reduction and Water Oxidation Catalyzed by Dinuclear $[Co^{III}_2(trpy)_2(\mu\text{-bpp})(\mu\text{-1,2-O}_2)]^{3+}$ Complex, 21[a]

catalytic cycle led to the conclusion that PCET from the Fc derivative to **21** is the rate-limiting step. Fascinated by the possibility of the reverse reaction of water oxidation by this unique peroxide-linkage containing $[Co^{III}\text{-}(O-O)\text{-}Co^{III}]^{3+}$ or analogous superoxido intermediates, practically underexplored in the field of $H_2O \rightarrow O_2$ conversion by first-row transition metal complexes, the authors developed the related binuclear cobalt complex with end-on superoxido moiety and a coordinated water molecule (**21b**, Scheme 11).[213] The shift in vibrational resonance Raman (rR) for O–O bond stretching in the peroxide intermediate **21** at 839 cm^{-1}, 814 and 795 cm^{-1} to 1121 cm^{-1}, 1088 and 1055 cm^{-1} for different oxygen isotopologues such as $^{16}O^{16}O$, $^{17}O^{17}O$, and $^{18}O^{18}O$, respectively, clearly demonstrated the formation of the superoxide linkage in intermediate **21b**.[213] As shown in Scheme 11, it is hypothesized that initial oxidation of **21** with Ce^{IV} leads to the superoxido complex, **21a** $[Co^{III}\text{-}O^\bullet O\text{-}Co^{III}]^{4+}$, which quickly undergoes hydrolysis to the water coordinated intermediate, **21b** $[H_2O\text{-}Co^{III}Co^{III}\text{-}OO^\bullet]^{4+}$. In fact, DFT studies at M11-L/6-311G(2f,d)/SMD(water) level of theory further emphasized that the end-on complex **21b** is ~20 kcal/mol stable than the superoxido-bridged complex, **21a**. Furthermore, an EPR signal at g = 1.98 and DFT calculations of singly occupied molecular orbital and spin-density plots confirmed the presence of the unpaired electron, predicted to mainly localize on the superoxido group. Intermediate **21b** undergoes further oxidation at 1.81 V vs NHE to generate diradical hydroxyl–superoxido intermediate $[HO^\bullet\text{-}Co^{III}Co^{III}\text{-}OO^\bullet]^{4+}$ (proposed with DFT and not shown here), that releases O_2 with concomitant solvent association in intermediate **21c** (Scheme 11). Intermediate **21c** is hypothesized to undergo 2e$^-$/2H$^+$ oxidation to an oxyl–hydroxyl species, $[HO^\bullet\text{-}Co^{III}Co^{III}\text{-}O^\bullet]^{4+}$, which can release one proton to regenerate complex **21**. Alternatively, due to its transient existence, the entropically

disfavored O–O bond formation is highly unlikely in $[HO^\bullet\text{-}Co^{III}Co^{III}\text{-}O^\bullet]^{4+}$. Rather intermediate **21c** is expected to undergo 1e$^-$ reduction and participate in the oxygen reduction cycle. Thus, Scheme 11 demonstrates the beautiful coordination between the oxygen reduction and water oxidation cycles as initiated from the cobalt complex **21**. Further, in order to validate whether molecular catalyst **21** is responsible for water oxidation at pH = 2.1, rather than heterogeneous water oxidation by cobalt-oxide films and nanoparticles, Nam, Llobet, Stahl, and others developed complex **22** (Figure 20) with more electronically rich bis(N-methyl-imidazolyl)-pyridine (Me$_2$bimpy).[210] As expected, the catalytic onset potential in **22** is significantly reduced (at 1.35 and 1.84 V) as compared to **21**.[209]

In the quest for inexpensive polynuclear metal catalysts, Co$_4$O$_4$ cubane (**23**, Figure 20) complex, coordinated by four bidentate acetate and four monodentate pyridine ligands, analogous to the Mn-based oxygen evolving complex, is extensively studied. Dismukes and co-workers described this complex capable of undergoing photochemical and electrochemical oxidation.[214] Photoexcitation was carried out with the employment of $[Ru^{II}(bpy)_3]^{2+}$, in the presence of a sacrificial persulfate acceptor (Scheme 12). With the help of varied spectroscopic techniques including XAS and Kβ RIXS and DFT modeling, Chen et al. characterized the plausible high-valent intermediates during oxygen evolution reaction as a Co(IV) species.[211] This is in line with the previous observation of Co(IV) during OER in thin-film electrodeposited Co-Pi catalyst.[215]

3.7. Copper and Nickel Catalysts. Recently, coordination complexes of copper have garnered attention as catalysts for oxygen evolution reaction and water oxidation, presumably due to their versatility in biological chemistry as copper–oxygen intermediates in reactive cores of several metalloenzymes.[216]

Scheme 12. Proposed Mechanism of Water Splitting by Co₄O₄(OAc)₄(py)₄ Cubane, 23
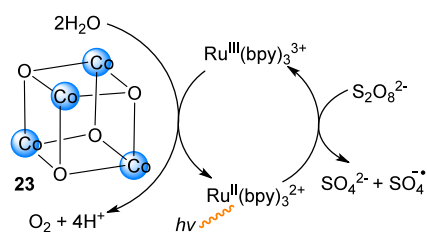
Reprinted with permission from ref 214. Copyright 2011 American Chemical Society.

Hence, mononuclear and multinuclear Cu-oxo complexes can function as intermediates for facile O−O bond formation and exhibit reversal to the starting configurations, promoting OER and WO catalysis under different conditions (Scheme 13). In

Scheme 13. Catalytically Active Cu−O Intermediates for O−O Bond Cleavage in Cu-Enzymes and O−O Bond Formation in Cu-Based Complexes for OER and WO Catalysis, Respectively
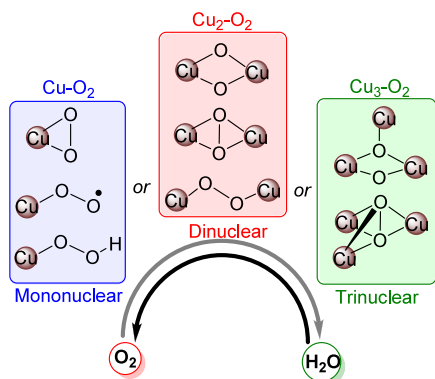
2012, the Mayer group developed the first Cu-based WOC catalyst, $[(bpy)Cu(\mu\text{-}OH)_2]$ (**24**, Figure 21), starting from simple copper salts and bipyridine at high pH.[217] Notably, this water-soluble catalyst demonstrated a very high turnover frequency (TOF) of 100 s^{-1} for electrocatalytic water oxidation at pH > 12, evolution of O₂ being confirmed by electrochemical fluorescence probe. One remarkable characteristic of this catalyst is its ability to reorganize from simple mononuclear neutral complex to a mononuclear positively charged aquated complex, with the intermediacy of a positively charged binuclear hydroxo species (Figure 21). This has been verified by EPR probes which registered a mononuclear bis-hydroxo species, $[(bpy)Cu(\mu\text{-}OH)_2]$, in quartet state at high catalytic pH. However, lowering the pH results in disappearance of the EPR signal, indicating an antiferromagnetically coupled dimeric species, $[(bpy)Cu(\mu\text{-}OH)]_2^{2+}$ (Figure 21). Further lowering to pH 8 produces a new quartet signal in the EPR spectra due to a resultant monomeric aqua-complex, $[(bpy)Cu(H_2O)_2]^{2+}$ (Figure 21), consistent with the hypothesized monomer−dimer equilibrium for this catalyst. Moreover, EPR double integration confirms that at pH 13, the reaction consists predominantly of monomeric μ-hydroxo species, emphasizing on its role as the active catalytic compound during water oxidation. However, necessity of strong alkaline conditions coupled with high overpotential requirement (∼750
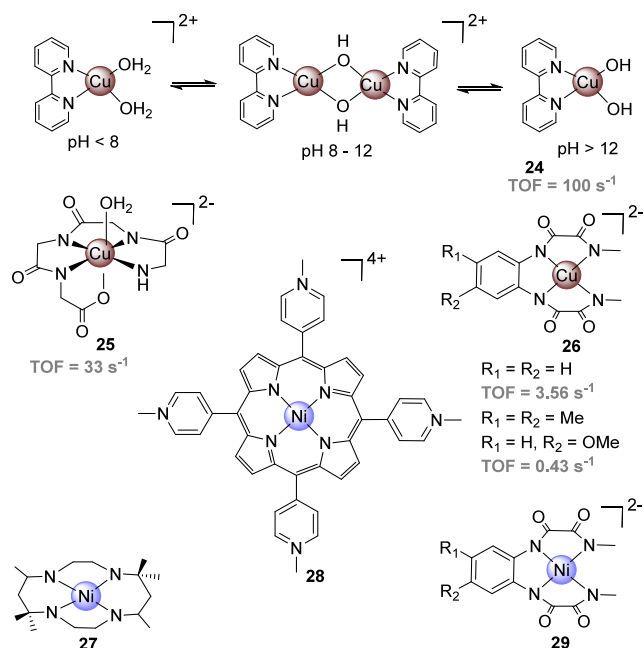
Figure 21. Copper and nickel based molecular water oxidation catalysts.[136,217−221]

mV) provide little credence to the utility of this complex as an efficient, robust, and inexpensive homogeneous WOC, performing conversion of electrical energy to chemical fuels.

To tackle these drawbacks in Mayer's catalyst, Lin et al.,[222] and Papish et al.[223] separately designed 6,6′-dihydroxy-2,2′-bipyridine (6,6′-dhbpy) with 6,6′-dhbpy and Cu(II) in ratios of 1:1 and 2:1, respectively. These structurally modified analogues of Mayer's complex demonstrated electrocatalysis at lowered overpotential of 640 and 477 mV, respectively, for catalytic turnover of dioxygen. However, the pseudo-first-order rate constant for water oxidation turns out to be merely 0.4 and 0.356 s^{-1}, respectively, which is much lower than that reported for Mayer's catalyst.[217,222,223]

Later, Meyer and co-workers reported a triglycylglycine (TGG) macrocyclic ligand based polypeptide Cu(II) complex, $[(TGG^{4-})Cu^{II}-OH_2]^{2-}$ (**25**, Figure 21), which carries out water oxidation at an onset potential of 1.10 V, featuring an overpotential of 520 mV, in alkaline phosphate buffer (pH 11).[218] This complex exhibits exceptional stability and displays a turnover frequency (TOF) of 33 s^{-1} at room temperature. Notably, during water oxidation, the reported k_{Cat} for catalyst **25** is equivalent to 100 s^{-1}, albeit at a higher pH of 13, and well in comparison with that reported for Mayer's bipyridine catalyst.[217]

Cyclic voltammetric and electrochemical kinetic studies provide in-depth insights on the mechanism of the crucial O−O bond formation during water oxidation by catalyst **25** (Scheme 14). As mentioned earlier, the key step in water oxidation by transition metal complexes commonly involve either concomitant O atom transfer to a residual water molecule in the first coordination sphere of the metal followed by proton loss to a sacrificial base or an additional water molecule (Scheme 6), or O−O bond formation in an intramolecular fashion (Scheme 8, Figure 20). Here, a PCET from Cu(II) in $[(TGG^{4-})Cu^{II}-OH_2]^{2-}$ generates a Cu(III)-hydroxo intermediate, $[(TGG^{4-})Cu^{III}-OH]^{2-}$. Thereafter, development of a second oxidation wave linearly dependent

Scheme 14. Proposed Mechanism of Water Oxidation Catalyzed by 25
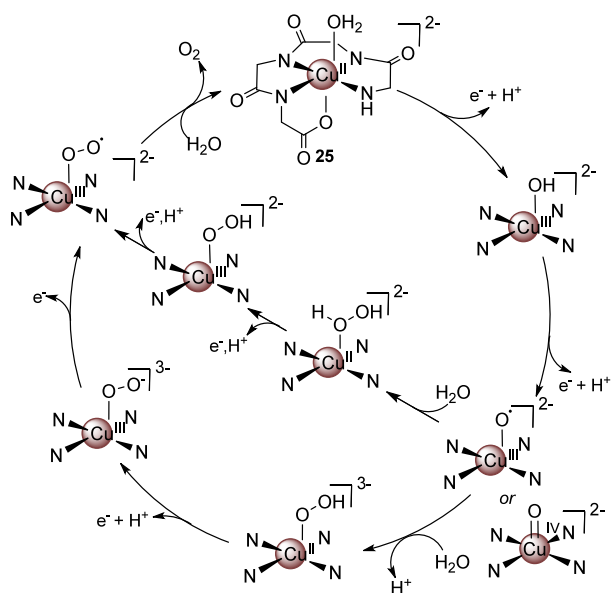
Reprinted with permission from ref 218. Copyright 2013 American Chemical Society.

on the concentration of copper, with enhanced pH dependency and demonstrating irreversibility at a peak potential of 1.32 V, certainly indicate further removal of protons. Hence, the second PCET process is predicted to generate a formal d^7 $[Cu^{IV}-O]^{2-}$ intermediate (Scheme 14). Indeed, this intermediate is reminiscent of a ligand-centered Cu(III)-oxyl radical species by Winkler and Gray[224] and our recent identification of a hydroxyl-radical character on two electron oxidation of complex 26 (Figure 21),[136] i.e., intermediate $[(L1^\bullet)$-$Cu^{II}(OH^\bullet)]^{1-}$, where L1 = o-phenylenebis(oxamidate), obtained by DFT studies and discussed later.[225] The high-valent Cu(IV)-oxo/Cu(III)-oxyl species attacks a water molecule to produce a peroxide linkage containing intermediate, $[Cu^{II}-OOH]^{3-}$ or $[Cu^{II}(HOOH)]^{2-}$. The authors further argue that the irreversibility of the second oxidation wave emphasizes on the fact that $[Cu^{IV}-O]^{2-}$ species undergoes oxidation to the peroxide intermediate with subsequent release of dioxygen and regeneration of $[(TGG^{4-})$-$Cu^{II}-OH_2]^{2-}$, through solvent water coordination, to gain access to the catalytic cycle.[218] Thus, the mechanistic intricacies and favorable kinetic results indicate that bio-relevant anionic polypeptide ligands could be used during water oxidation by non-noble metals, analogous to Ru-polypyridyl based water oxidation.[226] Indeed, this led to the study of water oxidation by two structurally modified Cu(II) complexes with branched-polypeptide ligands.[227] Pap, Szyrwiel, and others show that a Cu(II) complex constituting similar tetrapeptide ligands, for instance H-Gly-dap(H-Gly)-His-NH₂ (where dap = 2,3-diaminopropionic acid), with an equatorial histidine positioning, delivers an improved TOF of 53 s⁻¹ at pH 11, presumably due to a favorable proton−π interaction.[227]

One of the first nickel-based water oxidizing homogeneous molecular catalyst was developed by Lu and co-workers in 2014 (27, Figure 21). Incidentally, this macrocyclic nickel(II) complex, $[Ni(meso\text{-}L)](ClO_4)_2$ (L = 5,5,7,12,12,14-hexamethyl-1,4,8,11-tetraazacyclotetradecane) was found to catalyze

water oxidation at a neutral pH.[219] Furthermore, the O−O bond formation was operative through an intramolecular HO−OH coupling, residing atop a Ni(IV) cis intermediate. DFT calculations indicated the formation of a $[Ni^{III}-(OH^\bullet-OH)]$ radical species in the transition state with a barrier of 24.6 kcal/mol. The cationic nickel(II) complex, Ni(II)-meso-tetrakis(4-N-methylpyridyl)porphyrin, 28 (Figure 21), also exhibit a similar catalytic cycle for water oxidation with the intermediacy of a formal Ni(IV) intermediate $[Por-Ni^{III}-O^\bullet]^{4+}$ (where Por = porphyrin) in neutral aqueous conditions with an onset potential for catalytic wave at merely 1.0 V (pH 7.0).[220] Interestingly, catalyst 28 work under acidic to semialkaline conditions between pH 2−8, without showing any traces of NiOx film deposition which is a usual drawback in designing nickel based molecular catalyst for water oxidation.

Unlike Lai, Cao, and other's Ni(II)-porphyrin complex (28),[188] Llobet's Ni(II)-phenylenebis(oxamidate) complex (29, Figure 21) demonstrates borderline chemistry between homogeneous and heterogeneous water oxidation pathway, ultimately being decomposed to NiOx.[189] Intriguingly, the Ni(II) complex (29) and its aryl substituted analogues are quite distinct from the series of Cu(II)-bis(oxamidate) complexes (26) developed by the same group earlier.[193] While, the Ni(II) complexes face counteraction between water oxidation and molecular species deactivation, the Cu(II) analogues display robust and predominant molecular water oxidation behavior. Our recent theoretical endeavors reveal that a single-electron transfer water nucleophilic attack (SET-WNA) mechanism is operative for water oxidation in both the complexes, whereas the molecular species degradation occurs due to a potential H⁺ attack in acidic medium through proton transfer water electrophilic attack (PT-WEA) pathway (Scheme 15).[189,193] Electronic structure analysis reveals that 2e- oxidation of complexes 29 and 26 generate the anionic intermediates, $[(L1^\bullet)Ni^{III}(OH)]^{1-}$ (29a, Scheme 15) and $[(L1^\bullet)Cu^{II}(OH^\bullet)]^{1-}$ (26a, Scheme 15), respectively. Incidentally, the former intermediate promotes ligand deactivation with a comparatively higher driving force than the latter in an

Scheme 15. Two-Electron Oxidized Anionic Intermediates of 26 and 29, such as 26a and 29a, Respectively, Undergoing SET-WNA and PT-WEA Pathways
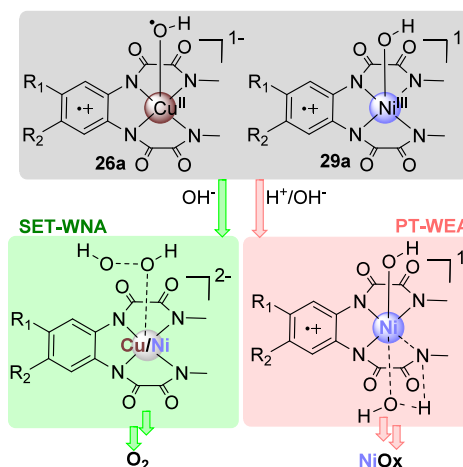
Reprinted with permission from ref 225. Copyright 2023 John Wiley and Sons.

acidic medium. In fact, the copper intermediate display radical character on the hydroxyl ligand which improves the prospect of nucleophilic attack by OH^- and prohibits catalyst deactivation.[193]

4. SUPRAMOLECULAR CATALYSTS

In the last few decades, supramolecular strategies have emerged as crucial tools to develop directional, self-sorted, and programmed self-assembly of elementary molecular donor—acceptor chromophores to complex oligomers, polymers, nanofibers, dendrimers etc.[57] Supramolecular strategies are also adapted to device artificial photosynthetic arrangements, with explicit control on the molecular architectures.[36,37] Recently, supramolecular approaches have been widely integrated in organization of molecular water oxidizing catalysts to enhance their catalytic activity. Such approaches minimize the potential loopholes of conventional artificial photosynthesis, utilizing light-harvesting and charge separation techniques. Undoubtedly, this leads to longer lifetime of excited triplets generated by photosensitizers, curtailing the possibility of decomposition and recombination, or photoproduction of singlet dioxygen that damages the ligand framework.

Noncovalent interactions can be beautifully integrated in organized supramolecular assemblies, like Nature's enzymatic resources. As highlighted in previous sections, biological water oxidation catalysis involving transfer of protons and electrons within the PSII framework firmly depends on the electron/proton wire mechanism promoted by the various amino acid residues surrounding the $CaMnO_4$ cluster within the protein domain. Unfortunately, such rigorous transmission of protons and electrons in functional synthetic multimetallic cluster mimics of PSII are incomprehensible and therefore lacks the recommended stability and activity. Fortunately, supramolecular multicomponent systems render vital nonbonding or purely covalent confinement that afford enhanced performance of existing water oxidation catalysts. In this section, we highlight some of the classic examples of transition-metal dependent supramolecular water oxidation activity while readers are encouraged to undergo recent overview articles for a holistic knowledge of supramolecular strategies in applied artificial photosynthesis and state-of-the-art devices.[6,59]

4.1. Metallosupramolecular Cluster. The challenges associated with catalyst design and loss of structural integrity of molecular water oxidation catalysts in strongly alkaline or acidic aqueous medium[221] with manifold noble and non-noble earth abundant metal active units led to the development of a limited number of systems being considered for further integration into supramolecular frameworks, albeit with the utilization of sacrificial reagents.[229] One such distinct example of a single-component metallo-supramolecular cluster was reported by Sun and co-workers in 2012 (**30**, Scheme 16).[228] Apparently, the Ru-based metallic triad (Scheme 16) undergoes an oxidative quenching mechanism on visible light irradiation at >400 nm, in a $H_2O/MeCN$ (9:1) solution containing $Na_2S_2O_8$ as the sacrificial oxidant, with a TON of 38 for O_2 evolution. As hypothesized for an oxidative quenching mechanism (Scheme 17),[229] the Ru-bpy photosensitizer in **30** is expected to undergo photoexcitation, followed by electron transfer to sodium persulfate. The oxidized $Ru(bpy)_3^{2+}$ photosensitizer would then trigger the removal of an electron from the centrally placed mononuclear Ru^{II} complex, $[RuL(pic)_2]$ (L = 2,2′-bipyridine-6,6′-dicarbox-

Scheme 16. Metallo-supramolecular Triad 30 Containing Both $Ru(bpy)_3^{2+}$ Photosensitizer and a Ru-Based Water Oxidation Catalyst
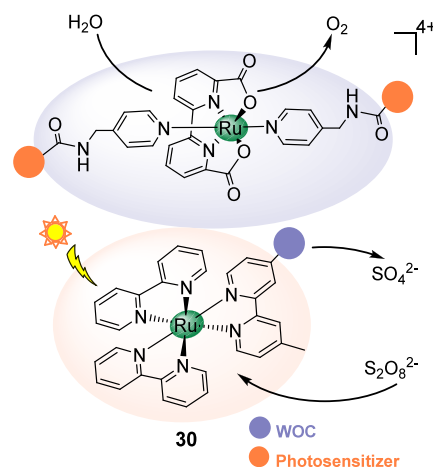
Reprinted with permission from ref 228. Copyright 2012 John Wiley and Sons.

Scheme 17. Hypothesized Oxidative Quenching Mechanism Taking Triad 30 as a Reference[229]
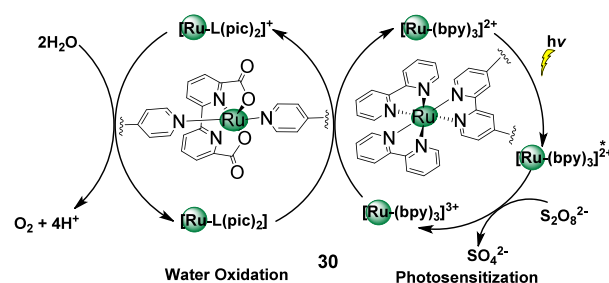
ylate; pic = 4-picoline), regenerating itself and oxidizing the catalyst to facilitate electron capture during water oxidation (Scheme 17). This event should undergo for four consecutive cycles before the catalytic turnover is reached to enable four electron water oxidation process. Notably, dissociation of the Ru-photosensitizers from the central molecular catalysts resulted in gradual decrease in the catalytic activity.[228]

Construction of photosensitizer—catalyst supramolecular combinations are not always successful to the same extent. For instance, utilizing $Ru(tpy)_2^{2+}$ (tpy = 2,2′:6′,2″-terpyridine) as the photosensitizer did not demonstrate any oxygen evolution in **31** (Figure 22),[228] perhaps due to its shorter excited-state lifetime. The photosensitizer-catalyst dyad **32** (Figure 22) consisting of a bipyridyl-Ru(II) based photosensitizer linked to a polypyridyl-Ru catalyst was reported by Thummel and co-workers in 2012.[230] Employing similar experimental conditions such as a blue light-emitting diode of wavelength 472 nm and persulfate as the sacrificial oxidant, **32** furnished a mere 6 turnover cycles, although using four times the concentration of the photosensitizer. Furthermore, **33** (Figure 22),[231] featuring a perylenebisimide (PBI) sensitizer coupled to the well-known complex $[(Cp^*)-Ir^{III}(ppy)Cl]$, (**7a**, Figure 9),[162] is photoactivated at 550 nm that leads to electron transfer from the Ir(III) core to the PBI moiety at a rate of 1.8 ps. However, the apparent charge separation is slated for an even faster electron—hole recombination (14 and 75 ps), ultimately resulting in a
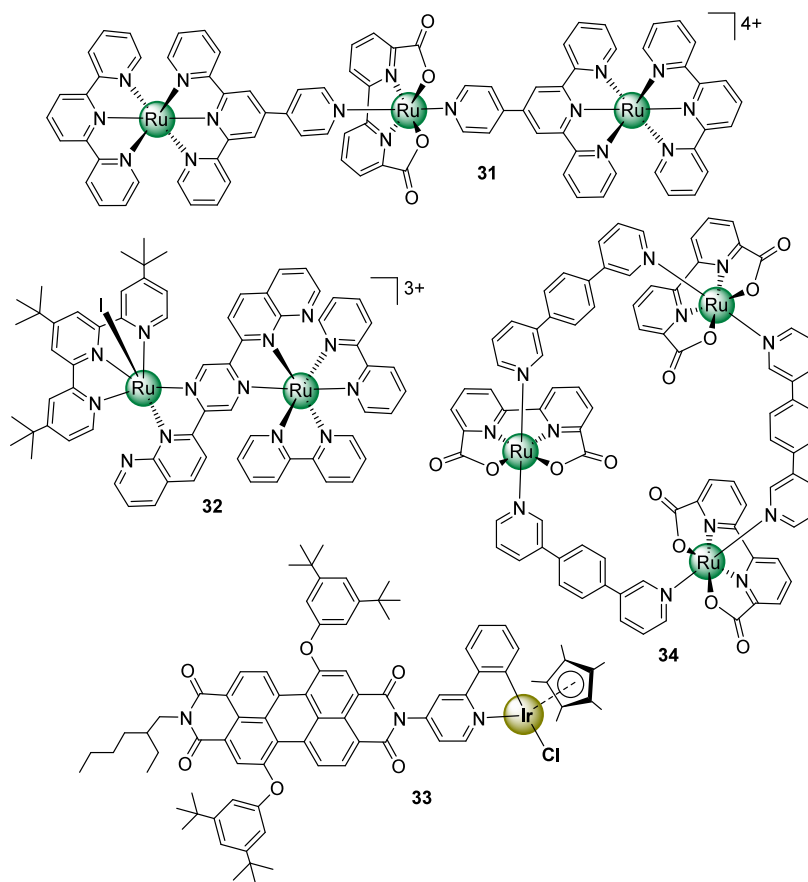
Figure 22. Structures of photosensitizer−catalyst metallo-supramolecular complexes.

short-lived PBI$^{\bullet-}$Ir(IV) radical state, not conducive for photocatalytic oxygen evolution.

To develop an efficient artificial supramolecular macrocycle, reflecting the sophistication and efficiency of the OEC in the biochemical setup, Würthner and others reported a ruthenium containing closed-loop complex (**34**, Figure 22), featuring three [Ru(bda)] subunits (similar to complex **3**)[141] coordinated through axial bpb (bpb= 1,4-bis(pyrid-3-yl) benzene) linkers, with remarkable catalytic activity (TOF > 100 s^{-1}).[232] Indeed, **34** demonstrated a TOF of >13.1 s^{-1} even in nM concentration of the system.

Mechanistic study with ^{18}O isotope labeling and spectro-electrochemical experiments show crucial difference in water oxidation carried out by **34** (Scheme 18),[232] as compared to the traditional Ru-bda complexes, **3** or **4** (Figure 8).[141,153] As mentioned in section 3, [Ru(bda)pic$_2$] complex (**3**), demonstrates a second order reaction kinetics with respect to the catalyst, i.e., a **3:3** dimer is predicted in the O−O bond forming transition state (as shown in Figure 8 for complex **4**),[141] with zeroth order dependence on the sacrificial oxidant and absence of a PCET process in the RDS.[233] Contrarily, **34** shows first order in macrocycle and first order in Ce^{4+} concentration, with a characteristic involvement on the O−H bond breaking step.[232] This certainly eliminates the possibility of a water nucleophilic attack (step 4, Scheme 18) or bimolecular radical coupling (step 4′, Scheme 18), as opposed to the radical mechanism predicted for complex **3**.[141] Incidentally, ^{18}O isotope labeling and thereafter mass spectrometry experiments demonstrate 43% of H$_2$^{18}O, emphasizing on the WNA as the most-acceptable mechanism

Scheme 18. Mechanism of Light-Induced Water Oxidation with Metallo-supramolecular Macrocyle 34^a
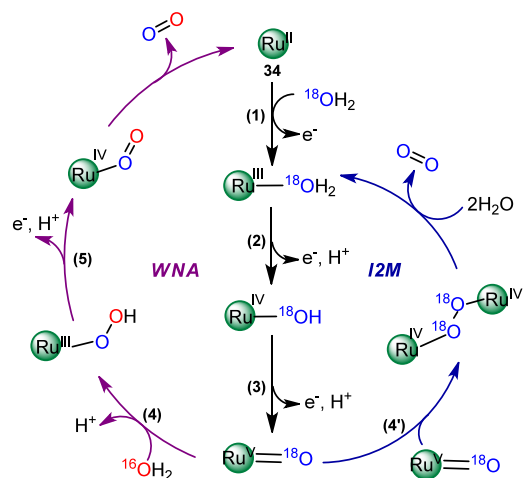
Reprinted with permission from ref 232. Copyright 2012 Springer Nature. ^{a}[Ru(bpy)$_3$]Cl$_2$ works as the photosensitizer.

undertaken by the macrocyclic complex, **34**. This suggests that the [Ru(bda)bpb]$_3$ architecture promotes a WNA pathway at a very low activation barrier, that enables the drastic change in the O$_2$ evolution kinetic activity on going from axially water coordinated mononuclear [Ru^{III}(bda)(mmi)(OH$_2$)] (mmi = 1,3-dimethylimidazolium-2-ylidene)[234] catalyst with k_{O_2} ∼ 0.04 s^{-1} to supramolecular template formation in [Ru(bda)-bpb]$_3$, demonstrating an unprecedented TOF of 155 s^{-1}.[232]

4.2. Supramolecular Self-Assembly and Encapsulation.

Understanding the chemical drive in bringing two mononuclear units in proximal and favorable orientation, and enhancement in reactivity due to $\pi-\pi$ stacking in Ru-bda complexes,[141,153] laid premises for unchartered avenues on development of catalysts within confined media, utilizing the well-known host–guest chemistry. Indeed, supramolecular encapsulation is an efficient technique to proliferate intermolecular dispersion forces to achieve higher activity and stability of molecular catalysts. One such unique example was put forth by Yang, Li, and co-workers where the authors prepared a nanocage of mesoporous silica for confining $Ru^{II}(bda)(pic)_2$ (3) and develop an efficient "homogeneous in heterogeneous" solid catalyst (35, Figure 23).[235] Inciden-
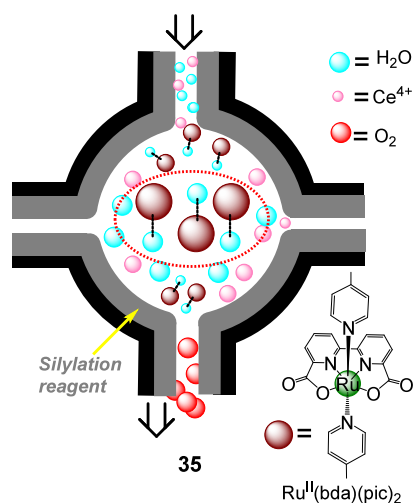
Figure 23. WOC encapsulated in mesoporous silica (35). Reprinted with permission from ref 235. Copyright 2012 Royal Society of Chemistry.

tally, the TOF is improved from 1.2 to 8.7 s^{-1} with successive increment in the number of ruthenium complexes (3), starting from one to seven units, confined within the nonaqueous condense environment of the solid host. Notably, π-stacking interactions are considered as key factors for the self-assembly process of the metal catalyst that promotes "cooperative activation" of the various binuclear units during the convergent O–O bond formation.[141,235] In fact, judicious design of catalysts and supramolecular techniques are recommended for extremely fast water oxidation reaction that could be utilized for assembling molecular devices and designing efficient photoanodes.[16]

As mentioned in 4.1, the metallo-supramolecular ruthenium triad 30 showed remarkable 5-fold enhancement (TON increased from 8 to 38) in catalytic activity as compared to its analogous molecular components.[196] However, further exploration of 30 by Sun and co-workers with mass spectrometry showed dissociation of the photosensitizer from the metallic triad, resulting in lowered quantum yield efficiency for O$_2$ evolution.[228,236] To meet the demand for high quantum yield during artificial photosynthesis, the authors anticipated to overcome the dissociation challenge with recombination of the sensitizer and the catalyst encapsulated in a supramolecular coverage. Hence, β-cyclodextrin was functionalized (β-CD) to incorporate $Ru(bpy)^{2+}$ through an ester bond [CD-Ru-(bpy)$_3$]$^{2+}$, while the central ruthenium catalyst consisted of

the hydrophobic 4-phenylpyridine (ppy) axial ligand (36, Figure 24). As a result of host–guest interaction, the

Figure 24. Supramolecular dye-WOC assembly (36) formed by encapsulation within cyclodextrin. Reprinted with permission from ref 236. Copyright 2015 American Chemical Society.
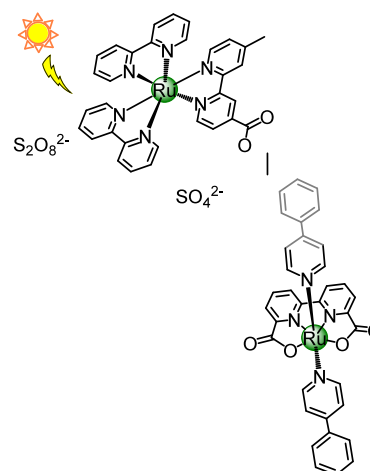
hydrophobic cavity captured the phenylpyridine axial ligands of the WOC through noncovalent interactions, resulting in an inclusion complex identified with ESI-MS spectrometry.[236] Efficient movement of electrons within the nondissociated metallo-supramolecular cluster prolonged the quantum yield efficiency to 84% at 450 nm, highlighting the noncovalent interactions as a crucial strategy in future development of artificial photosynthetic systems or dye-sensitized photo-electrochemical cells.

Unlike various synthetic ruthenium catalysts including the celebrated Meyer's blue dimer which follow the WNA mechanism (Scheme 3),[133,152] the Ru-bda based catalysts developed by Llobet, Sun and co-workers[141,153,238] follow the radical coupling I2M mechanism during the O–O bond formation (Scheme 3). Moreover, utilization of organic solvents imposes the challenges related to undesired molecular complex deactivation pathways due to the solvent coordination. Additionally, the possibility of oxidation of accessible organic/inorganic species other than the redox events related to the targeted catalyst over the wide window of redox potential increase the complexity of an already convoluted operation. Furthermore, the feasibility of both WNA and I2M pathways through comparable activation barriers by subtle modification of the ligand scaffold of two analogous binuclear ruthenium WOCs having bridging pyrazolate ligands such as $\{[Ru^{II}(py\text{-}SO_3)_2(OH)]_2(\mu\text{-Mebbp})\}^{3-}$, (where Mebbp = 4-methylbis(bipyridyl)pyrazolate), and the aqua complex, $\{[Ru^{II}(trpy)(H_2O)]_2(\mu\text{-Hbpp})\}_3$, (where trpy = 2,2′:6′,2″-terpyridine; Hbpp$^-$ = 3,5-bis(2-pyridyl)pyrazolate) emphasizes on the crucial role of the compartmental ligand design in determining the mechanistic landscape of molecular water oxidation.[237] Such a mechanistic difference probably stems from the bis-facial disposition of the Mebbp$^-$ ligand in the former complex that impedes the rotation of the pyridyl chelate arms to stabilize the putative Ru^{IV}=O or Ru^V=O oxidants.[237] These findings were inspirational for Yang et al. who developed amphiphilic supramolecular Ru-bda catalysts, self-assembled due to the interactions between the hydrophilic ether chains or sulfonate axial ligands in 37 (Scheme 19,

Scheme 19. Schematic Representation of Amphiphilic Axial Alkyl Chain Mediated Self-Assembly of Ru-bda-based WOCs into Micellar Vesicles in Water

Reprinted with permission from ref 237. Copyright 2016 John Wiley and Sons.

Figure 25. Assembled guanidinium nanosphere and catalyst encapsulation process of $Ru(bda)(PySO_3TBA)_2$ (**39**). Reprinted with permission from ref 240. Copyright 2018 John Wiley and Sons.

5. HYBRID CATALYSTS

As discussed earlier, biomimetic artificial metalloenzymes and model complexes are mostly found to have limited catalytic activity owing to deactivation and suicidal oxidation.[242,243] Hence, immobilization of synthetic structures on porous materials like metal−organic frameworks, metal-exchanged zeolites, carbon nanotubes etc., with persistent chemical environment like protein scaffolds would not only heterogenize these catalysts, but also prevent their immature deactivation, and provide the necessary molecular recognition of substrates to generate highly efficient biomimetic catalytic materials.[242] Unlike irregular allocation of active sites on oxides or silica supports, installation of molecular catalysts at regular intervals on suitable porous supports provide highly economic catalysts with superior heterogeneity and structural integrity. Thus, the large gap between effective artificial photosynthetic devices and the existing plethora of molecular and supramolecular catalysts could be eliminated with heterogenization of the latter into molecular catalyst-anchored on metal-oxo nodes or photoanodes.[18] Rational design of biomimetic hybrid organic/inorganic materials also ensures that selectivity is controlled in competing reaction pathways. This strategic combination enables the development of innovative electrochemical and photochemical processes that enhance activity, selectivity, and stability, leading to more efficient catalysis. In this context, molecular catalysts displaying low overpotential are preferred for design of efficient model of artificial photosynthetic devices.[18] Since the redox potential of organometallic complexes depend on the adjoining ligand environment, engineering the coordination environment lowers the overvoltage to explore new frontiers in water oxidation. In this part, therefore, we briefly discuss efficient hybridized molecular catalysts developed in the first stage that have shown success in catalytic splitting of water and ensure a continuous flow of oxygen and hydrogen for implementation in artificial photosynthetic devices.

5.1. Direct Hybridization on Photoanodes. Immobilization of molecular catalyst on electroconductive substrates or solid electrodes is one of the many conceivable engineered approaches for a hybrid (photo)electrocatalyst. Carboxylic, phosphate, or silicate groups are commonly utilized for

OTEG = $OCH_2CH_2OCH_2CH_2OCH_3$) and **38** (Scheme 19, $PySO_3^-$ = pyridine-3-sulfonate).[239] This amphiphilic nature of the axial ligands and the hydrophobic bda^{2-} core ensured aggregation of **37** and **38** to vesicular arrangement that undertook different O−O bond formation pathways with variation in the chain length. While the longer amphiphilic chain in **37** drifted the ruthenium centers apart, preventing the radical coupling mechanism (Scheme 19), the shorter alkyl chain in **38** favored the interaction between two M−O moieties through radical coupling (Scheme 19).[239] This fundamental understanding demonstrate the dependence of the water oxidation reaction mechanism on noncovalent interactions. Thus, it unfurled the domain of supramolecular water oxidation catalysis in natural photosynthesis for further investigation.

Later, supramolecular interactions were tweaked to achieve larger concentrations of the working catalyst. Reek and co-workers encapsulated Ru(bda) complexes with sulfonated pyridine axial ligands within a self-assembled guanidinium functionalized $M_{12}L_{24}$ nanosphere (M = Pt^{2+} or Pd^{2+}, L = bis-pyridyl building block) (**39**, Figure 25),[240] with a rigid shell outer framework and an inner amorphous medium, originally built by Fujita.[241] This primarily occurs due to strong H-bonding between the ligand $-SO_3^-$ and guanidium $-NH_2$ groups. Interestingly, the aggregation of multiple Ru-bda scaffolds (up to 12) within the supramolecular cage results in high catalytic concentration (0.54 M), facilitating preorganization of the binuclear setup to achieve greater catalytic activity. Indeed, compared to the molecular catalyst, the reaction rate increases 2-fold, following a diffusion-controlled RDS, rather than a radical coupling mechanism.
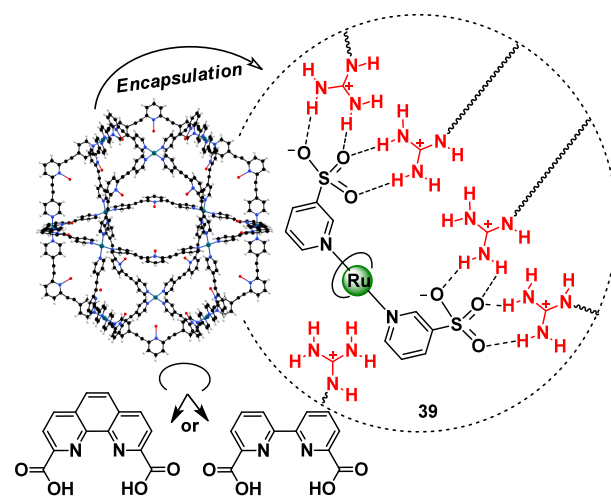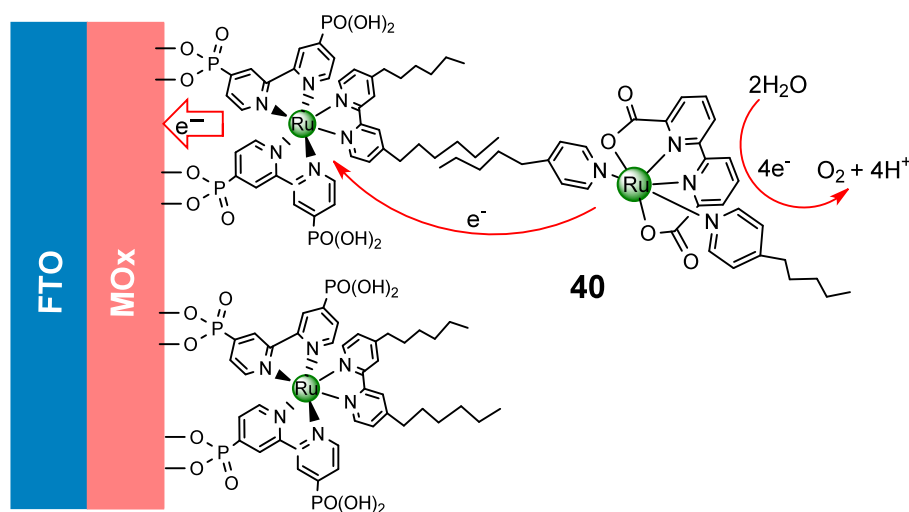
Figure 26. Chromophore-catalyst assemblies on a SnO_2/TiO_2 core/shell oxide surface (**40**) for water oxidation. Reprinted with permission from ref 249. Copyright 2019 American Chemical Society.

entrapment of molecular homogeneous catalysts on metal oxides which amount to low catalyst loading and vulnerability of the system in aqueous media,[244] while thiol group containing molecular catalysts are easily grafted on Au anodes.[245] Several techniques are also put forth for grafting on glass carbon electrodes, carbon nanotubes or graphene. The planar all-carbon monomolecular layers are covalently functionalized by alkyne−azide click reaction[246] or diazonium ion reduction reactions.[247] Alternatively, noncovalent interactions such as $\pi-\pi$ stacking are utilized to introduce molecular catalysts over carbon nanotubes and graphene sheets through physisorption.[248] Interestingly, the carbon-based platforms offer large surface area with oxidative stability and feasibility of structural modification that provide easy access to charge transfer for practical applications.

Recently, a new approach has been proposed by Concepcion, Meyer and others on development of water oxidation photoanodes consisting of a self-assembled chromophore and catalyst combination on mesoporous SnO_2/TiO_2 core/shell electrode for photoelectro synthetic water splitting in a dye-sensitized cell (**40**, Figure 26).[249] Here long-alkyl chain substituents on the Ru(bpy)$^{2+}$ chromophore and Ru-bda catalyst are noncovalently attached to generate a self-assembly that is further grafted on the anode through the phosphate groups on the photosensitizer (Figure 26). The oxygen generation efficiencies are found to be remarkable (73%) at 450 nm and pH 7, signifying the utility of such strategies for a varied number of catalyst-chromophore combinations in future water-splitting explorations.[249]

5.2. Anchorage on Metal-Oxo Nodes. Supramolecular preorganization of molecular catalysts on polyoxometalates and metal-oxo nodes through electrostatic and other non-covalent interactions are also interesting developments in the field of water oxidation.[59] Bonchio *et. al* utilized this technique for self-assembly of multiperylene-bis-imide chromophores, π-intercalated with poly ruthenium-oxo metalate water oxidation catalyst, to develop a robust and dynamic amphiphilic catalyst.[250] The two-dimensional para-crystalline aggregates resembled the architecture of PSII, with appreciable quantum efficiency (>40%) using green light ($\lambda > 500$ nm).[250] However, a low TON (~3) precludes its practical utility. Nevertheless, the simplicity in modulation of the building blocks due to

feasibility of tweaking the various noncovalent interactions offer scope for further investigation of innovative solutions toward artificial photosynthesis.

Earth-abundant 3d transition metal containing coordination complexes are incorporated within MOFs by bridging the linkers, demonstrating intriguing alternatives to traditional water oxidation catalysts. Crystalline porous MOFs with self-assembled extended networks of inorganic connectors (nodes) of metal ions or metallic clusters coordinated to the organic ligands (linkers), having tailored functionalities are excellent platforms, connecting the breaches between molecular and material oxygen evolution catalysis. The large surface area and high density provide the appropriate disposition of catalytic active sites, comparable to the catalytic properties of homogeneous catalysts. In fact, recent results show that a Ni(II) *meso*-tetrakis(4-carboxyphenyl) porphyrin (TCPP) functionalized Zr(IV)-based porous coordination network (PCN-224) MOF is a highly reactive supermolecule (**41**, Scheme 20),[251] catalyzing water oxidation at neutral conditions, with an overpotential of 450 mV. Interestingly,

Scheme 20. Proposed Mechanism of Water Oxidation Using Ni(II)-TCPP Immobilized over Zr-oxo Nodes (41)
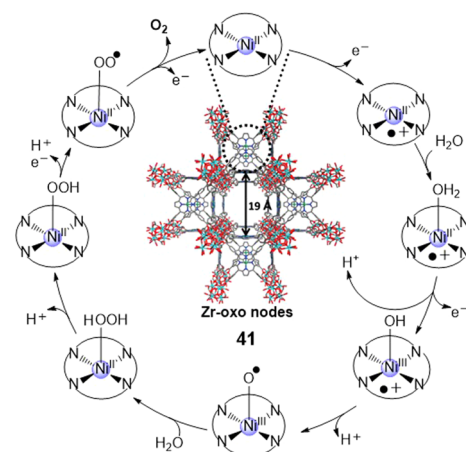
Reprinted with permission from ref 251. Copyright 2016 the Royal Society of Chemistry.

the Ni(II)-TCPP linkers bound to the PCN-224 MOF are the active catalytic units, which retain homogeneity of the water oxidation reaction mechanism (Scheme 20). Octahedral Zr(IV)-based MOF nodes or the secondary building units are connected to six Ni(II)-TCPP ligands, at node-to-node distance of 23.7 and 15.1 Å through two open channels, with a pore diameter of ~19 Å (Scheme 20). Thus, the large distance between two nickel centers in **41** and the rigidity of the MOF inhibits the possibility of binuclear participation in water oxidation reaction. In fact, **41** is expected to undergo water oxidation reaction, similar to catalyst **28** (Figure 21),[220] with a formal Por−Ni(III)−O● intermediate facilitating the O−O bond formation through PCET processes. The Por−Ni(II) active catalytic site is regenerated on O_2 evolution (Scheme 20).[251]

6. CONCLUDING REMARKS

The worldwide attention toward clean energy has triggered development of several promising catalysts for production of chemical fuels from solar energy, forming the genesis of successful artificial photosynthesis (AP). Primarily, tremendous efforts are concentrated on dealing with water oxidation catalysts which is the major bottleneck in practical implementation of this strategy. Over the past few years, both homogeneous and heterogeneous systems[252,253] have been investigated in detail to bring forward new design principles in WOCs. As summarized in this review, molecular homogeneous transition metal containing catalysts serve as excellent model systems and provide enormous advantages to understand the mechanistic intricacies of water oxidation, which in turn facilitate to understand the structural trajectory at an atomistic level. The fundamental insights gained on the versatile interplay of ligand and metal centers over the catalytic reaction pathways are inspirational for future development of molecular catalysts. Further, strategies have been intensified to develop molecular catalysts with higher nuclearity, utilizing self-assembly and encapsulation techniques to integrate them into hybrid structural motifs. With the progress in mechanistic studies on "homogeneous in heterogenous catalysts", new dimensions for rational design of WOCs are now available, thus eliminating the analytical challenges associated with the active sites on heterogeneous catalysts.

Some of the key factors that needs to be addressed for the development of new-age economical WOCs for alternative renewable energy generation are (1) identification of earth-abundant 3*d* transition metal based robust and efficient molecular catalysts, working effectively in acidic aqueous conditions, overcoming the possibility of ligand deactivation. It is, therefore, important that such catalysts show low over potential and high TON and TOF, analogous to their noble metal counterparts, especially the ruthenium and iridium-based complexes. Moreover, the design of catalysts should not be biased toward certain organic solvents. (2) Homogeneous electrocatalysts generally require a sacrificial oxidizing reagent such as Ce^{4+}, $Na_2S_2O_8$, and others. However, it is imperative that such catalysts are immobilized on electrodes for efficient electrochemical oxygen evolution. Although the development of molecular electrocatalysts is promising, the involvement of the sacrificial oxidizing agent including its instability, presence of reactive oxygen atoms and dependence on pH limits the functionality of those WOCs. In fact, such vigorous oxidative conditions are detrimental toward the ligand framework and leads to decomposition of the molecular catalyst. Hence, more

efforts should be invested to identify molecular electrocatalysts working in milder conditions and excluding the role of the sacrificial oxidant. (3) Heterogenization of molecular/supra-molecular catalysts on inorganic materials and photoanodes to develop potential catalysts for industrial applications. Care should be taken to enhance the stability and activity of molecular catalysts engineered into hybrid materials. The performance of the catalyst incorporated into electrochemical setup should be evaluated under the influence of different external parameters such as oxidants, reductants, solvent, and pH. Understanding the complications related to molecular and heterogenized water oxidation catalysis would be a key step to "blur" the borderline chemistry between homogeneous and heterogeneous catalysis, and expedite the search for permanent solutions toward "greener" technological advancements.

■ AUTHOR INFORMATION

Corresponding Author

Lisa Roy − *Institute of Chemical Technology Mumbai−IOC Odisha Campus Bhubaneswar, IIT Kharagpur Extension Centre, Bhubaneswar 751013, India;* orcid.org/0000-0003-4205-1626; Email: l.roy@iocb.ictmumbai.edu.in

Author

Ajeet Kumar Singh − *Institute of Chemical Technology Mumbai−IOC Odisha Campus Bhubaneswar, IIT Kharagpur Extension Centre, Bhubaneswar 751013, India;* orcid.org/0000-0003-3026-881X

Complete contact information is available at:
https://pubs.acs.org/10.1021/acsomega.3c07847

Author Contributions

L.R. designed the project. A.K.S. wrote the initial draft. L.R. wrote the final version. A.K.S. and L.R. both contributed to graphics. Both authors have given approval to the final version.

Notes

The authors declare no competing financial interest.

■ REFERENCES

(1) Lewis, N. S.; Nocera, D. G. Powering the Planet: Chemical Challenges in Solar Energy Utilization. *Proc. Natl. Acad. Sci. U. S. A.* **2006**, *103*, 15729−15735.

(2) Nocera, D. G. Chemistry of Personalized Solar Energy. *Inorg. Chem.* **2009**, *48*, 10001−10017.

(3) Gust, D.; Moore, T. A.; Moore, A. L. Solar Fuels via Artificial Photosynthesis. *Acc. Chem. Res.* **2009**, *42*, 1890−1898.

(4) Berardi, S.; Drouet, S.; Francàs, L.; Gimbert-Suriñach, C.; Guttentag, M.; Richmond, C.; Stoll, T.; Llobet, A. Molecular Artificial Photosynthesis. *Chem. Soc. Rev.* **2014**, *43*, 7501−7519.

(5) Barber, J. Photosynthetic Energy Conversion: Natural and Artificial. *Chem. Soc. Rev.* **2009**, *38*, 185−196.

(6) Nocera, D. G. The Artificial Leaf. *Acc. Chem. Res.* **2012**, *45*, 767−776.

(7) Stahel, W. R. The Circular Economy. *Nature* **2016**, *531*, 435−438.

(8) Dillon, A. C.; Jones, K. M.; Bekkedahl, T. A.; Kiang, C. H.; Bethune, D. S.; Heben, M. J. Storage of Hydrogen in Single-Walled Carbon Nanotubes. *Nature* **1997**, *386*, 377−379.

(9) Tsivion, E.; Long, J. R.; Head-Gordon, M. Hydrogen Physisorption on Metal−Organic Framework Linkers and Metalated

Linkers: A Computational Study of the Factors That Control Binding Strength. *J. Am. Chem. Soc.* **2014**, *136*, 17827−17835.

(10) Roy, L.; Mittal, S.; Paul, A. Breaking the Myth of the Recalcitrant Chemisorbed Hydrogens on Boron Nitride Nanotubes: A Theoretical Perspective. *Angew. Chem., Int. Ed.* **2012**, *51*, 4152−4156.

(11) Roy, L.; Bhunya, S.; Paul, A. A Metal-Free Strategy to Release Chemisorbed H_2 from Hydrogenated Boron Nitride Nanotubes. *Angew. Chem., Int. Ed.* **2014**, *53*, 12430−12435.

(12) Roy, L.; Paul, A. Computational Design of an Iridium Based Catalyst for Releasing H_2 from Hydrogenated BN Nanotubes. *Chem. Commun.* **2015**, *51*, 10532−10535.

(13) Roy, L. Theoretical Investigation of an Acid Catalyst for Viable Release of H_2 from BN Nanotubes: A Local Pair Natural Orbital Coupled Cluster Approach. *Int. J. Quantum Chem.* **2020**, *120*, No. e26257.

(14) Agarwala, P.; Pati, S. K.; Roy, L. Unravelling the Possibility of Hydrogen Storage on Naphthalene Dicarboxylate-Based MOF Linkers: A Theoretical Perspective. *Mol. Phys.* **2020**, *118*, No. e1757169.

(15) Matheu, R.; Garrido-Barros, P.; Gil-Sepulcre, M.; Ertem, M. Z.; Sala, X.; Gimbert-Suriñach, C.; Llobet, A. The Development of Molecular Water Oxidation Catalysts. *Nat. Rev. Chem.* **2019**, *3*, 331−341.

(16) Li, X.; Lei, H.; Xie, L.; Wang, N.; Zhang, W.; Cao, R. Metalloporphyrins as Catalytic Models for Studying Hydrogen and Oxygen Evolution and Oxygen Reduction Reactions. *Acc. Chem. Res.* **2022**, *55*, 878−892.

(17) Zhang, L.; Mathew, S.; Hessels, J.; Reek, J. N. H.; Yu, F. Homogeneous Catalysts Based on First-Row Transition-Metals for Electrochemical Water Oxidation. *ChemSusChem* **2021**, *14*, 234−250.

(18) Zhang, B.; Sun, L. Artificial Photosynthesis: Opportunities and Challenges of Molecular Catalysts. *Chem. Soc. Rev.* **2019**, *48*, 2216−2264.

(19) Blakemore, J. D.; Crabtree, R. H.; Brudvig, G. W. Molecular Catalysts for Water Oxidation. *Chem. Rev.* **2015**, *115*, 12974−13005.

(20) Lubitz, W.; Chrysina, M.; Cox, N. Water Oxidation in Photosystem II. *Photosynth. Res.* **2019**, *142*, 105−125.

(21) Kärkäs, M. D.; Verho, O.; Johnston, E. V.; Åkermark, B. Artificial Photosynthesis: Molecular Systems for Catalytic Water Oxidation. *Chem. Rev.* **2014**, *114*, 11863−12001.

(22) Young, K. J.; Martini, L. A.; Milot, R. L.; Snoeberger, R. C.; Batista, V. S.; Schmuttenmaer, C. A.; Crabtree, R. H.; Brudvig, G. W. Light-Driven Water Oxidation for Solar Fuels. *Coord. Chem. Rev.* **2012**, *256*, 2503−2520.

(23) Soriano-López, J.; Schmitt, W.; García-Melchor, M. Computational Modelling of Water Oxidation Catalysts. *Curr. Opin. Electrochem.* **2018**, *7*, 22−30.

(24) Croce, R.; Van Amerongen, H. Natural Strategies for Photosynthetic Light Harvesting. *Nat. Chem. Biol.* **2014**, *10*, 492−501.

(25) Nelson, N.; Ben-Shem, A. The Complex Architecture of Oxygenic Photosynthesis. *Nat. Rev. Mol. Cell Biol.* **2004**, *5*, 971−982.

(26) Vinyard, D. J.; Brudvig, G. W. Progress Toward a Molecular Mechanism of Water Oxidation in Photosystem II. *Annu. Rev. Phys. Chem.* **2017**, *68*, 101−116.

(27) Junge, W. Oxygenic Photosynthesis: History, Status and Perspective. *Q. Rev. Biophys.* **2019**, *52*, No. e1.

(28) Yano, J.; Yachandra, V. Mn4Ca Cluster in Photosynthesis: Where and How Water Is Oxidized to Dioxygen. *Chem. Rev.* **2014**, *114*, 4175−4205.

(29) Ferreira, K. N.; Iverson, T. M.; Maghlaoui, K.; Barber, J.; Iwata, S. Architecture of the Photosynthetic Oxygen-Evolving Center. *Science* **2004**, *303*, 1831−1838.

(30) Messinger, J. Evaluation of Different Mechanistic Proposals for Water Oxidation in Photosynthesis on the Basis of Mn4OxCa Structures for the Catalytic Site and Spectroscopic Data. *Phys. Chem. Chem. Phys.* **2004**, *6*, 4764.

(31) Lubitz, W.; Reijerse, E. J.; Messinger, J. Solar Water-Splitting into H_2 and O_2: Design Principles of Photosystem II and Hydrogenases. *Energy Environ. Sci.* **2008**, *1*, 15.

(32) De Lichtenberg, C.; Messinger, J. Substrate Water Exchange in the S_2 State of Photosystem II Is Dependent on the Conformation of the Mn_4 Ca Cluster. *Phys. Chem. Chem. Phys.* **2020**, *22*, 12894−12908.

(33) Haumann, M.; Müller, C.; Liebisch, P.; Iuzzolino, L.; Dittmer, J.; Grabolle, M.; Neisius, T.; Meyer-Klaucke, W.; Dau, H. Structural and Oxidation State Changes of the Photosystem II Manganese Complex in Four Transitions of the Water Oxidation Cycle (S0 → S1, S1 → S2, S2 → S3, and S3,4 → S0) Characterized by X-Ray Absorption Spectroscopy at 20 K and Room Temperature†. *Biochemistry* **2005**, *44*, 1894−1908.

(34) Song, X.; Wang, B. O−O Bond Formation and Oxygen Release in Photosystem II Are Enhanced by Spin-Exchange and Synergetic Coordination Interactions. *J. Chem. Theory Comput.* **2023**, *19*, 2684−2696.

(35) Ogata, K.; Hatakeyama, M.; Sakamoto, Y.; Nakamura, S. Investigation of a Pathway for Water Delivery in Photosystem II Protein by Molecular Dynamics Simulation. *J. Phys. Chem. B* **2019**, *123*, 6444−6452.

(36) Doyle, M. D.; Bhowmick, A.; Wych, D. C.; Lassalle, L.; Simon, P. S.; Holton, J.; Sauter, N. K.; Yachandra, V. K.; Kern, J. F.; Yano, J.; Wall, M. E. Water Networks in Photosystem II Using Crystalline Molecular Dynamics Simulations and Room-Temperature XFEL Serial Crystallography. *J. Am. Chem. Soc.* **2023**, *145*, 14621−14635.

(37) Young, I. D.; Ibrahim, M.; Chatterjee, R.; Gul, S.; Fuller, F. D.; Koroidov, S.; Brewster, A. S.; Tran, R.; Alonso-Mori, R.; Kroll, T.; Michels-Clark, T.; Laksmono, H.; Sierra, R. G.; Stan, C. A.; Hussein, R.; Zhang, M.; Douthit, L.; Kubin, M.; De Lichtenberg, C.; Vo Pham, L.; Nilsson, H.; Cheah, M. H.; Shevela, D.; Saracini, C.; Bean, M. A.; Seuffert, I.; Sokaras, D.; Weng, T. C.; Pastor, E.; Weninger, C.; Fransson, T.; Lassalle, L.; Bräuer, P.; Aller, P.; Docker, P. T.; Andi, B.; Orville, A. M.; Glownia, J. M.; Nelson, S.; Sikorski, M.; Zhu, D.; Hunter, M. S.; Lane, T. J.; Aquila, A.; Koglin, J. E.; Robinson, J.; Liang, M.; Boutet, S.; Lyubimov, A. Y.; Uervirojnangkoorn, M.; Moriarty, N. W.; Liebschner, D.; Afonine, P. V.; Waterman, D. G.; Evans, G.; Wernet, P.; Dobbek, H.; Weis, W. I.; Brunger, A. T.; Zwart, P. H.; Adams, P. D.; Zouni, A.; Messinger, J.; Bergmann, U.; Sauter, N. K.; Kern, J.; Yachandra, V. K.; Yano, J. Structure of Photosystem II and Substrate Binding at Room Temperature. *Nature* **2016**, *540*, 453−457.

(38) Hirata, K.; Shinzawa-Itoh, K.; Yano, N.; Takemura, S.; Kato, K.; Hatanaka, M.; Muramoto, K.; Kawahara, T.; Tsukihara, T.; Yamashita, E.; Tono, K.; Ueno, G.; Hikima, T.; Murakami, H.; Inubushi, Y.; Yabashi, M.; Ishikawa, T.; Yamamoto, M.; Ogura, T.; Sugimoto, H.; Shen, J.-R.; Yoshikawa, S.; Ago, H. Determination of Damage-Free Crystal Structure of an X-Ray−Sensitive Protein Using an XFEL. *Nat. Methods* **2014**, *11*, 734−736.

(39) Suga, M.; Akita, F.; Hirata, K.; Ueno, G.; Murakami, H.; Nakajima, Y.; Shimizu, T.; Yamashita, K.; Yamamoto, M.; Ago, H.; Shen, J. R. Native Structure of Photosystem II at 1.95Å Resolution Viewed by Femtosecond X-Ray Pulses. *Nature* **2015**, *517*, 99−103.

(40) Ibrahim, M.; Fransson, T.; Chatterjee, R.; Cheah, M. H.; Hussein, R.; Lassalle, L.; Sutherlin, K. D.; Young, I. D.; Fuller, F. D.; Gul, S.; Kim, I.-S.; Simon, P. S.; De Lichtenberg, C.; Chernev, P.; Bogacz, I.; Pham, C. C.; Orville, A. M.; Saichek, N.; Northen, T.; Batyuk, A.; Carbajo, S.; Alonso-Mori, R.; Tono, K.; Owada, S.; Bhowmick, A.; Bolotovsky, R.; Mendez, D.; Moriarty, N. W.; Holton, J. M.; Dobbek, H.; Brewster, A. S.; Adams, P. D.; Sauter, N. K.; Bergmann, U.; Zouni, A.; Messinger, J.; Kern, J.; Yachandra, V. K.; Yano, J. Untangling the Sequence of Events during the S_2 → S_3 Transition in Photosystem II and Implications for the Water Oxidation Mechanism. *Proc. Natl. Acad. Sci. U. S. A.* **2020**, *117*, 12624−12635.

(41) Simon, P. S.; Makita, H.; Bogacz, I.; Fuller, F.; Bhowmick, A.; Hussein, R.; Ibrahim, M.; Zhang, M.; Chatterjee, R.; Cheah, M. H.; Chernev, P.; Doyle, M. D.; Brewster, A. S.; Alonso-Mori, R.; Sauter,

N. K.; Bergmann, U.; Dobbek, H.; Zouni, A.; Messinger, J.; Kern, J.; Yachandra, V. K.; Yano, J. Capturing the Sequence of Events during the Water Oxidation Reaction in Photosynthesis Using XFELs. *FEBS Lett.* **2023**, *597*, 30−37.

(42) Najafpour, M. M.; Renger, G.; Hołyńska, M.; Moghaddam, A. N.; Aro, E.-M.; Carpentier, R.; Nishihara, H.; Eaton-Rye, J. J.; Shen, J.-R.; Allakhverdiev, S. I. Manganese Compounds as Water-Oxidizing Catalysts: From the Natural Water-Oxidizing Complex to Nanosized Manganese Oxide Structures. *Chem. Rev.* **2016**, *116*, 2886−2936.

(43) Li, W.; Li, F.; Yang, H.; Wu, X.; Zhang, P.; Shan, Y.; Sun, L. A Bio-Inspired Coordination Polymer as Outstanding Water Oxidation Catalyst via Second Coordination Sphere Engineering. *Nat. Commun.* **2019**, *10*, 5074.

(44) Fukuzumi, S.; Hong, D.; Yamada, Y. Bioinspired Photocatalytic Water Reduction and Oxidation with Earth-Abundant Metal Catalysts. *J. Phys. Chem. Lett.* **2013**, *4*, 3458−3467.

(45) Wang, D.; Sampaio, R. N.; Troian-Gautier, L.; Marquard, S. L.; Farnum, B. H.; Sherman, B. D.; Sheridan, M. V.; Dares, C. J.; Meyer, G. J.; Meyer, T. J. Molecular Photoelectrode for Water Oxidation Inspired by Photosystem II. *J. Am. Chem. Soc.* **2019**, *141*, 7926−7933.

(46) Wei, J.; Feng, Y.; Zhou, P.; Liu, Y.; Xu, J.; Xiang, R.; Ding, Y.; Zhao, C.; Fan, L.; Hu, C. A Bioinspired Molecular Polyoxometalate Catalyst with Two Cobalt(II) Oxide Cores for Photocatalytic Water Oxidation. *ChemSusChem* **2015**, *8*, 2630−2634.

(47) Wieghardt, K. The Active Sites in Manganese-Containing Metalloproteins and Inorganic Model Complexes. *Angew. Chem., Int. Ed. Engl.* **1989**, *28*, 1153−1172.

(48) Christou, G. Manganese Carboxylate Chemistry and Its Biological Relevance. *Acc. Chem. Res.* **1989**, *22*, 328−335.

(49) Tsui, E. Y.; Kanady, J. S.; Agapie, T. Synthetic Cluster Models of Biological and Heterogeneous Manganese Catalysts for O$_2$ Evolution. *Inorg. Chem.* **2013**, *52*, 13833−13848.

(50) Najafpour, M. M.; Nayeri, S.; Pashaei, B. Nano-Size Amorphous Calcium−Manganese Oxide as an Efficient and Biomimetic Water Oxidizing Catalyst for Artificial Photosynthesis: Back to Manganese. *Dalton Trans.* **2011**, *40*, 9374−9378.

(51) Koellner, C. A.; Gau, M. R.; Polyak, A.; Bayana, M.; Zdilla, M. J. Hemicubane Topological Analogs of the Oxygen-Evolving Complex of Photosystem II Mediating Water-Assisted Propylene Carbonate Oxidation. *Chem. Commun.* **2022**, *58*, 2532−2535.

(52) Rivalta, I.; Brudvig, G. W.; Batista, V. S. Computational Studies of the Oxygen-Evolving Complex of Photosystem II and Biomimetic Oxomanganese Complexes for Renewable Energy Applications. In *ACS Symposium Series*; Fitzgerald, G., Govind, N., Eds.; American Chemical Society: Washington, DC, 2013; Vol. *1133*, pp 203−215.

(53) Brimblecombe, R.; Swiegers, G. F.; Dismukes, G. C.; Spiccia, L. Sustained Water Oxidation Photocatalysis by a Bioinspired Manganese Cluster. *Angew. Chem., Int. Ed.* **2008**, *47*, 7335−7338.

(54) Tran, P. D.; Wong, L. H.; Barber, J.; Loo, J. S. C. Recent Advances in Hybrid Photocatalysts for Solar Fuel Production. *Energy Environ. Sci.* **2012**, *5*, 5902.

(55) Schley, N. D.; Blakemore, J. D.; Subbaiyan, N. K.; Incarvito, C. D.; D'Souza, F.; Crabtree, R. H.; Brudvig, G. W. Distinguishing Homogeneous from Heterogeneous Catalysis in Electrode-Driven Water Oxidation with Molecular Iridium Complexes. *J. Am. Chem. Soc.* **2011**, *133*, 10473−10481.

(56) Kondo, M.; Tatewaki, H.; Masaoka, S. Design of Molecular Water Oxidation Catalysts with Earth-Abundant Metal Ions. *Chem. Soc. Rev.* **2021**, *50*, 6790−6831.

(57) Wehner, M.; Würthner, F. Supramolecular Polymerization through Kinetic Pathway Control and Living Chain Growth. *Nat. Rev. Chem.* **2020**, *4*, 38−53.

(58) Vallavoju, N.; Sivaguru, J. Supramolecular Photocatalysis: Combining Confinement and Non-Covalent Interactions to Control Light Initiated Reactions. *Chem. Soc. Rev.* **2014**, *43*, 4084−4101.

(59) Keijer, T.; Bouwens, T.; Hessels, J.; Reek, J. N. H. Supramolecular Strategies in Artificial Photosynthesis. *Chem. Sci.* **2021**, *12*, 50−70.

(60) Blakemore, J. D.; Crabtree, R. H.; Brudvig, G. W. Molecular Catalysts for Water Oxidation. *Chem. Rev.* **2015**, *115*, 12974−13005.

(61) Smith, P. T.; Nichols, E. M.; Cao, Z.; Chang, C. J. Hybrid Catalysts for Artificial Photosynthesis: Merging Approaches from Molecular, Materials, and Biological Catalysis. *Acc. Chem. Res.* **2020**, *53*, 575−587.

(62) Li, J.; Triana, C. A.; Wan, W.; Adiyeri Saseendran, D. P.; Zhao, Y.; Balaghi, S. E.; Heidari, S.; Patzke, G. R. Molecular and Heterogeneous Water Oxidation Catalysts: Recent Progress and Joint Perspectives. *Chem. Soc. Rev.* **2021**, *50*, 2444−2485.

(63) Hunter, B. M.; Gray, H. B.; Müller, A. M. Earth-Abundant Heterogeneous Water Oxidation Catalysts. *Chem. Rev.* **2016**, *116*, 14120−14136.

(64) Stracke, J. J.; Finke, R. G. Distinguishing Homogeneous from Heterogeneous Water Oxidation Catalysis When Beginning with Polyoxometalates. *ACS Catal.* **2014**, *4*, 909−933.

(65) Rappaport, F.; Guergova-Kuras, M.; Nixon, P. J.; Diner, B. A.; Lavergne, J. Kinetics and Pathways of Charge Recombination in Photosystem II. *Biochemistry* **2002**, *41*, 8518−8527.

(66) Saito, K.; Shen, J.-R.; Ishida, T.; Ishikita, H. Short Hydrogen Bond between Redox-Active Tyrosine Y$_Z$ and D1-His190 in the Photosystem II Crystal Structure. *Biochemistry* **2011**, *50*, 9836−9844.

(67) Shevela, D.; Kern, J. F.; Govindjee, G.; Messinger, J. Solar Energy Conversion by Photosystem II: Principles and Structures. *Photosynth. Res.* **2023**, *156*, 279−307.

(68) Kok, B.; Forbush, B.; McGloin, M. Cooperation Of Charges In Photosynthetic O$_2$ Evolution−I. A Linear Four Step Mechanism. *Photochem. Photobiol.* **1970**, *11*, 457−475.

(69) Joliot, P.; Barbieri, G.; Chabaud, R. Un Nouveau Modele Des Centres Photochimiques Du Systeme Ii*. *Photochem. Photobiol.* **1969**, *10*, 309−329.

(70) Klauss, A.; Haumann, M.; Dau, H. Alternating Electron and Proton Transfer Steps in Photosynthetic Water Oxidation. *Proc. Natl. Acad. Sci. U. S. A.* **2012**, *109*, 16035−16040.

(71) Siegbahn, P. E. M. Structures and Energetics for O$_2$ Formation in Photosystem II. *Acc. Chem. Res.* **2009**, *42*, 1871−1880.

(72) Suzuki, H.; Sugiura, M.; Noguchi, T. Monitoring Water Reactions during the S-State Cycle of the Photosynthetic Water-Oxidizing Center: Detection of the DOD Bending Vibrations by Means of Fourier Transform Infrared Spectroscopy. *Biochemistry* **2008**, *47*, 11024−11030.

(73) Shen, J.-R. The Structure of Photosystem II and the Mechanism of Water Oxidation in Photosynthesis. *Annu. Rev. Plant Biol.* **2015**, *66*, 23−48.

(74) Kim, C. J.; Debus, R. J. One of the Substrate Waters for O$_2$ Formation in Photosystem II Is Provided by the Water-Splitting Mn$_4$CaO$_5$ Cluster's Ca^{2+} Ion. *Biochemistry* **2019**, *58*, 3185−3192.

(75) Cox, N.; Pantazis, D. A.; Lubitz, W. Current Understanding of the Mechanism of Water Oxidation in Photosystem II and Its Relation to XFEL Data. *Annu. Rev. Biochem.* **2020**, *89*, 795−820.

(76) Orio, M.; Pantazis, D. A. Successes, Challenges, and Opportunities for Quantum Chemistry in Understanding Metalloenzymes for Solar Fuels Research. *Chem. Commun.* **2021**, *57*, 3952−3974.

(77) Deisenhofer, J.; Epp, O.; Miki, K.; Huber, R.; Michel, H. Structure of the Protein Subunits in the Photosynthetic Reaction Centre of Rhodopseudomonas Viridis at 3Å Resolution. *Nature* **1985**, *318*, 618−624.

(78) Zouni, A.; Witt, H.-T.; Kern, J.; Fromme, P.; Krauss, N.; Saenger, W.; Orth, P. Crystal Structure of Photosystem II from Synechococcus Elongatus at 3.8 Å Resolution. *Nature* **2001**, *409*, 739−743.

(79) Krewald, V.; Neese, F.; Pantazis, D. A. Redox Potential Tuning by Redox-Inactive Cations in Nature's Water Oxidizing Catalyst and Synthetic Analogues. *Phys. Chem. Chem. Phys.* **2016**, *18*, 10739−10750.

(80) Umena, Y.; Kawakami, K.; Shen, J. R.; Kamiya, N. Crystal Structure of Oxygen-Evolving Photosystem II at a Resolution of 1.9Å. *Nature* **2011**, *473*, 55−60.

(81) Hussein, R.; Ibrahim, M.; Bhowmick, A.; Simon, P. S.; Chatterjee, R.; Lassalle, L.; Doyle, M.; Bogacz, I.; Kim, I.-S.; Cheah, M. H.; Gul, S.; De Lichtenberg, C.; Chernev, P.; Pham, C. C.; Young, I. D.; Carbajo, S.; Fuller, F. D.; Alonso-Mori, R.; Batyuk, A.; Sutherlin, K. D.; Brewster, A. S.; Bolotovsky, R.; Mendez, D.; Holton, J. M.; Moriarty, N. W.; Adams, P. D.; Bergmann, U.; Sauter, N. K.; Dobbek, H.; Messinger, J.; Zouni, A.; Kern, J.; Yachandra, V. K.; Yano, J. Structural Dynamics in the Water and Proton Channels of Photosystem II during the S2 to S3 Transition. *Nat. Commun.* **2021**, *12*, 6531.

(82) Pantazis, D. A.; Ames, W.; Cox, N.; Lubitz, W.; Neese, F. Two Interconvertible Structures That Explain the Spectroscopic Properties of the Oxygen-Evolving Complex of Photosystem II in the S 2 State. *Angew. Chem. - Int. Ed.* **2012**, *51*, 9935−9940.

(83) Dismukes, G. C.; Siderer, Y. Intermediates of a Polynuclear Manganese Center Involved in Photosynthetic Oxidation of Water. *Proc. Natl. Acad. Sci. U. S. A.* **1981**, *78*, 274−278.

(84) De Paula, J. C.; Beck, W. F.; Miller, A.-F.; Wilson, R. B.; Brudvig, G. W. Studies of the Manganese Site of Photosystem II by Electron Spin Resonance Spectroscopy. *J. Chem. Soc. Faraday Trans. 1 Phys. Chem. Condens. Phases* **1987**, *83*, 3635−3651.

(85) Haddy, A. EPR Spectroscopy of the Manganese Cluster of Photosystem II. *Photosynth. Res.* **2007**, *92*, 357−368.

(86) Chatterjee, R.; Lassalle, L.; Gul, S.; Fuller, F. D.; Young, I. D.; Ibrahim, M.; De Lichtenberg, C.; Cheah, M. H.; Zouni, A.; Messinger, J.; Yachandra, V. K.; Kern, J.; Yano, J. Structural Isomers of the S 2 State in Photosystem II: Do They Exist at Room Temperature and Are They Important for Function? *Physiol. Plant.* **2019**, *166*, 60−72.

(87) Boussac, A.; Ugur, I.; Marion, A.; Sugiura, M.; Kaila, V. R. I.; Rutherford, A. W. The Low Spin - High Spin Equilibrium in the S2-State of the Water Oxidizing Enzyme. *Biochim. Biophys. Acta BBA - Bioenerg.* **2018**, *1859*, 342−356.

(88) Boussac, A.; Girerd, J.-J.; Rutherford, A. W. Conversion of the Spin State of the Manganese Complex in Photosystem II Induced by Near-Infrared Light. *Biochemistry* **1996**, *35*, 6984−6989.

(89) Krewald, V.; Retegan, M.; Cox, N.; Messinger, J.; Lubitz, W.; DeBeer, S.; Neese, F.; Pantazis, D. A. Metal Oxidation States in Biological Water Splitting. *Chem. Sci.* **2015**, *6*, 1676−1695.

(90) Chrysina, M.; Heyno, E.; Kutin, Y.; Reus, M.; Nilsson, H.; Nowaczyk, M. M.; DeBeer, S.; Neese, F.; Messinger, J.; Lubitz, W.; Cox, N. Five-Coordinate Mn IV Intermediate in the Activation of Nature's Water Splitting Cofactor. *Proc. Natl. Acad. Sci. U. S. A.* **2019**, *116*, 16841−16846.

(91) Cox, N.; Pantazis, D. A.; Neese, F.; Lubitz, W. Biological Water Oxidation. *Acc. Chem. Res.* **2013**, *46*, 1588−1596.

(92) Noguchi, T.; Sugiura, M. Flash-Induced FTIR Difference Spectra of the Water Oxidizing Complex in Moderately Hydrated Photosystem II Core Films: Effect of Hydration Extent on S-State Transitions. *Biochemistry* **2002**, *41*, 2322−2330.

(93) Siegbahn, P. E. M. Water Oxidation Mechanism in Photosystem II, Including Oxidations, Proton Release Pathways, O−−−O Bond Formation and O2 Release. *Biochim. Biophys. Acta BBA - Bioenerg.* **2013**, *1827*, 1003−1019.

(94) Suga, M.; Akita, F.; Yamashita, K.; Nakajima, Y.; Ueno, G.; Li, H.; Yamane, T.; Hirata, K.; Umena, Y.; Yonekura, S.; Yu, L.-J.; Murakami, H.; Nomura, T.; Kimura, T.; Kubo, M.; Baba, S.; Kumasaka, T.; Tono, K.; Yabashi, M.; Isobe, H.; Yamaguchi, K.; Yamamoto, M.; Ago, H.; Shen, J.-R. An Oxyl/Oxo Mechanism for Oxygen-Oxygen Coupling in PSII Revealed by an x-Ray Free-Electron Laser. *Science* **2019**, *366*, 334−338.

(95) Gao, Y.; Åkermark, T.; Liu, J.; Sun, L.; Åkermark, B. Nucleophilic Attack of Hydroxide on a Mn V Oxo Complex: A Model of the O−O Bond Formation in the Oxygen Evolving Complex of Photosystem II. *J. Am. Chem. Soc.* **2009**, *131*, 8726−8727.

(96) Kim, S. H.; Park, H.; Seo, M. S.; Kubo, M.; Ogura, T.; Klajn, J.; Gryko, D. T.; Valentine, J. S.; Nam, W. Reversible O−O Bond Cleavage and Formation between Mn(IV)-Peroxo and Mn(V)-Oxo Corroles. *J. Am. Chem. Soc.* **2010**, *132*, 14030−14032.

(97) Bao, H.; Burnap, R. L. Structural Rearrangements Preceding Dioxygen Formation by the Water Oxidation Complex of Photosystem II. *Proc. Natl. Acad. Sci. U. S. A.* **2015**, *112*, E6139−E6147.

(98) Siegbahn, P. E. M. Recent Theoretical Studies of Water Oxidation in Photosystem II. *J. Photochem. Photobiol., B* **2011**, *104*, 94−99.

(99) McEvoy, J. P.; Brudvig, G. W. Water-Splitting Chemistry of Photosystem II. *Chem. Rev.* **2006**, *106*, 4455−4483.

(100) Siegbahn, P. E. M. The Effect of Backbone Constraints: The Case of Water Oxidation by the Oxygen-Evolving Complex in PSII. *ChemPhysChem* **2011**, *12*, 3274−3280.

(101) Siegbahn, P. E. M. Nucleophilic Water Attack Is Not a Possible Mechanism for O−O Bond Formation in Photosystem II. *Proc. Natl. Acad. Sci. U. S. A.* **2017**, *114*, 4966−4968.

(102) Li, X.-C.; Li, J.; Siegbahn, P. E. M. A Theoretical Study of the Recently Suggested Mn VII Mechanism for O−O Bond Formation in Photosystem II. *J. Phys. Chem. A* **2020**, *124*, 8011−8018.

(103) Guo, Y.; Messinger, J.; Kloo, L.; Sun, L. Alternative Mechanism for O 2 Formation in Natural Photosynthesis via Nucleophilic Oxo−Oxo Coupling. *J. Am. Chem. Soc.* **2023**, *145*, 4129−4141.

(104) Krewald, V.; Neese, F.; Pantazis, D. A. Implications of Structural Heterogeneity for the Electronic Structure of the Final Oxygen-Evolving Intermediate in Photosystem II. *J. Inorg. Biochem.* **2019**, *199*, No. 110797.

(105) Renger, G. Mechanism of Light Induced Water Splitting in Photosystem II of Oxygen Evolving Photosynthetic Organisms. *Biochim. Biophys. Acta BBA - Bioenerg.* **2012**, *1817*, 1164−1176.

(106) Corry, T. A.; O'Malley, P. J. Evidence of O−O Bond Formation in the Final Metastable S 3 State of Nature's Water Oxidizing Complex Implying a Novel Mechanism of Water Oxidation. *J. Phys. Chem. Lett.* **2018**, *9*, 6269−6274.

(107) Corry, T. A.; O'Malley, P. J. Electronic−Level View of O−O Bond Formation in Nature's Water Oxidizing Complex. *J. Phys. Chem. Lett.* **2020**, *11*, 4221−4225.

(108) Shoji, M.; Isobe, H.; Shigeta, Y.; Nakajima, T.; Yamaguchi, K. Nonadiabatic One-Electron Transfer Mechanism for the O−O Bond Formation in the Oxygen-Evolving Complex of Photosystem II. *Chem. Phys. Lett.* **2018**, *698*, 138−146.

(109) Pushkar, Y.; Davis, K. M.; Palenik, M. C. Model of the Oxygen Evolving Complex Which Is Highly Predisposed to O−O Bond Formation. *J. Phys. Chem. Lett.* **2018**, *9*, 3525−3531.

(110) Armstrong, F. A. Why Did Nature Choose Manganese to Make Oxygen? *Philos. Trans. R. Soc. B Biol. Sci.* **2008**, *363*, 1263−1270.

(111) Dau, H.; Haumann, M. Eight Steps Preceding O−O Bond Formation in Oxygenic Photosynthesis—A Basic Reaction Cycle of the Photosystem II Manganese Complex. *Biochim. Biophys. Acta BBA - Bioenerg.* **2007**, *1767*, 472−483.

(112) Jensen, S. C.; Davis, K. M.; Sullivan, B.; Hartzler, D. A.; Seidler, G. T.; Casa, D. M.; Kasman, E.; Colmer, H. E.; Massie, A. A.; Jackson, T. A.; Pushkar, Y. X-Ray Emission Spectroscopy of Biomimetic Mn Coordination Complexes. *J. Phys. Chem. Lett.* **2017**, *8*, 2584−2589.

(113) Koppenol, W. H.; Stanbury, D. M.; Bounds, P. L. Electrode Potentials of Partially Reduced Oxygen Species, from Dioxygen to Water. *Free Radic. Biol. Med.* **2010**, *49*, 317−322.

(114) Pantazis, D. A. Missing Pieces in the Puzzle of Biological Water Oxidation. *ACS Catal.* **2018**, *8*, 9477−9507.

(115) Dau, H.; Limberg, C.; Reier, T.; Risch, M.; Roggan, S.; Strasser, P. The Mechanism of Water Oxidation: From Electrolysis via Homogeneous to Biological Catalysis. *ChemCatChem.* **2010**, *2*, 724−761.

(116) Maayan, G.; Gluz, N.; Christou, G. A Bioinspired Soluble Manganese Cluster as a Water Oxidation Electrocatalyst with Low Overpotential. *Nat. Catal.* **2018**, *1*, 48−54.

(117) Paille, G.; Gomez-Mingot, M.; Roch-Marchal, C.; Lassalle-Kaiser, B.; Mialane, P.; Fontecave, M.; Mellot-Draznieks, C.; Dolbecq, A. A Fully Noble Metal-Free Photosystem Based on Cobalt-

Polyoxometalates Immobilized in a Porphyrinic Metal−Organic Framework for Water Oxidation. *J. Am. Chem. Soc.* **2018**, *140*, 3613−3618.

(118) Bergner, M.; Roy, L.; Dechert, S.; Neese, F.; Ye, S.; Meyer, F. Ligand Rearrangements at Fe/S Cofactors: Slow Isomerization of a Biomimetic [2Fe-2S] Cluster. *Angew. Chem., Int. Ed.* **2017**, *56*, 4882−4886.

(119) Elizarova, G. L.; Zhidomirov, G. M.; Parmon, V. N. Hydroxides of Transition Metals as Artificial Catalysts for Oxidation of Water to Dioxygen. *Catal. Today* **2000**, *58*, 71−88.

(120) Li, X.; Siegbahn, P. E. M. Water Oxidation Mechanism for Synthetic Co-Oxides with Small Nuclearity. *J. Am. Chem. Soc.* **2013**, *135*, 13804−13813.

(121) Roy, L. Theoretical Identification of the Factors Governing the Reactivity of C−H Bond Activation by Non-Heme Iron(IV)-Oxo Complexes. *ChemPlusChem.* **2019**, *84*, 893−906.

(122) Roy, L. Theoretical Insights into the Nature of Oxidant and Mechanism in the Regioselective *Syn* -Dihydroxylation of an Alkene with a Rieske Oxygenase Inspired Iron Catalyst. *ChemCatChem.* **2018**, *10*, 3683−3688.

(123) Siegbahn, P. E. M. O=O Bond Formation in the S4 State of the Oxygen-Evolving Complex in Photosystem II. *Chem.—Eur. J.* **2006**, *12*, 9217−9227.

(124) Pecoraro, V. L.; Baldwin, M. J.; Caudle, M. T.; Hsieh, W.-Y.; Law, N. A. A Proposal for Water Oxidation in Photosystem II. *Pure Appl. Chem.* **1998**, *70*, 925−929.

(125) Lee, C.-I.; Lakshmi, K. V.; Brudvig, G. W. Probing the Functional Role of Ca $^{2+}$ in the Oxygen-Evolving Complex of Photosystem II by Metal Ion Inhibition. *Biochemistry* **2007**, *46*, 3211−3223.

(126) Limburg, J.; Szalai, V. A.; Brudvig, G. W. A Mechanistic and Structural Model for the Formation and Reactivity of a MnV=O Species in Photosynthetic Water Oxidation. *J. Chem. Soc., Dalton Trans.* **1999**, No. 9, 1353−1362.

(127) Polander, B. C.; Barry, B. A. A Hydrogen-Bonding Network Plays a Catalytic Role in Photosynthetic Oxygen Evolution. *Proc. Natl. Acad. Sci. U. S. A.* **2012**, *109*, 6112−6117.

(128) Askerka, M.; Brudvig, G. W.; Batista, V. S. The O $_2$ -Evolving Complex of Photosystem II: Recent Insights from Quantum Mechanics/Molecular Mechanics (QM/MM), Extended X-Ray Absorption Fine Structure (EXAFS), and Femtosecond X-Ray Crystallography Data. *Acc. Chem. Res.* **2017**, *50*, 41−48.

(129) Wei, R. J.; Zhang, Y.; Mao, J.; Kaur, D.; Khaniya, U.; Gunner, M. R. Comparison of Proton Transfer Paths to the QA and QB Sites of the Rb. Sphaeroides Photosynthetic Reaction Centers. *Photosynth. Res.* **2022**, *152*, 153−165.

(130) Hillier, W.; Hendry, G.; Burnap, R. L.; Wydrzynski, T. Substrate Water Exchange in Photosystem II Depends on the Peripheral Proteins. *J. Biol. Chem.* **2001**, *276*, 46917−46924.

(131) Service, R. J.; Yano, J.; McConnell, I.; Hwang, H. J.; Niks, D.; Hille, R.; Wydrzynski, T.; Burnap, R. L.; Hillier, W.; Debus, R. J. Participation of Glutamate-354 of the CP43 Polypeptide in the Ligation of Manganese and the Binding of Substrate Water in Photosystem II. *Biochemistry* **2011**, *50*, 63−81.

(132) Nilsson, H.; Rappaport, F.; Boussac, A.; Messinger, J. Substrate−Water Exchange in Photosystem II Is Arrested before Dioxygen Formation. *Nat. Commun.* **2014**, *5*, 4305.

(133) Gersten, S. W.; Samuels, G. J.; Meyer, T. J. Catalytic Oxidation of Water by an Oxo-Bridged Ruthenium Dimer. *J. Am. Chem. Soc.* **1982**, *104*, 4029−4030.

(134) Gagliardi, C. J.; Vannucci, A. K.; Concepcion, J. J.; Chen, Z.; Meyer, T. J. The Role of Proton Coupled Electron Transfer in Water Oxidation. *Energy Environ. Sci.* **2012**, *5*, 7704−7717.

(135) Boyer, J. L.; Rochford, J.; Tsai, M.-K.; Muckerman, J. T.; Fujita, E. Ruthenium Complexes with Non-Innocent Ligands: Electron Distribution and Implications for Catalysis. *Coord. Chem. Rev.* **2010**, *254*, 309−330.

(136) Garrido-Barros, P.; Funes-Ardoiz, I.; Drouet, S.; Benet-Buchholz, J.; Maseras, F.; Llobet, A. Redox Non-Innocent Ligand

Controls Water Oxidation Overpotential in a New Family of Mononuclear Cu-Based Efficient Catalysts. *J. Am. Chem. Soc.* **2015**, *137*, 6758−6761.

(137) Chattopadhyay, S.; Ghatak, A.; Ro, Y.; Guillot, R.; Halime, Z.; Aukauloo, A.; Dey, A. Ligand Radical Mediated Water Oxidation by a Family of Copper O-Phenylene Bis-Oxamidate Complexes. *Inorg. Chem.* **2021**, *60*, 9442−9455.

(138) Gil-Sepulcre, M.; Garrido-Barros, P.; Oldengott, J.; Funes-Ardoiz, I.; Bofill, R.; Sala, X.; Benet-Buchholz, J.; Llobet, A. Consecutive Ligand-Based Electron Transfer in New Molecular Copper-Based Water Oxidation Catalysts. *Angew. Chem., Int. Ed.* **2021**, *60*, 18639−18644.

(139) Hessels, J.; Detz, R. J.; Koper, M. T. M.; Reek, J. N. H. Rational Design Rules for Molecular Water Oxidation Catalysts Based on Scaling Relationships. *Chem.—Eur. J.* **2017**, *23*, 16413−16418.

(140) Sens, C.; Romero, I.; Rodríguez, M.; Llobet, A.; Parella, T.; Benet-Buchholz, J. A New Ru Complex Capable of Catalytically Oxidizing Water to Molecular Dioxygen. *J. Am. Chem. Soc.* **2004**, *126*, 7798−7799.

(141) Duan, L.; Fischer, A.; Xu, Y.; Sun, L. Isolated Seven-Coordinate Ru(IV) Dimer Complex with [HOHOH]- Bridging Ligand as an Intermediate for Catalytic Water Oxidation. *J. Am. Chem. Soc.* **2009**, *131*, 10397−10399.

(142) Duan, L.; Araujo, C. M.; Ahlquist, M. S. G.; Sun, L. Highly Efficient and Robust Molecular Ruthenium Catalysts for Water Oxidation. *Proc. Natl. Acad. Sci. U. S. A.* **2012**, *109*, 15584−15588.

(143) Wang, L.; Duan, L.; Wang, Y.; Ahlquist, M. S. G.; Sun, L. Highly Efficient and Robust Molecular Water Oxidation Catalysts Based on Ruthenium Complexes. *Chem. Commun.* **2014**, *50*, 12947−12950.

(144) Gilbert, J. A.; Eggleston, D. S.; Murphy, W. R.; Geselowitz, D. A.; Gersten, S. W.; Hodgson, D. J.; Meyer, T. J. Structure and Redox Properties of the Water-Oxidation Catalyst [(Bpy)2(OH2)RuORu-(OH2)(Bpy)2]4+. *J. Am. Chem. Soc.* **1985**, *107*, 3855−3864.

(145) Nagoshi, K.; Yamashita, S.; Yagi, M.; Kaneko, M. Catalytic Activity of [(Bpy)2(H2O)Ru−O−Ru(H2O)(Bpy)2]4+ for Four-Electron Water Oxidation. *J. Mol. Catal. Chem.* **1999**, *144*, 71−76.

(146) Collin, J. P.; Sauvage, J. P. Synthesis and Study of Mononuclear Ruthenium(II) Complexes of Sterically Hindering Diimine Chelates. Implications for the Catalytic Oxidation of Water to Molecular Oxygen. *Inorg. Chem.* **1986**, *25*, 135−141.

(147) Binstead, R. A.; Chronister, C. W.; Ni, J.; Hartshorn, C. M.; Meyer, T. J. Mechanism of Water Oxidation by the μ-Oxo Dimer [(Bpy) $_2$ (H $_2$ O)Ru ^{III} ORu ^{III} (OH $_2$)(Bpy) $_2$] $^{4+}$. *J. Am. Chem. Soc.* **2000**, *122*, 8464−8473.

(148) Clark, A. E.; Hurst, J. K. Mechanisms of Water Oxidation Catalyzed by Ruthenium Coordination Complexes. In *Progress in Inorganic Chemistry*; Karlin, K. D., Ed.; Wiley, 2011; Vol. 57, pp 1−54. DOI: 10.1002/9781118148235.ch1

(149) Hurst, J. K.; Zhou, J.; Lei, Y. Pathways for Water Oxidation Catalyzed by the (.Mu.-Oxo)Bis[Aquabis(Bipyridine)Ruthenium]-(4+) Ion. *Inorg. Chem.* **1992**, *31*, 1010−1017.

(150) Liu, F.; Concepcion, J. J.; Jurss, J. W.; Cardolaccia, T.; Templeton, J. L.; Meyer, T. J. Mechanisms of Water Oxidation from the Blue Dimer to Photosystem II. *Inorg. Chem.* **2008**, *47*, 1727−1752.

(151) Yang, X.; Baik, M.-H. *Cis,Cis*-[(Bpy)$_2$RuVO]$_2$O^{4+} Catalyzes Water Oxidation Formally via *in Situ* Generation of Radicaloid Ru^{IV}−O$^{•}$. *J. Am. Chem. Soc.* **2006**, *128*, 7476−7485.

(152) Li, X.; Chen, G.; Schinzel, S.; Siegbahn, P. E. M. A Comparison between Artificial and Natural Water Oxidation. *Dalton Trans.* **2011**, *40*, 11296−11307.

(153) Richmond, C. J.; Matheu, R.; Poater, A.; Falivene, L.; Benet-Buchholz, J.; Sala, X.; Cavallo, L.; Llobet, A. Supramolecular Water Oxidation with Ru-Bda-Based Catalysts. *Chem.—Eur. J.* **2014**, *20*, 17282−17286.

(154) Concepcion, J. J.; Tsai, M.-K.; Muckerman, J. T.; Meyer, T. J. Mechanism of Water Oxidation by Single-Site Ruthenium Complex Catalysts. *J. Am. Chem. Soc.* **2010**, *132*, 1545−1557.

(155) Kaveevivitchai, N.; Zong, R.; Tseng, H.-W.; Chitta, R.; Thummel, R. P. Further Observations on Water Oxidation Catalyzed by Mononuclear Ru(II) Complexes. *Inorg. Chem.* **2012**, *51*, 2930−2939.

(156) Nyhlén, J.; Duan, L.; Åkermark, B.; Sun, L.; Privalov, T. Evolution of O2 in a Seven-Coordinate RuIV Dimer Complex with a [HOHOH]- Bridge: A Computational Study. *Angew. Chem. - Int. Ed.* **2010**, *49*, 1773−1777.

(157) McDaniel, N. D.; Coughlin, F. J.; Tinker, L. L.; Bernhard, S. Cyclometalated Iridium(III) Aquo Complexes: Efficient and Tunable Catalysts for the Homogeneous Oxidation of Water. *J. Am. Chem. Soc.* **2008**, *130*, 210−217.

(158) Hull, J. F.; Balcells, D.; Blakemore, J. D.; Incarvito, C. D.; Eisenstein, O.; Brudvig, G. W.; Crabtree, R. H. Highly Active and Robust Cp* Iridium Complexes for Catalytic Water Oxidation. *J. Am. Chem. Soc.* **2009**, *131*, 8730−8731.

(159) Li, M.; Takada, K.; Goldsmith, J. I.; Bernhard, S. Iridium(III) Bis-Pyridine-2-Sulfonamide Complexes as Efficient and Durable Catalysts for Homogeneous Water Oxidation. *Inorg. Chem.* **2016**, *55*, 518−526.

(160) Sharninghausen, L. S.; Sinha, S. B.; Shopov, D. Y.; Choi, B.; Mercado, B. Q.; Roy, X.; Balcells, D.; Brudvig, G. W.; Crabtree, R. H. High Oxidation State Iridium Mono-*μ*-Oxo Dimers Related to Water Oxidation Catalysis. *J. Am. Chem. Soc.* **2016**, *138*, 15917−15926.

(161) Vilella, L.; Vidossich, P.; Balcells, D.; Lledós, A. Basic Ancillary Ligands Promote O−O Bond Formation in Iridium-Catalyzed Water Oxidation: A DFT Study. *Dalton Trans.* **2011**, *40*, 11241−11247.

(162) Hull, J. F.; Balcells, D.; Blakemore, J. D.; Incarvito, C. D.; Eisenstein, O.; Brudvig, G. W.; Crabtree, R. H. Highly Active and Robust Cp* Iridium Complexes for Catalytic Water Oxidation. *J. Am. Chem. Soc.* **2009**, *131*, 8730−8731.

(163) Blakemore, J. D.; Schley, N. D.; Balcells, D.; Hull, J. F.; Olack, G. W.; Incarvito, C. D.; Eisenstein, O.; Brudvig, G. W.; Crabtree, R. H. Half-Sandwich Iridium Complexes for Homogeneous Water-Oxidation Catalysis. *J. Am. Chem. Soc.* **2010**, *132*, 16017−16029.

(164) Brewster, T. P.; Blakemore, J. D.; Schley, N. D.; Incarvito, C. D.; Hazari, N.; Brudvig, G. W.; Crabtree, R. H. An Iridium(IV) Species, [Cp*Ir(NHC)Cl]⁺, Related to a Water-Oxidation Catalyst. *Organometallics* **2011**, *30*, 965−973.

(165) Navarro, M.; Smith, C. A.; Li, M.; Bernhard, S.; Albrecht, M. Optimization of Synthetically Versatile Pyridylidene Amide Ligands for Efficient Iridium-Catalyzed Water Oxidation. *Chem. − Eur. J.* **2018**, *24*, 6386−6398.

(166) Lalrempuia, R.; McDaniel, N. D.; Müller-Bunz, H.; Bernhard, S.; Albrecht, M. Water Oxidation Catalyzed by Strong Carbene-Type Donor-Ligand Complexes of Iridium. *Angew. Chem., Int. Ed.* **2010**, *49*, 9765−9768.

(167) Hintermair, U.; Sheehan, S. W.; Parent, A. R.; Ess, D. H.; Richens, D. T.; Vaccaro, P. H.; Brudvig, G. W.; Crabtree, R. H. Precursor Transformation during Molecular Oxidation Catalysis with Organometallic Iridium Complexes. *J. Am. Chem. Soc.* **2013**, *135*, 10837−10851.

(168) Hu, G.; Troiano, J. L.; Tayvah, U. T.; Sharninghausen, L. S.; Sinha, S. B.; Shopov, D. Y.; Mercado, B. Q.; Crabtree, R. H.; Brudvig, G. W. Accessing Molecular Dimeric Ir Water Oxidation Catalysts from Coordination Precursors. *Inorg. Chem.* **2021**, *60*, 14349−14356.

(169) Crabtree, R. H. Resolving Heterogeneity Problems and Impurity Artifacts in Operationally Homogeneous Transition Metal Catalysts. *Chem. Rev.* **2012**, *112*, 1536−1554.

(170) Wang, C.; Xie, Z.; deKrafft, K. E.; Lin, W. Doping Metal−Organic Frameworks for Water Oxidation, Carbon Dioxide Reduction, and Organic Photocatalysis. *J. Am. Chem. Soc.* **2011**, *133*, 13445−13454.

(171) Paul, S.; Neese, F.; Pantazis, D. A. Structural Models of the Biological Oxygen-Evolving Complex: Achievements, Insights, and Challenges for Biomimicry. *Green Chem.* **2017**, *19*, 2309−2325.

(172) Wieghardt, K.; Bossek, U.; Gebert, W. Synthesis of a Tetranuclear Manganese(IV) Cluster with Adamantane Skeleton: [(C6H15N3)4Mn4O6]4+. *Angew. Chem., Int. Ed. Engl.* **1983**, *22*, 328−329.

(173) Dubé, C. E.; Mukhopadhyay, S.; Bonitatebus, P. J., Jr.; Staples, R. J.; Armstrong, W. H. Tuning Tetranuclear Manganese−Oxo Core Electronic Properties: Adamantane-Shaped Complexes Synthesized by Ligand Exchange. *Inorg. Chem.* **2005**, *44*, 5161−5175.

(174) Ruettinger, W. F.; Campana, C.; Dismukes, G. C. Synthesis and Characterization of Mn₄O₄L₆ Complexes with Cubane-like Core Structure: A New Class of Models of the Active Site of the Photosynthetic Water Oxidase. *J. Am. Chem. Soc.* **1997**, *119*, 6670−6671.

(175) Vincent, J. B.; Christmas, C.; Huffman, J. C.; Christou, G.; Chang, H.-R.; Hendrickson, D. N. Modelling the Photosynthetic Water Oxidation Centre: Synthesis, Structure, and Magnetic Properties of [Mn4O2(OAc)7(Biphy)2ClO4]3H2O (Bipy = 2,2′-Bipyridine). *J. Chem. Soc. Chem. Commun.* **1987**, No. 4, 236−238.

(176) Kanady, J. S.; Tsui, E. Y.; Day, M. W.; Agapie, T. A Synthetic Model of the Mn₃Ca Subsite of the Oxygen-Evolving Complex in Photosystem II. *Science* **2011**, *333*, 733−736.

(177) Zhang, C.; Chen, C.; Dong, H.; Shen, J.-R.; Dau, H.; Zhao, J. A Synthetic Mn₄Ca-Cluster Mimicking the Oxygen-Evolving Center of Photosynthesis. *Science* **2015**, *348*, 690−693.

(178) Gerey, B.; Gouré, E.; Fortage, J.; Pécaut, J.; Collomb, M.-N. Manganese-Calcium/Strontium Heterometallic Compounds and Their Relevance for the Oxygen-Evolving Center of Photosystem II. *Coord. Chem. Rev.* **2016**, *319*, 1−24.

(179) Mathe, Z.; Pantazis, D. A.; Lee, H. B.; Gnewkow, R.; Van Kuiken, B. E.; Agapie, T.; DeBeer, S. Calcium Valence-to-Core X-Ray Emission Spectroscopy: A Sensitive Probe of Oxo Protonation in Structural Models of the Oxygen-Evolving Complex. *Inorg. Chem.* **2019**, *58*, 16292−16301.

(180) Kanady, J. S.; Lin, P.-H.; Carsch, K. M.; Nielsen, R. J.; Takase, M. K.; Goddard, W. A.; Agapie, T. Toward Models for the Full Oxygen-Evolving Complex of Photosystem II by Ligand Coordination To Lower the Symmetry of the Mn₃CaO₄ Cubane: Demonstration That Electronic Effects Facilitate Binding of a Fifth Metal. *J. Am. Chem. Soc.* **2014**, *136*, 14373−14376.

(181) Zhang, C.; Chen, C.; Dong, H.; Shen, J. R.; Dau, H.; Zhao, J. A Synthetic Mn4Ca-Cluster Mimicking the Oxygen-Evolving Center of Photosynthesis. *Science* **2015**, *348*, 690−693.

(182) Paul, S.; Cox, N.; Pantazis, D. A. What Can We Learn from a Biomimetic Model of Nature's Oxygen-Evolving Complex? *Inorg. Chem.* **2017**, *56*, 3875−3888.

(183) Johansson, A.; Abrahamsson, M.; Magnuson, A.; Huang, P.; Mårtensson, J.; Styring, S.; Hammarström, L.; Sun, L.; Åkermark, B. Synthesis and Photophysics of One Mononuclear Mn(III) and One Dinuclear Mn(III,III) Complex Covalently Linked to a Ruthenium-(II) Tris(Bipyridyl) Complex. *Inorg. Chem.* **2003**, *42*, 7502−7511.

(184) Naruta, Y.; Sasayama, M.-a.; Sasaki, T. Oxygen Evolution by Oxidation of Water with Manganese Porphyrin Dimers. *Angew. Chem., Int. Ed. Engl.* **1994**, *33*, 1839−1841.

(185) Blackman, A. G.; Huffman, J. C.; Lobkovsky, E. B.; Christou, G. Towards Functional Models of the Photosynthetic Water Oxidation Centre: Synthesis and Structure of the Asymmetric Complex [Mn2O(O2CMe)2(Bpy)2(H2O)(S2O8)]·H2O (Bpy = 2,2′-Bipyridine), Containing Coordinated H2O and S2O8²⁻. *J. Chem. Soc. Chem. Commun.* **1991**, No. 15, 989−991.

(186) Collomb, M.-N.; Deronzier, A.; Richardot, A.; Pe′caut, J. Synthesis and Characterization of a New Kind of Mn2III,IV *μ*-Oxo Complex: [Mn2O2(Terpy)2(H2O)2](NO3)3·6H2O, Terpy = 2,2′:6′,2″-Terpyridine. *New J. Chem.* **1999**, *23*, 351−354.

(187) Ruiz, R.; Sangregorio, C.; Caneschi, A.; Rossi, P.; Gaspar, A. B.; Real, J. A.; Muñoz, M. C. A Novel Dimer of Oxo-Di(Acetato)-Bridged Manganese(III) Dimers Complex of Potential Biological Significance. *Inorg. Chem. Commun.* **2000**, *3*, 361−367.

(188) Kärkäs, M. D.; Johnston, E. V.; Verho, O.; Åkermark, B. Artificial Photosynthesis: From Nanosecond Electron Transfer to Catalytic Water Oxidation. *Acc. Chem. Res.* **2014**, *47*, 100−111.

(189) Shimazaki, Y.; Nagano, T.; Takesue, H.; Ye, B.-H.; Tani, F.; Naruta, Y. Characterization of a Dinuclear MnV=O Complex and Its Efficient Evolution of O₂ in the Presence of Water. *Angew. Chem., Int. Ed.* **2004**, *43*, 98−100.

(190) Lundberg, M.; Blomberg, M. R. A.; Siegbahn, P. E. M. Oxyl Radical Required for O−O Bond Formation in Synthetic Mn-Catalyst. *Inorg. Chem.* **2004**, *43*, 264−274.

(191) Limburg, J.; Vrettos, J. S.; Liable-Sands, L. M.; Rheingold, A. L.; Crabtree, R. H.; Brudvig, G. W. A Functional Model for O-O Bond Formation by the O₂-Evolving Complex in Photosystem II. *Science* **1999**, *283*, 1524−1527.

(192) Limburg, J.; Vrettos, J. S.; Chen, H.; De Paula, J. C.; Crabtree, R. H.; Brudvig, G. W. Characterization of the O₂-Evolving Reaction Catalyzed by [(Terpy)(H₂O)Mn^III^(O)₂Mn^IV^(OH₂)(Terpy)](NO₃)₃ (Terpy = 2,2′:6,2″-Terpyridine). *J. Am. Chem. Soc.* **2001**, *123*, 423−430.

(193) Young, K. J.; Brennan, B. J.; Tagore, R.; Brudvig, G. W. Photosynthetic Water Oxidation: Insights from Manganese Model Chemistry. *Acc. Chem. Res.* **2015**, *48*, 567−574.

(194) Seidler-Egdal, R. K.; Nielsen, A.; Bond, A. D.; Bjerrum, M. J.; McKenzie, C. J. High Turnover Catalysis of Water Oxidation by Mn(II) Complexes of Monoanionic Pentadentate Ligands. *Dalton Trans.* **2011**, *40*, 3849−3858.

(195) Baffert, C.; Collomb, M.-N.; Deronzier, A.; Kjærgaard-Knudsen, S.; Latour, J.-M.; Lund, K. H.; McKenzie, C. J.; Mortensen, M.; Nielsen, L. P.; Thorup, N. Biologically Relevant Mono- and Di-Nuclear Manganese II/III/IV Complexes of Mono-negative Pentadentate Ligands. *Dalton Trans.* **2003**, No. 9, 1765−1772.

(196) Sameera, W. M. C.; McKenzie, C. J.; McGrady, J. E. On the Mechanism of Water Oxidation by a Bimetallic Manganese Catalyst: A Density Functional Study. *Dalton Trans.* **2011**, *40*, 3859−3870.

(197) Rardin, R. L.; Tolman, W. B.; Lippard, S. J. Monodentate Carboxylate Complexes and The Carboxylate Shift: Implications for Polymetalloprotein Structure and Function. *New J. Chem.* **1991**, *15*, 417−430.

(198) Ellis, W. C.; McDaniel, N. D.; Bernhard, S.; Collins, T. J. Fast Water Oxidation Using Iron. *J. Am. Chem. Soc.* **2010**, *132*, 10990−10991.

(199) Liu, T.; Zhang, B.; Sun, L. Iron-Based Molecular Water Oxidation Catalysts: Abundant, Cheap, and Promising. *Chem.—Asian J.* **2019**, *14*, 31−43.

(200) Ertem, M. Z.; Gagliardi, L.; Cramer, C. J. Quantum Chemical Characterization of the Mechanism of an Iron-Based Water Oxidation Catalyst. *Chem. Sci.* **2012**, *3*, 1293−1299.

(201) Liao, R.; Li, X.; Siegbahn, P. E. M. Reaction Mechanism of Water Oxidation Catalyzed by Iron Tetraamido Macrocyclic Ligand Complexes − A DFT Study. *Eur. J. Inorg. Chem.* **2014**, *2014*, 728−741.

(202) Liao, R. Z.; Siegbahn, P. E. M. Quantum Chemical Modeling of Homogeneous Water Oxidation Catalysis. *ChemSusChem* **2017**, *10*, 4236−4263.

(203) Fillol, J. L.; Codolà, Z.; Garcia-Bosch, I.; Gómez, L.; Pla, J. J.; Costas, M. Efficient Water Oxidation Catalysts Based on Readily Available Iron Coordination Complexes. *Nat. Chem.* **2011**, *3*, 807−813.

(204) Codolà, Z.; Garcia-Bosch, I.; Acuña-Parés, F.; Prat, I.; Luis, J. M.; Costas, M.; Lloret-Fillol, J. Electronic Effects on Single-Site Iron Catalysts for Water Oxidation. *Chem.—Eur. J.* **2013**, *19*, 8042−8047.

(205) Coggins, M. K.; Zhang, M.-T.; Vannucci, A. K.; Dares, C. J.; Meyer, T. J. Electrocatalytic Water Oxidation by a Monomeric Amidate-Ligated Fe(III)−Aqua Complex. *J. Am. Chem. Soc.* **2014**, *136*, 5531−5534.

(206) Kanan, M. W.; Yano, J.; Surendranath, Y.; Dincă, M.; Yachandra, V. K.; Nocera, D. G. Structure and Valency of a Cobalt−Phosphate Water Oxidation Catalyst Determined by in Situ X-ray Spectroscopy. *J. Am. Chem. Soc.* **2010**, *132*, 13692−13701.

(207) Wasylenko, D. J.; Ganesamoorthy, C.; Borau-Garcia, J.; Berlinguette, C. P. Electrochemical Evidence for Catalytic Water

Oxidation Mediated by a High-Valent Cobalt Complex. *Chem. Commun.* **2011**, *47*, 4249−4251.

(208) Dogutan, D. K.; McGuire, R.; Nocera, D. G. Electrocatalytic Water Oxidation by Cobalt(III) Hangman β-Octafluoro Corroles. *J. Am. Chem. Soc.* **2011**, *133*, 9178−9180.

(209) Fukuzumi, S.; Mandal, S.; Mase, K.; Ohkubo, K.; Park, H.; Benet-Buchholz, J.; Nam, W.; Llobet, A. Catalytic Four-Electron Reduction of O₂ via Rate-Determining Proton-Coupled Electron Transfer to a Dinuclear Cobalt-μ-1,2-Peroxo Complex. *J. Am. Chem. Soc.* **2012**, *134*, 9906−9909.

(210) Rigsby, M. L.; Mandal, S.; Nam, W.; Spencer, L. C.; Llobet, A.; Stahl, S. S. Cobalt Analogs of Ru-Based Water Oxidation Catalysts: Overcoming Thermodynamic Instability and Kinetic Lability to Achieve Electrocatalytic O₂ Evolution. *Chem. Sci.* **2012**, *3*, 3058−3062.

(211) Hadt, R. G.; Hayes, D.; Brodsky, C. N.; Ullman, A. M.; Casa, D. M.; Upton, M. H.; Nocera, D. G.; Chen, L. X. X-Ray Spectroscopic Characterization of Co(IV) and Metal−Metal Interactions in Co₄O₄: Electronic Structure Contributions to the Formation of High-Valent States Relevant to the Oxygen Evolution Reaction. *J. Am. Chem. Soc.* **2016**, *138*, 11017−11030.

(212) Crandell, D. W.; Ghosh, S.; Berlinguette, C. P.; Baik, M.-H. How a [Co^IV^−O]²⁺ Fragment Oxidizes Water: Involvement of a Biradicaloid [Co^II^−(O)]²⁺ Species in Forming the O−O Bond. *ChemSusChem* **2015**, *8*, 844−852.

(213) Gimbert-Suriñach, C.; Moonshiram, D.; Francàs, L.; Planas, N.; Bernales, V.; Bozoglian, F.; Guda, A.; Mognon, L.; López, I.; Hoque, M. A.; Gagliardi, L.; Cramer, C. J.; Llobet, A. Structural and Spectroscopic Characterization of Reaction Intermediates Involved in a Dinuclear Co−Hbpp Water Oxidation Catalyst. *J. Am. Chem. Soc.* **2016**, *138*, 15291−15294.

(214) McCool, N. S.; Robinson, D. M.; Sheats, J. E.; Dismukes, G. C. A Co₄O₄ "Cubane" Water Oxidation Catalyst Inspired by Photosynthesis. *J. Am. Chem. Soc.* **2011**, *133*, 11446−11449.

(215) McAlpin, J. G.; Surendranath, Y.; Dincă, M.; Stich, T. A.; Stoian, S. A.; Casey, W. H.; Nocera, D. G.; Britt, R. D. EPR Evidence for Co(IV) Species Produced During Water Oxidation at Neutral pH. *J. Am. Chem. Soc.* **2010**, *132*, 6882−6883.

(216) Kondo, M.; Masaoka, S. Water Oxidation Catalysts Constructed by Biorelevant First-Row Metal Complexes. *Chem. Lett.* **2016**, *45*, 1220−1231.

(217) Barnett, S. M.; Goldberg, K. I.; Mayer, J. M. A Soluble Copper−Bipyridine Water-Oxidation Electrocatalyst. *Nat. Chem.* **2012**, *4*, 498−502.

(218) Zhang, M. T.; Chen, Z.; Kang, P.; Meyer, T. J. Electrocatalytic Water Oxidation with a Copper(II) Polypeptide Complex. *J. Am. Chem. Soc.* **2013**, *135*, 2048−2051.

(219) Zhang, M.; Zhang, M.-T.; Hou, C.; Ke, Z.-F.; Lu, T.-B. Homogeneous Electrocatalytic Water Oxidation at Neutral pH by a Robust Macrocyclic Nickel(II) Complex. *Angew. Chem.* **2014**, *126*, 13258−13264.

(220) Han, Y.; Wu, Y.; Lai, W.; Cao, R. Electrocatalytic Water Oxidation by a Water-Soluble Nickel Porphyrin Complex at Neutral pH with Low Overpotential. *Inorg. Chem.* **2015**, *54*, 5604−5613.

(221) Garrido-Barros, P.; Grau, S.; Drouet, S.; Benet-Buchholz, J.; Gimbert-Surinach, C.; Llobet, A. Can Ni Complexes Behave as Molecular Water Oxidation Catalysts? *ACS Catal.* **2019**, *9*, 3936−3945.

(222) Zhang, T.; Wang, C.; Liu, S.; Wang, J.-L.; Lin, W. A Biomimetic Copper Water Oxidation Catalyst with Low Over-potential. *J. Am. Chem. Soc.* **2014**, *136*, 273−281.

(223) Gerlach, D. L.; Bhagan, S.; Cruce, A. A.; Burks, D. B.; Nieto, I.; Truong, H. T.; Kelley, S. P.; Herbst-Gervasoni, C. J.; Jernigan, K. L.; Bowman, M. K.; Pan, S.; Zeller, M.; Papish, E. T. Studies of the Pathways Open to Copper Water Oxidation Catalysts Containing Proximal Hydroxy Groups During Basic Electrocatalysis. *Inorg. Chem.* **2014**, *53*, 12689−12698.

(224) Winkler, J. R.; Gray, H. B. Electronic Structures of Oxo-Metal Ions. In *Molecular Electronic Structures of Transition Metal Complexes I*;

Mingos, D. M. P., Day, P., Dahl, J. P., Eds.; Structure and Bonding; Springer: Berlin, 2011; Vol. *142*, pp 17−28.

(225) Singh, A. K.; Roy, L. Computational Mechanistic Insights on Homogeneous Water Oxidation Versus Catalyst Deactivation: A Case Study with Mononuclear Nickel and Copper Complexes. *Eur. J. Inorg. Chem.* **2023**, *26*, No. e202300412.

(226) Chen, Z.; Concepcion, J. J.; Hu, X.; Yang, W.; Hoertz, P. G.; Meyer, T. J. Concerted O Atom−Proton Transfer in the O−O Bond Forming Step in Water Oxidation. *Proc. Natl. Acad. Sci. U. S. A.* **2010**, *107*, 7225−7229.

(227) Pap, J. S.; Szyrwiel, Ł.; Srankó, D.; Kerner, Z.; Setner, B.; Szewczuk, Z.; Malinka, W. Electrocatalytic Water Oxidation by Cu^{II} Complexes with Branched Peptides. *Chem. Commun.* **2015**, *51*, 6322−6324.

(228) Li, F.; Jiang, Y.; Zhang, B.; Huang, F.; Gao, Y.; Sun, L. Towards A Solar Fuel Device: Light-Driven Water Oxidation Catalyzed by a Supramolecular Assembly. *Angew. Chem., Int. Ed.* **2012**, *51*, 2417−2420.

(229) Frischmann, P. D.; Mahata, K.; Würthner, F. Powering the Future of Molecular Artificial Photosynthesis with Light-Harvesting Metallosupramolecular Dye Assemblies. *Chem. Soc. Rev.* **2013**, *42*, 1847−1870.

(230) Kaveevivitchai, N.; Chitta, R.; Zong, R.; El Ojaimi, M.; Thummel, R. P. A Molecular Light-Driven Water Oxidation Catalyst. *J. Am. Chem. Soc.* **2012**, *134*, 10721−10724.

(231) Vagnini, M. T.; Smeigh, A. L.; Blakemore, J. D.; Eaton, S. W.; Schley, N. D.; D'Souza, F.; Crabtree, R. H.; Brudvig, G. W.; Co, D. T.; Wasielewski, M. R. Ultrafast Photodriven Intramolecular Electron Transfer from an Iridium-Based Water-Oxidation Catalyst to Perylene Diimide Derivatives. *Proc. Natl. Acad. Sci. U. S. A.* **2012**, *109*, 15651−15656.

(232) Schulze, M.; Kunz, V.; Frischmann, P. D.; Würthner, F. A Supramolecular Ruthenium Macrocycle with High Catalytic Activity for Water Oxidation That Mechanistically Mimics Photosystem II. *Nat. Chem.* **2016**, *8*, 576−583.

(233) Duan, L.; Wang, L.; Li, F.; Li, F.; Sun, L. Highly Efficient Bioinspired Molecular Ru Water Oxidation Catalysts with Negatively Charged Backbone Ligands. *Acc. Chem. Res.* **2015**, *48*, 2084−2096.

(234) Staehle, R.; Tong, L.; Wang, L.; Duan, L.; Fischer, A.; Ahlquist, M. S. G.; Sun, L.; Rau, S. Water Oxidation Catalyzed by Mononuclear Ruthenium Complexes with a 2,2′-Bipyridine-6,6′-Dicarboxylate (Bda) Ligand: How Ligand Environment Influences the Catalytic Behavior. *Inorg. Chem.* **2014**, *53*, 1307−1319.

(235) Li, B.; Li, F.; Bai, S.; Wang, Z.; Sun, L.; Yang, Q.; Li, C. Oxygen Evolution from Water Oxidation on Molecular Catalysts Confined in the Nanocages of Mesoporous Silicas. *Energy Environ. Sci.* **2012**, *5*, 8229−8233.

(236) Li, H.; Li, F.; Zhang, B.; Zhou, X.; Yu, F.; Sun, L. Visible Light-Driven Water Oxidation Promoted by Host−Guest Interaction between Photosensitizer and Catalyst with A High Quantum Efficiency. *J. Am. Chem. Soc.* **2015**, *137*, 4332−4335.

(237) Neudeck, S.; Maji, S.; López, I.; Meyer, S.; Meyer, F.; Llobet, A. New Powerful and Oxidatively Rugged Dinuclear Ru Water Oxidation Catalyst: Control of Mechanistic Pathways by Tailored Ligand Design. *J. Am. Chem. Soc.* **2014**, *136*, 24−27.

(238) Duan, L.; Bozoglian, F.; Mandal, S.; Stewart, B.; Privalov, T.; Llobet, A.; Sun, L. A Molecular Ruthenium Catalyst with Water-Oxidation Activity Comparable to That of Photosystem II. *Nat. Chem.* **2012**, *4*, 418−423.

(239) Yang, B.; Jiang, X.; Guo, Q.; Lei, T.; Zhang, L.; Chen, B.; Tung, C.; Wu, L. Self-Assembled Amphiphilic Water Oxidation Catalysts: Control of O−O Bond Formation Pathways by Different Aggregation Patterns. *Angew. Chem., Int. Ed.* **2016**, *55*, 6229−6234.

(240) Yu, F.; Poole, D.; Mathew, S.; Yan, N.; Hessels, J.; Orth, N.; Ivanović-Burmazović, I.; Reek, J. N. H. Control over Electrochemical Water Oxidation Catalysis by Preorganization of Molecular Ruthenium Catalysts in Self-Assembled Nanospheres. *Angew. Chem., Int. Ed.* **2018**, *57*, 11247−11251.

(241) Sato, S.; Iida, J.; Suzuki, K.; Kawano, M.; Ozeki, T.; Fujita, M. Fluorous Nanodroplets Structurally Confined in an Organopalladium Sphere. *Science* **2006**, *313*, 1273−1276.

(242) Zhao, M.; Ou, S.; Wu, C.-D. Porous Metal−Organic Frameworks for Heterogeneous Biomimetic Catalysis. *Acc. Chem. Res.* **2014**, *47*, 1199−1207.

(243) Snyder, B. E. R.; Bols, M. L.; Schoonheydt, R. A.; Sels, B. F.; Solomon, E. I. Iron and Copper Active Sites in Zeolites and Their Correlation to Metalloenzymes. *Chem. Rev.* **2018**, *118*, 2718−2768.

(244) Materna, K. L.; Crabtree, R. H.; Brudvig, G. W. Anchoring Groups for Photocatalytic Water Oxidation on Metal Oxide Surfaces. *Chem. Soc. Rev.* **2017**, *46*, 6099−6110.

(245) Mukherjee, S.; Mukherjee, A.; Bhagi-Damodaran, A.; Mukherjee, M.; Lu, Y.; Dey, A. A Biosynthetic Model of Cytochrome c Oxidase as an Electrocatalyst for Oxygen Reduction. *Nat. Commun.* **2015**, *6*, 8467.

(246) Meldal, M.; Tornøe, C. W. Cu-Catalyzed Azide−Alkyne Cycloaddition. *Chem. Rev.* **2008**, *108*, 2952−3015.

(247) Allongue, P.; Delamar, M.; Desbat, B.; Fagebaume, O.; Hitmi, R.; Pinson, J.; Savéant, J.-M. Covalent Modification of Carbon Surfaces by Aryl Radicals Generated from the Electrochemical Reduction of Diazonium Salts. *J. Am. Chem. Soc.* **1997**, *119*, 201−207.

(248) Tran, P. D.; Le Goff, A.; Heidkamp, J.; Jousselme, B.; Guillet, N.; Palacin, S.; Dau, H.; Fontecave, M.; Artero, V. Noncovalent Modification of Carbon Nanotubes with Pyrene-Functionalized Nickel Complexes: Carbon Monoxide Tolerant Catalysts for Hydrogen Evolution and Uptake. *Angew. Chem., Int. Ed.* **2011**, *50*, 1371−1374.

(249) Wang, D.; Wang, L.; Brady, M. D.; Dares, C. J.; Meyer, G. J.; Meyer, T. J.; Concepcion, J. J. Self-Assembled Chromophore−Catalyst Bilayer for Water Oxidation in a Dye-Sensitized Photo-electrosynthesis Cell. *J. Phys. Chem. C* **2019**, *123*, 30039−30045.

(250) Bonchio, M.; Syrgiannis, Z.; Burian, M.; Marino, N.; Pizzolato, E.; Dirian, K.; Rigodanza, F.; Volpato, G. A.; La Ganga, G.; Demitri, N.; Berardi, S.; Amenitsch, H.; Guldi, D. M.; Caramori, S.; Bignozzi, C. A.; Sartorel, A.; Prato, M. Hierarchical Organization of Perylene Bisimides and Polyoxometalates for Photo-Assisted Water Oxidation. *Nat. Chem.* **2019**, *11*, 146−153.

(251) Usov, P. M.; Ahrenholtz, S. R.; Maza, W. A.; Stratakes, B.; Epley, C. C.; Kessinger, M. C.; Zhu, J.; Morris, A. J. Cooperative Electrochemical Water Oxidation by Zr Nodes and Ni−Porphyrin Linkers of a PCN-224 MOF Thin Film. *J. Mater. Chem. A* **2016**, *4*, 16818−16823.

(252) Li, X.; Zhang, H.; Hu, Q.; Zhou, W.; Shao, J.; Jiang, X.; Feng, C.; Yang, H.; He, C. Amorphous NiFe Oxide-based Nanoreactors for Efficient Electrocatalytic Water Oxidation. *Angew. Chem., Int. Ed.* **2023**, *62*, No. e202300478.

(253) Li, X.; Deng, C.; Kong, Y.; Huo, Q.; Mi, L.; Sun, J.; Cao, J.; Shao, J.; Chen, X.; Zhou, W.; Lv, M.; Chai, X.; Yang, H.; Hu, Q.; He, C. Unlocking the Transition of Electrochemical Water Oxidation Mechanism Induced by Heteroatom Doping. *Angew. Chem., Int. Ed.* **2023**, *62*, No. e202309732.